

OIL RETENTION AND ITS EFFECTS ON PRESSURE
DROP AND HEAT TRANSFER IN MICROCHANNEL
HEAT EXCHANGERS OF AIR CONDITIONING AND
REFRIGERATION SYSTEM

By

ARDIYANSYAH S. YATIM

Bachelor of Engineering
Universitas Indonesia
Depok, Indonesia
2003

Master of Engineering
Chonnam National University
Chonnam, Republic of Korea
2006

Submitted to the Faculty of the
Graduate College of the
Oklahoma State University
in partial fulfillment of
the requirements for
the Degree of
DOCTOR OF PHILOSOPHY
July, 2015

OIL RETENTION AND ITS EFFECTS ON PRESSURE
DROP AND HEAT TRANSFER IN MICROCHANNEL
HEAT EXCHANGERS OF AIR CONDITIONING AND
REFRIGERATION SYSTEM

Dissertation Approved:

Dr. Lorenzo Cremaschi

Dissertation Adviser

Dr. Daniel E. Fisher

Dr. Brian R. Elbing

Dr. Clint P. Aichele

ACKNOWLEDGEMENTS

I wish to express my sincere appreciation and grateful to my advisor, Dr. Lorenzo Cremaschi, for his continuous support, patience and guidance. I would also like to extend my appreciation to my committee members, Dr. Daniel E. Fisher, Dr. Brian R. Elbing and Dr. Clint P. Aichele for all the advices and suggestions given during my PhD study. I also would to thank Dr. Jeffrey Spitler for his inputs during the first and second years of the research.

I sincerely thank fellow graduate students: Pratik Deokar and Sarath Mulugurthi for the construction and operation of the experimental setups, Andrea Bigi, Stefano Del'Orto, Ellyn Jespersen for the modelling works. I would also like to thank other research group members: Jeremy Smith, Shanshan Cai, Weiwei Zu, Xiaoxiao Wu, Pedro Perez, Thiam Wong, and Auvi Biswas for their help and friendships. Without your help, I cannot go this far.

Special thanks to my wife, Dwi Rahmawati for her endless love and support through the ups and downs in my personal and professional life.

Name: ARDIYANSYAH S. YATIM

Date of Degree: JULY, 2015

Title of Study: OIL RETENTION AND ITS EFFECTS ON PRESSURE DROP AND HEAT TRANSFER IN MICROCHANNEL HEAT EXCHANGERS OF AIR CONDITIONING AND REFRIGERATION SYSTEM

Major Field: MECHANICAL AND AEROSPACE ENGINEERING

Abstract: In vapor compression, a small portion of the compressor oil circulates with the refrigerant through the cycle components, while most of the oil stays in the compressor. The presence of oil increases the pressure losses and results in an additional thermal resistance to the heat exchange process. The goals of this study were to investigate the oil retention and its effects on heat transfer and pressure drop of refrigerants and oil mixtures in microchannel type condenser and evaporator.

Two different louvered-fin aluminum microchannel heat exchangers set as condenser and evaporator were tested. The experiments were conducted in a custom-made test facility built ad-hoc for this study that controlled the amount of oil released to the heat exchangers and measured the corresponding oil retention, the heat transfer rates, and the pressure drops. The refrigerants used were R410A and R134a in combination with synthetic polyol ester (POE) oil. The saturation temperatures for condenser applications varied from 85 to 130 °F (29 to 54°C) while for evaporator applications, the range was from 33 to 48°F (0.5 to 9°C). The oil mass fraction (OMF) were varied from 0 to 5 wt.%. For microchannel type condenser, the results from the present work indicated that the oil retained in the condenser strongly depended on the OMF of the mixture. The oil retention volume increased if the OMF increased and it was measured up to 11% of the total condenser internal volume. The oil retention volume for high mass flux conditions were higher than those for low mass flux conditions and the effect of mass flux on the oil retention was small for low OMFs but it became more evident for OMFs of 3 wt.% and higher. Oil affected the heat transfer rate of the microchannel condenser and it penalized the heat transfer capacity by as much as 10 percent if the oil mass fraction was 3 wt.%. For both refrigerant R410A and POE mixture and refrigerant R134a and POE oil mixture, the heat transfer rate at low saturation temperature increased slightly if the OMF increased up to about 3 wt.%; then the heat transfer rate started to decline at higher OMFs. Oil also increased the refrigerant-side pressure losses of the microchannel condenser up to 19 percent with respect to oil free conditions.

The oil retention volume in the microchannel evaporator was measured up to 13 % of total internal volume of evaporator. Oil affected the heat transfer rate of the microchannel evaporator and it penalized the heat transfer capacities by as much as 11% if the oil mass fraction was 3 wt.%. For air-conditioning and refrigeration systems, when OMFs were equal to or less than 1 wt. %, the decrease in heat transfer rates were within 4 %. The oil decreased the heat transfer rate and its impact was also depended on the mass flux. The refrigerant-side pressure drop across the microchannel evaporators increased by 10 to 25 percent when oil was present inside the heat exchangers and the OMF was in the range of 1 wt.%.

TABLE OF CONTENTS

CHAPTER I.....	1
1 Introduction.....	1
1.1 Background	1
1.2 Study Objectives	6
1.3 Scope of Work and Experimental Test Matrix.....	7
1.4 Dissertation Organization.....	10
CHAPTER II.....	12
2 Literature review	12
2.1 Relevant Studies on POE lubricant and Refrigerant Properties	12
2.2 Effect of Lubricant during Refrigerant Condensation.....	16
2.3 Effect of Lubricant during Refrigerant Evaporation	23
2.4 Oil Retention Models	30
2.5 Oil Retention Experimental Methodology	34
CHAPTER III	38
3 Experimental methodology	38
3.1 Introduction	38
3.2 Microchannel Heat Exchangers	39

3.2.1	Microchannel Condenser That Was Tested in the Research	40
3.2.2	Microchannel Evaporator That Was Tested in the Present Study	44
3.3	Experimental Setup	46
3.3.1	Psychrometric chamber used to control the inlet air streams	47
3.3.2	Oil Retention Measurements in the Microchannel Condenser	50
3.3.3	Oil Retention Measurement in Microchannel Evaporator	69
3.3.4	Verification that the Two Methods Adopted in the Present Work for Measuring Oil Retention in the Microchannel Heat Exchangers Provided the Same Experimental Data.....	94
3.4	Test Conditions and flow rates for the condenser and evaporators tests	.99
3.5	Further Details of the Equipment and Instrumentation of the Experimental Facility.....	100
3.5.1	Air Tunnel Apparatus	103
3.5.2	Chiller and Secondary Coolant Loop	109
3.6	Instrumentation and Data Acquisition System.....	111
3.6.1	Temperature Measurements	119
3.6.2	Oil and Refrigerant Pressure Measurements	123
3.6.3	Air Humidity Measurements	125
3.6.4	Air Flow Measurements	125
3.6.5	Oil Volume Measurements.....	128

CHAPTER IV	137
4 Data Reduction and Uncertainty Analysis	137
4.1 Data Reduction	137
4.2 Uncertainty Analysis	144
4.2.1 Uncertainty Analysis of Microchannel Condenser Tests	146
4.2.2 Uncertainty Analysis of Microchannel Evaporator Tests	150
CHAPTER V	155
5 Experimental Results and Discussion	155
5.1 Microchannel Condenser	155
5.1.1 Oil retention	155
5.1.2 Effect of oil retention on the heat transfer rate of the condenser	167
5.1.3 Pressure drop on the refrigerant side of the heat exchanger	175
5.1.4 Thermodynamic and Heat Transfer Analysis of Condenser Experimental Results for the Heat Transfer Factor	180
5.2 Microchannel Evaporator	185
5.2.1 Oil retention volume in the evaporators	185
5.2.2 Heat transfer factors (HTFs) for microchannel evaporator	198
5.2.3 Pressure drop factor of microchannel evaporator	207
CHAPTER VI	215
6 Oil Retention Model	215

6.1	Microchannel Condenser Model	215
6.2	Microchannel Condenser Model Validation	217
6.2.1	Air Conditioning Application with R410A and POE lubricant	217
CHAPTER VII.....		231
7	Conclusions and Recommendations for Future Work.....	231
7.1	Conclusions from the Present Study	231
7.2	Recommendations for Future Work on this Research Topic	242
Nomenclature		246
References.....		251

List of Figures

Figure 2.1: Example of oil retention volume, expressed in percentage of oil volume charged inside the compressor, in components of an R134a/POE refrigeration system (reprinted, by permission, from Cremaschi (2004))...	36
Figure 3.1: Schematic of the microchannel condenser tested in the research	41
Figure 3.2: Use of an infrared image to locate the partition inside the header of the microchannel condenser (Deokar, 2013).....	43
Figure 3.3: Microchannel evaporator A: (top) actual picture of the first heat exchanger, A, tested in the present study and (bottom) schematic of the heat exchanger A with refrigerant flow direction during the evaporator tests	44
Figure 3.4: Psychrometric chamber at Oklahoma State University (Deokar, 2013)	47
Figure 3.5: Layout of the oil retention test set up in the large scale psychrometric chamber (Deokar, 2013).....	49
Figure 3.6: Schematic of the initial compressor based test facility designed and constructed for the research – later it was modified and upgraded to a pump boiler based test facility (Deokar, 2013)	53
Figure 3.7: P-h diagram of Vapor Compression cycle and Pump-Boiler systems (Deokar, 2013).....	55
Figure 3.8: Schematic of the experimental setup for condenser tests (modified from Deokar (2013)).....	60

Figure 3.9: Oil extraction system (left) and mass balance at the oil extractor (right, the oil extractor consisted of the two oil separators connected in series, as indicated inside the red dashed square on the left side of the figure).....	62
Figure 3.10: Oil retention calculation: (a) injection at inlet of MCHX; (b) injection at outlet of MCHX.....	66
Figure 3.11: Schematic of the pump-boiler based experimental setup used in the evaporator oil retention tests	70
Figure 3.12: Section of pump boiler loop from exit of oil separators until preheater tubes (Deokar, 2013)	74
Figure 3.13: Variable power preheater and constant power preheater tube heat exchangers of the pump boiler loop	74
Figure 3.14: Example of an electric heater wrapped around a refrigerant copper tube and used as preheater for the evaporator tests	76
Figure 3.15: The four differential pressure transducers installed in parallel and used in the evaporator tests	77
Figure 3.16: Photo of the position of sight glass S1 and sight glass S2 with respect to oil separators (the sight glasses S1 and S2 were used as visual aid to see when refrigerant and oil mixture layer first appears in those sight glasses).	79
Figure 3.17: Test sections and Air sampling device in front of test section.....	80
Figure 3.18: Thermocouple grid arrangement during Evaporator A installation	82
Figure 3.19: Infrared Image of microchannel evaporator A for one medium temperature test; this image indicates refrigerant flowing vertically from	

bottom to top of the heat exchanger and fairly uniform refrigerant flow distribution.....	84
Figure 3.20: Examples of a measurement of the time at which the oil reached the sight glass; a digital chronometer was video recorded next to the sight glass to synchronize the data (the uncertainty of the measured time was of max 2 seconds)	86
Figure 3.21: Example of time for the oil to travel along the pipeline versus OMF	90
Figure 3.22: Mass of oil measured when injected at the outlet of the test section (M (OMF% _{@outlet}) versus OMF and for two locations of the fight glasses.....	90
Figure 3.23: Screenshot of the Labview graphic interface DAQ displaying the psychrometric conditions of the air at the inlet of microchannel evaporator	92
Figure 3.24: Example of a case in which frost formation on the microchannel evaporator A occurred during the experiments (the test was interrupted, the evaporator was defrosted, and then the test was repeated in frost-less conditions)	93
Figure 3.25: Display of the Labview graphic interface DAQ for the air blower and for the flow nozzles used to measure the air flow rate during the heat transfer experiments	94
Figure 3.26: P-h diagram and corresponding components for condenser tests	96
Figure 3.27: P-h diagram and corresponding components for evaporator tests	96
Figure 3.28: Comparison between oil retention measurements in the condenser by using the two equivalent experimental techniques of the research.	98

Figure 3.29: Air flow loop inside the psychrometric chamber at Oklahoma State University (Deokar, 2013).....	103
Figure 3.30: Front side of the microchannel heat exchanger exposed to the ambient air (air flow direction is entering the heat exchanger as indicated by the yellow dashed arrow (Deokar, 2013))	104
Figure 3.31: Back side (in the direction of the air flow) of the microchannel heat exchanger (air flow direction is exiting the heat exchanger moving toward the fan (Deokar, 2013))	105
Figure 3.32: Instrumentation and configuration of refrigerant and oil lines connecting the microchannel heat exchanger	107
Figure 3.33: Chiller and heat sink loop.....	110
Figure 3.34: Labview control and graphic interface for oil retention tests.....	112
Figure 3.35: Calibration curve for the oil level tank to measure the volume of oil extracted during initial test setup (Deokar, 2013)	132
Figure 3.36: Relation between the flow meter accuracy and the mass flow rate.....	135
Figure 4.1: Uncertainty of ORV with $t \pm 2$ seconds	152
Figure 4.2: Oil layer observed for various OMFs.....	153
Figure 5.1: Oil retention volume at low degree of superheat for R410A+POE oil in microchannel condenser	158
Figure 5.2: Oil retention volume at high degree of superheat for R410A+POE oil in microchannel condenser	160
Figure 5.3: Oil retention volume at high degree of inlet superheat for R134a+POE oil in microchannel condenser	165

Figure 5.4: Heat transfer factor at low degree of superheat for R410A+POE oil in microchannel condenser	169
Figure 5.5: Heat transfer factor at high degree of superheat for R410A+POE oil in microchannel condenser	170
Figure 5.6: Heat transfer factor at high degree of superheat for R134a+POE oil in microchannel condenser	174
Figure 5.7: Pressure drop at low degree of superheat for R410A+POE oil in microchannel condenser	176
Figure 5.8: Pressure drop at high degree of superheat for R410A+POE oil in microchannel condenser	177
Figure 5.9: Pressure drop factor at high degree of superheat for R134a+POE oil in microchannel condenser	180
Figure 5.10: Oil retention volume (ORV_N) in microchannel evaporator A with R410A and POE oil.....	191
Figure 5.11: Oil retention volume (ORV_N) in microchannel evaporator A with respect to sight glass S1, sight glass S2, and effect of the variation of the observed time by 2 seconds (the results for series H)	192
Figure 5.12: Oil retention volume for R134a+POE oil in microchannel evaporator A...	197
Figure 5.13: Heat transfer factor in microchannel evaporator A with R410A and POE oil	202
Figure 5.14: Simulation results of the local convective heat transfer coefficient in one microchannel tube of evaporator A with R410A and POE oil mixture (Dell'orto, 2014, printed with permission).....	203

Figure 5.15: Heat transfer rate measured from the air-side (<i>Q_{evap, A}</i>) in microchannel evaporator A with R410A and POE oil at OMF at 0.5%	203
Figure 5.16: <i>Q_{evap, A}</i> in microchannel evaporator A with R410A and POE oil at OMF 1%	203
Figure 5.17: <i>Q_{evap, A}</i> in microchannel evaporator A with R410A and POE oil at OMF 3%	204
Figure 5.18: <i>Q_{evap, A}</i> in microchannel evaporator A with R410A and POE oil at OMF 5%	204
Figure 5.19: Heat transfer factor in microchannel evaporator A with R134a and POE oil	207
Figure 5.20: Pressure drop factor in microchannel evaporator A with R410A and POE oil	210
Figure 5.21: Pressure drop factor in microchannel evaporator A with R134a and POE oil	213
Figure 6.1: Verification of the local refrigerant and oil mixture heat transfer coefficients during two phase flow condensation in microchannel tubes with data from the literature (Bigi, 2014)	219
Figure 6.2: Infrared images of a small sample of microchannel heat exchanger inside (a) and outside (b) an oven; the images were taken to calibrate the emissivity factors of the thermal camera (Bigi, 2014)	220
Figure 6.3: Infrared image of the microchannel condenser inlet with R410A and POE lubricant (a) and comparison of infrared image surface temperature with simulation results (b) for two different temperatures (Bigi, 2014)	222

Figure 6.4 Comparison between experimental data and predicted results for the oil retention volume (ORV) at low superheat conditions (top) and at high superheat conditions (bottom) of the microchannel condenser with refrigerant R410A and POE oil mixture.....	225
Figure 6.5 Comparison between experimental data and predicted results for the oil retention volume (ORV) at high superheat conditions of the microchannel condenser with refrigerant R134a and POE oil mixture.....	226
Figure 6.6: Comparison between experimental data and predicted results for the HTF (top) and PDF (bottom) of the microchannel condenser with refrigerant R410A and POE oil mixture at 105°F (41°C), low mass flux, and low superheat conditions	227
Figure 6.7: Comparison between experimental data and predicted results for the HTF (top) and PDF (bottom) of the microchannel condenser with refrigerant R410A and POE oil mixture at 105°F (41°C), low mass flux, and high superheat conditions	228
Figure 6.8: Comparison between experimental data and predicted results for the HTF (top) and PDF (bottom) of the microchannel condenser with refrigerant R134a and POE oil mixture at 105°F (41°C), low mass flux, and high superheat conditions	230

List of Tables

Table 1-1: Test matrix of oil retention experiments in microchannel heat exchangers for air conditioning and refrigeration applications	8
Table 3-1 Dimensions of the microchannel condenser that was tested in the present study	42
Table 3-2 Dimensions of the Microchannel Heat Exchanger-Evaporator That Was Tested in the Present Study	45
Table 3-3: Range of the differential pressure transducers used in the experimental setup.....	77
Table 3-4 Test matrix for typical air conditioning and refrigeration systems	99
Table 3-5 Main equipment and sensors of the psychrometric chamber used in this study	100
Table 3-6 Specification of the components used in the oil retention tests.....	113
Table 3-7 Specifications of Resistance Temperature Detectors	120
Table 3-8 Specifications of the Thermocouples	121
Table 3-9 Specifications of the Absolute Pressure Transducers.....	124
Table 3-10 Specifications of the Differential Pressure Transducers	124
Table 3-11 Specifications of the Relative Humidity Sensors	125
Table 3-12 Specifications of the Air flow Nozzles.....	126
Table 3-13 Specifications of the Very Low Differential Pressure Transducers	127
Table 3-14 Specifications of the Refrigerant Mass Flow Meter.....	133

Table 3-15 Specifications of the Oil-Refrigerant Mixture Injection and Extraction	
Mass Flow Meter	134
Table 3-16 Specification of the Weighing Scale	136
Table 4-1 Accuracy of the main instrumentation for the study	145
Table 4-2 Range and Uncertainty Limits of the Main Variables in Condenser Tests	149
Table 5-1 Legend of the letters and symbols used in the figures reporting the tests	
results of microchannel condenser with R410A and POE	157
Table 5-2 Legend of the letters and symbols used in the figures reporting the tests	
results of microchannel condenser with R134a and POE	164
Table 5-3 Legend of the letters and symbols used in the figures reporting the tests	
results of microchannel evaporators with R410A and POE	187
Table 5-4: Legend of the letters and symbols used in the figures reporting the tests	
results of microchannel evaporator A with R134a and POE	195

CHAPTER I

1 Introduction

1.1 Background

In a refrigeration cycle, a small portion of oil circulates with the refrigerant flow through the cycle components, while most of the oil stays in the compressor. The compressor in a refrigeration system needs oil for the following reasons: to prevent surface-to-surface contact, to remove heat, to provide sealing, to keep out contaminants, to prevent corrosion, and to dispose of debris created by wear (Vaughn, 1971). Most compressor mechanical failures are due to improper oil management that leads to a lack of proper lubrication inside the compressor. This means taking into account the fact that oil might be missing from the compressor because it can be held up inside the heat exchangers during actual system operating conditions.

Oil retention is a complex function of fluid properties as well as geometry and configuration aspects. The circulating oil, which is missing from the compressor, can form a fairly homogeneous mixture with the liquid refrigerant or it can exist as a separate oil film inside the tubes and headers of the heat exchangers; the amount of oil is affected by the system conditions. Each heat exchanger in a refrigeration cycle has different oil retention characteristics, and large amounts of oil retention cause a decrease in heat transfer and an increase of pressure drop (Cremaschi *et al.*, 2005). As a result, proper oil

management is necessary in order to improve the compressor reliability, increase the overall efficiency of the system, and minimize the system cost by avoiding redundancy.

Abundant literature can be found on oil and refrigerant flow inside simple geometries. Sundaresan and Radermacher (1996) studied oil return characteristics in residential heat pump systems using R22, R407C, and R410A with mineral oil (MO) and synthetic polyol ester (POE) oils. From their experiments, they recommended the use of POE oils with new refrigerant blends such as R407C and R410A. Biancardi *et al.* (1996) conducted experimental and analytical efforts to determine the lubricant circulation characteristics of R134a/POE and R134a/MO pairs in a residential heat pump system and compared the behavior with a R22/MO mixture. The minimum flow rate for “the worst-case” scenario, in which the critical velocities occurred in the vertical vapor suction line, were determined by visual observations. They reported that minimum flow velocities ranging from 1.8 to 1.9 m/s (354 to 374 fpm) were required in the vertical upward suction lines when the system operated in the cooling mode. Oil return characteristic in vertical upward flows was also experimentally and theoretically investigated by Mehendale and Radermacher (2000) whereof the critical mass flow rates for preventing oil film reversal in a vertical pipe were estimated.

Although most of the oil circulated in the system returns to the compressor, a small portion of the oil is retained in heat exchangers. The oil retained affects the heat exchanger performance through heat transfer degradation and pressure drop augmentation. In order to determine the oil retention volume, one option might be to measure the thickness of the oil film created during annular flow on the interior wall of the refrigerant tubes. Shedd and Newell (1998) proposed a non-intrusive, automated,

optical film thickness measurement technique to be used with a wide range of fluids and flow configurations. Later, Bai and Newell (2002), Shedd and Newell (2004) and Schubring *et al.* (2009) used a similar approach to describe the characteristics of annular two-phase viscous flow of air and water or air and 300 SUS Alkybenzene oil. Extensive experimental flow visualization in horizontal and vertical pipes was required and the oil film thicknesses were correlated with the oil mass flow rates, vapor velocity and pipe diameter. Shear stress correlations were developed and verified with the experimental data. Unfortunately this technique requires optical access to the refrigerant flow and might not be practical for microchannel heat exchangers. Not only the tubes in microchannel heat exchangers are likely to be too small to provide accurate measurements of the oil film thickness by optical methods, but also creating an optical access to the tubes of a microchannel heat exchanger might interfere with the real operation of the heat exchanger during refrigerant condensation. The flow regime during refrigerant condensation in the actual air conditioning applications of the microchannel heat exchanger is mostly annular and the oil film thickness is generally not uniform along the heat exchanger refrigerant path. Oil retention is affected by the flow pattern of the refrigerant-oil mixture because the magnitude of the forces exerted on the fluid element depends on the type of motion of the fluid, relative interfacial surface area between the two phases, and velocity slip ratio between gas and liquid phases. Few researchers investigated flow patterns for refrigerant-oil mixtures used in air conditioning industry while many researchers studied the flow characteristics for mixtures of air/water or air/pure oil. Riedle *et al.* (1972) were among the first researchers to characterize systematically the flow of oil-refrigerant mixtures. Their analytical model, based on

minimum gas velocities, introduced the concepts of void fraction, oil entrainment, and liquid film thickness for oil-refrigerant mixtures. An extensive review of flow boiling characteristics and flow patterns of refrigerant-oil mixture was presented in Bandarra Filho *et al.* (2009).

While studies of oil return and oil transport in suction liners are quite numerous in the literature, measurements of oil retention in condensers and evaporators for air conditioning and refrigeration systems are rather sporadic in the open domain state-of-the-art work. Oil retention is affected by the flow pattern of the refrigerant-oil mixture because the magnitude of the forces exerted on the fluid element depends on the type of motion of the fluid, relative interfacial surface area between the two phases, and velocity slip ratio between gas and liquid phases. Few researchers investigated flow patterns for refrigerant-oil mixtures used in air conditioning industry while many researchers studied the flow characteristics for mixtures of air/water or air/pure oil. Riedle *et al.* (1972) were among the first researchers to characterize systematically the flow of oil-refrigerant mixtures. Their analytical model, based on minimum gas velocities, introduced the concepts of void fraction, oil entrainment, and liquid film thickness for oil-refrigerant mixtures. Schlager *et al.* (1990) conducted experiments in order to determine the quantity of oil in smooth and micro-fin tubes during evaporation and condensation of refrigerant-oil mixtures. They showed that the parameters that affect the oil retention were mass flux, oil mass fraction, viscosity, evaporator exit conditions (i.e., vapor quality at the evaporator outlet), and evaporation pressure. They used R22 in combination with 150 to 300 SUS mineral oil.

Lee (2002) proposed a model for oil retention in Carbon Dioxide (CO₂) air conditioning systems. The lubricant used was polyalkylene glycole (PAG) oil, which is partially miscible with CO₂. Lee also showed the effect of the oil retention on pressure drops in the suction line, evaporator, and gas cooler. Pressure drops were easily doubled when the oil mass fraction increases up to 5 percent in mass concentration. Thus, design pressure drop correlations needed to consider this penalty factor due to oil accumulation in the heat exchangers. The oil effects on the evaporation heat transfer in microchannel heat exchangers were experimentally investigated by Zhao *et al.* (2002). Later, Hwang *et al.* (2004) were able to characterize the pressure drop and heat transfer capacity degradation of a low temperature CO₂ refrigeration system based on the oil circulation. They used capacitive sensors to detect the trace of oil in the refrigerant flow. Cremaschi (2004) focused on measuring the oil retention in fin-and-tube evaporators and condensers of air conditioning and refrigeration systems. The refrigerants adopted were R22, R410A, and R134a in combination with three different types of oils: mineral oil (MO), polyol ester (POE), and polyalkylene glycole (PAG) synthetic lubricants. The effects of different refrigerant mass fluxes, solubility, and miscibility of the carrier fluid were experimentally investigated.

In summary, there appears to be a growing number of studies on the oil effects on heat exchanger performance for conventional fin-and-tube heat exchangers. However, studies of the effects of oil on microchannel type heat exchangers are still limited in the open domain literature. The objective of this study is to measure the oil retention and its effects on heat transfer and pressure drop in microchannel evaporators and condensers used in air conditioning and refrigeration applications.

1.2 Study Objectives

The overarching goal of the research was to investigate experimentally the effect of lubricant on heat transfer and pressure drop of refrigerant during flow boiling and condensation in microchannels. The analysis also utilized the results from a preliminary model for oil retention in microchannel heat exchangers that was developed in a separate study.

The specific objectives of the research are as follows:

- 1) To construct an experimental apparatus capable of measuring the oil retention volume in microchannel heat exchangers used as both evaporators and condensers in R410A air conditioning systems and R134a coolers and refrigeration systems
- 2) To measure the quantity of oil held up in two microchannel heat exchangers, one for R410A air conditioning and one for R134a coolers applications, operating in evaporator and condenser modes
- 3) To provide data of oil retention in microchannel heat exchangers as function of oil mass fraction circulating in the heat exchangers, refrigerant flow rates, and refrigerant saturation temperatures
- 4) To experimentally determine the impact of the oil that was held up inside the microchannel heat exchanger on the heat transfer capacity degradation and refrigerant side pressure drop
- 5) To analyze the experimental results and use a model for oil retention in microchannel tubes of the condenser that was simple but accurate enough to be useful in practical engineering designs

- 6) To experimentally validate the oil retention model, including the predicted heat transfer rates and pressure drops for refrigerant and oil mixtures, with the data of the present work.

1.3 Scope of Work and Experimental Test Matrix

The research used two different louvered-fin aluminum microchannel heat exchangers: one type for the condenser and one type for the evaporator. All two microchannel type heat exchangers were commercially available and they were used in commercially available heat pump systems. The experiments were conducted in a custom-made test facility built ad-hoc for this study in order to replicate the real life operating conditions of the heat exchangers of air conditioning and refrigeration systems at Oklahoma State University (OSU) laboratory. The OSU test facility controlled the amount of oil released to the heat exchangers and it measured the corresponding oil retention, the heat transfer rates, and the pressure drops. The test conditions were selected based on typical applications of refrigerant R410A in air conditioning systems and of refrigerant R134a in vending machines and water/wine coolers refrigeration systems. The oil used in the present work was synthetic polyol ester (POE) with viscosity grade of VG 32 (that is, Emkarate RL32-3MAF POE oil). The saturation temperatures for condenser applications varied from 85 to 130 °F (29 to 54°C) while for evaporator applications, the range of saturation temperatures was ranging from 33 to 48°F (0.5 to 9°C). Over 135 tests were conducted in the present study and the test conditions are summarized in Table 2-1.

Tests were conducted for two refrigerant mass fluxes at each saturation temperature. The first mass flux was representative of the mass flux for full load design conditions of the heat exchangers. The second mass flux was representative of the mass flux for part load conditions of the heat exchangers and it was intentionally selected between 50 to 67 percent of the first mass flux in order to isolate the effect of mass flux on the oil retention. For each refrigerant mass flux, the oil mass fraction, (abbreviated as to OMF), was controlled and varied in a parametric fashion from 0 to 5 weight percent (abbreviated as to wt.%).

The mass flux of the refrigerant was controlled by a variable speed gear pump. The saturation pressures in the microchannel heat exchangers were controlled by a series of auxiliary refrigerant-to-water heat exchangers. An electrically heated water tank and a low temperature chiller served as the hot and cold reservoirs, respectively. The pressures during the actual experiments were also controlled by the temperature of the incoming air stream to the microchannel heat exchangers and by the refrigerant amount that was charged into the test apparatus. The refrigerant mass flux, the incoming air temperature, and the air speed determined the outlet refrigerant-side conditions of the microchannel heat exchangers. For the evaporator tests, the degree of vapor superheat at the outlet of the heat exchanger was controlled to 11 to 15°F (~6 to 8°C).

Table 1-1: Test matrix of oil retention experiments in microchannel heat exchangers for air conditioning and refrigeration applications

Test No.	Saturation Temp. [°F] (°C)	Refrigerant & Oil	Refrigerant Tube Mass Flux [lb _m /hr-ft ²] *	Oil Mass Fraction [wt.%]	Component function / application	Number of Tests data
1	130 (54)	R410A/POE	G _A	0 0.5 1 3 5	Condenser / AC units	3 x 2 x 5 = 30
2	105 (41)	R410A/POE	G _B			

3	85 (29)	R410A/POE								
4	130 (54)	R134a/POE	G_B G_C	0	0.5	1	3	5	Condenser / refrigeration condensing units	3 x 2 x 5 = 30
5	105 (41)	R134a/POE								
6	95 (35)	R134a/POE								
7	48 (9)	R410A/POE	G_C G_D	0	0.5	1	3	5	Evaporator (manufacturer A) / AC units	3 x 2 x 5 = 30
8	38 (3.3)	R410A/POE								
9	32 (0)	R410A/POE								
10	48 (9)	R134a/POE	G_F	0	0.5	1	3	5	Evaporator (manufacturer A) / AC units, Vending machines & water/wine coolers refrigeration systems	5 x 1 x 3 = 15
11	38 (3.3)	R134a/POE								
12	33 (0.5)	R134a/POE								
Total No. of Tests ----->									135	

*The mass flux varied due to difference in both mass flow rate and microchannel port geometry.

Details are provided in chapter 4: Experimental Methodology

1.4 Dissertation Organization

The present dissertation contains 7 chapters. Chapter 1 provides a background and description of the oil retention in microchannel heat exchangers and it summarizes the motivations for the present work. It also contains the objectives and scope of the present work. Chapter 2 discusses the literature review in detail and highlights the main lessons learned from the previous studies. It also provides some clarifications on the scope of this study, on why parts of the present work had to be analyzed in depth, and on questions that the present study aimed to address.

Chapter 3 describes the experimental methodology chosen for this research and explains the test facility and its components details. This chapter describes the geometry of microchannel heat exchangers tested in the present study, test matrix, test objectives and test procedures. Instrumentation and data acquisition system are also covered in this chapter. Chapter 4 discusses data processing, data reduction and uncertainty analysis of the present study.

Chapter 5 discusses the experimental results of the present study. Figures, plots, and charts obtained for tests listed in the test matrix are given and technical analysis of the experimental data is presented.

Chapter 6 describes the model of oil retention, heat transfer and pressure drop model for the microchannel heat exchangers used in the present study. The validation of the model and of existing heat transfer and pressure drop correlations with the experimental data of the present work is also presented in this chapter. Chapter 7 summarized the content of the dissertation and the conclusions from the present study. Some recommendations for

future follow up research on the topic area of oil retention in microchannel heat exchangers are also given in Chapter 7.

CHAPTER II

2 Literature review

There are vast publications available on refrigerant-oil mixture effect on the performance of a refrigeration system, particularly for compressor and heat exchanger equipments, i.e. evaporator and condenser. The effects are highly dependent on the lubricant thermophysical properties and interaction between refrigerant and lubricant especially during phase change process where two-phase, two-component flow occurs. In the first sections, literatures on lubricant properties and their influence to the refrigerant-oil mixture properties, evaporation and condensation processes are summarized. The oil retention models and previous experimental methods available in the literature are discussed next.

2.1 Relevant Studies on POE lubricant and Refrigerant Properties

Refrigerant lubricant requirements are not limited to provide lubrication for compressor moving parts. It also acts as a seal that separate high pressure gas on the discharge side from low pressure gas on the suction side. A high viscosity lubricant can provide good sealing; however it introduces higher frictional resistance. Mineral oil (MO) is one of the first refrigerant lubricants used in the refrigeration system. Due to solubility limitation, especially with non-CFC refrigerants such as R134a and R410A, synthetic oils were

introduced. Polyolester (POE) is synthetic oil commercially used as lubricant in the refrigeration system for all types of compressor with HFC refrigerant such as R134a and R410A. POEs are produced from alcohol and carboxylic acid, where acids are used to give correct viscosity and fluidity at low temperature to match miscibility requirement of the refrigerant. Properties of POE and other refrigeration lubricant are widely available in literatures.

The presence of lubricant in refrigeration system modifies the thermophysical properties of the refrigerant-oil mixture, especially during evaporation and condensation. The lubricant exists only as liquid phase, inducing a two phase-two component flow during both processes, and its concentration varies greatly as the quality changes. In addition, some refrigerant vapor is dissolved in liquid phase of oil-rich mixture which depends on temperature of the oil film and pressure of the refrigerant gas phase. These interactions between lubricant and refrigerant and their local behavior variations are responsible in the mixture properties changes. Study on lubricant properties, hence is uttermost important to understand the lubricant effect to heat transfer and pressure drop of refrigerant-oil mixture.

There are two methods to analyze the effect of lubricant properties to refrigerant-oil mixture behavior that have been used extensively (Thome, 1995;1998). First method is to use pure refrigerant properties, i.e. saturation temperature, and consider the oil as a contaminant then introduce correction factor to account for its effect. Another method is to consider the refrigerant-oil mixture as a binary zeotropic mixture. The author presented general methods for determining bubble-point temperatures, specific heats of oils and refrigerant-oil mixtures, local oil concentrations and temperature enthalpy curves.

Although the latter is considered more accurate from thermodynamic point of view, it was derived using totally miscible lubricant and required full knowledge of mixture properties.

The most apparent effect of the lubricant properties to refrigerant-oil mixture is its high viscosity, which are hundreds to thousands higher than pure refrigerant. Sunami (1999) presented tabulated values of viscosity, along with other physical and chemical properties, of mineral oils and synthetic oils- Polyolester and Alkylbenzene (AB). The viscosity of refrigerant-oil mixture is highly affected by the solubility of the refrigerant and lubricant combinations. The mixture is considered two-phase, two components mixture. While the vapor phase is essentially pure refrigerant, the liquid phase is composed of refrigerant and lubricant. The solubility of refrigerant-lubricant composition is a function of pressure and temperature. ASHRAE Handbook (2010) published solubility, viscosity and density charts of POE and R410A mixtures for ISO VG 32 and 68 in a wide range of temperature and pressure based on works from (Cavestri *et al.*, 1994). Separate study from Yokozeki (1994) and Teodorescu *et al.* (2003) proposed solubility models for various refrigerant/oil mixture using Soave-modified Redlich-Kwong (SRK) equations of state and validated the model with experimental data from literatures. Recent study from Wei *et al.* (2007) proposed simple correlations for various thermodynamic and transport properties of R410A/POE ISO VG 68 oil mixture, e.g. density, solubility, density, specific heat, viscosity, surface tension, thermal conductivity and enthalpy.

In microchannel flow, surface tension (capillary) force has more important role compared to that in conventional tube (Kandlikar, 2004;Thome, 2004). The addition of lubricant to

pure refrigerant will increase the surface tension of the mixture, which tends to provide better wetting characteristics and affect flow regime and heat transfer mechanism during boiling and condensation. Despite its important role, there are not many literatures available for the surface tension property of refrigerant-oil mixture. The surface tension of a mixture can be far lower than the value obtained just using interpolation method between two component properties Riedle *et al.* (1972). The refrigerant-oil mixture surface tension of R410A/POE increases almost double with 30% of oil concentration Wei *et al.* (2007). Based on their experimental results the authors suggested correlation by Jensen and Jackman (1984) for refrigerant-oil mixture surface tension calculation.

The miscibility of lubricant in the refrigerant also affects the performance of refrigeration and air conditioning system (Popovic *et al.*, 2000). In the evaporator, entering fluid consist mainly liquid refrigerant with small amount of lubricant. As it progresses along the evaporator, liquid refrigerant vaporizes and the liquid leaving the evaporator is mostly lubricant. The phase separation can occurs, especially in flooded evaporator, where lubricant-rich liquid layer adheres to the surface, causing obstruction to heat transfer between the wall and the refrigerant and increasing oil retention in the evaporator and suction line of the system. The effect of miscibility of the lubricant in the condenser is less important because liquid flow is in the turbulent region and at relatively high temperature.

The bubble point temperature of refrigerant-lubricant mixture can be estimated using correlation suggested by Thome (1995) as a function of vapor pressure and local oil concentration for different refrigerant and lubricant pairs. The local change of enthalpy for the mixture during evaporation can be contributed to the latent heat of the vaporized

liquid fraction, sensible heat of the liquid phase and vapor phase which are heated to higher bubble point temperature compared to that of pure refrigerant.

2.2 Effect of Lubricant during Refrigerant Condensation

A significant portion in this study was dedicated to determine the effect of lubricant in condensation process, including heat transfer and pressure drop. Despite the fact that the effect of lubricant in the condensation heat transfer was usually less significant compared to that in the evaporation, the study was particularly important in microchannel condenser. The difference can be attributed from the analysis of lubricant and refrigerant liquid phase separation that forms lubricant-rich liquid layers, which prevent optimum heat transfer (Shen and Groll, 2005;2005). For the condenser, these layers formed only at solid-liquid interfaces while for the evaporator the layers exist both at solid-liquid and liquid-vapor interface. In addition, as the mixture progresses in the condenser, the lubricant continuously dissolved into condensed liquid refrigerant, providing oil-free layers at the top side of the condenser tube and maintains high heat transfer performance. The effect of the phase separations due to miscibility of the refrigerant-lubricant mixture also less importance in the condenser as explained in the previous section compared to that in the evaporator.

The effect of oil mass fraction in the condensation heat transfer has been reported to vary non-linearly with oil mass concentration. Schlager *et al.* (1987), Eckels *et al.* (1993), and Bassi and Bansal (2003) indicated negligible effect of lubricant in the condensation heat transfer for oil mass fraction below 3%. However, the condensation heat transfer decreases as the oil mass fraction increases to higher values. Shao and Granryd (1995)

reported decreased mean heat transfer coefficient in a condensing tubes of 10 and 20% for oil mass fraction of 2 and 5%, respectively. The authors also noted different effect in condensation heat transfer at the beginning of the condenser and the latter parts. The difference was explained possibly due to higher condensation temperature for refrigerant-oil mixture compared to that of pure refrigerant, resulting in earlier condensation at the beginning of the condenser. Similar effect of oil mass fraction to convective condensation were also reported using numerical approach with 5% of oil mass fraction, resulting in decreasing condensation heat transfer by 9-16%. (Lottin *et al.*, 2003;Lottin *et al.*, 2003)

Convective condensation correlations for pure refrigerant in conventional channel are well-established in literature. Due to strong influence of flow pattern to heat and momentum transfer, proposed correlations were presented based on observed flow pattern. In a fully developed annular flow, which are commonly found in small diameter tubes, semi-empirical models were proposed by Shah (1979) and Tang *et al.* (2000). A more recent prediction method based on flow regime were presented by Thome *et al.* (2003) which were developed based on 15 refrigerants flow condensation with hydraulic diameter ranges from 3.1 to 21.4 mm. Other models proposed by Dobson and Chato (1998), Haraguchi *et al.* (1994) and Cavallini *et al.* (2004) attempted to predict convective condensation heat transfer coefficient which cover all flow regimes. A set of heat transfer coefficient correlations which cover three ranges of dimensionless parameters are still recommended in ASHRAE Handbook (2009) which were based on Ackers and Rosson (1960) and Ackers *et al.* (1959).

Research on convective condensation in small diameter tube, especially microchannel, have become interest only a decade back, driven by the potential application of

microchannel condenser for residential air conditioning system. These developments require more understanding on heat transfer characteristics inside small diameter channels. The apparent influence of significantly difference hydraulic diameter to flow regime transition was reported by Garimella (2004). As the diameter decrease, the annular flow dominates while the wavy and stratified flow regime decrease or disappear. The effect of surface tension becomes more important while gravitational effect become less and less important. Few literatures are available for condensation heat transfer with hydraulic diameter less than 3 mm. A study by Cavallini *et al.* (2005) measured and compared condensation heat transfer coefficient inside 1.4 mm D_h multiport microchannel with refrigerant R134a and R410A with available correlation for conventional channels. The authors reported that the models under-predicted their experimental results. Yang and Webb (1997) proposed model which account for surface tension forces in microchannel. Wang *et al.* (2004) developed correlation for condensation inside channel with 1 mm hydraulic diameter. Their model includes combination effect of surface tension, shear and gravity forces during condensation.

Available condensation heat transfer correlations for refrigerant-oil mixture employ several different approaches based on known pure refrigerant properties and established correlations for conventional or small diameter channel as described above. The first approach considers the lubricant as contaminant and introduces an oil-enhancement factor (EF) as correction for condensation heat transfer of pure refrigerant flow. Huang *et al.* (2010a) verified three correlations in this category, namely Schlager *et al.* (1990), Eckels *et al.* (1998), and Bassi and Bansal (2003) for EF . Cawte (1992) used different approach by using modified two phase multiplier to correct single phase heat transfer

coefficient in pure refrigerant flow. Here the author defined the multiplier as the ratio of two phase refrigerant-oil mixture and single phase liquid pure refrigerant.

The third category, which becomes more common, uses established correlation for pure refrigerant flow and replacing the pure refrigerant properties with refrigerant-oil mixture's properties. One of the methods was presented by Shao and Granryd (1995) who developed condensation heat transfer coefficient based on modified Tandon *et al.* (1995) correlation with R134a. Their correlations were developed for R134a/POE mixtures inside 6 mm inner diameter smooth tube with mass flux in the range of 120 to 160 kg/m²s, and oil mass fraction from 0 to 5.1%.

For $Re_{r,g} < 24,000$

$$Nu = 15.9 \cdot Pr_{mix,f}^{\frac{1}{3}} \left[\frac{h_{fg}}{C_{p,mix}(T_{sat} - T_w)} \right]^{\frac{1}{6}} \cdot Re_{r,f}^{0.15} \exp(-5.0\omega_0) \quad 2-1$$

For $Re_{r,g} > 24,000$

$$Nu = 0.084 \cdot Pr_{mix,f}^{\frac{1}{3}} \left[\frac{h_{fg}}{C_{p,mix}(T_{sat} - T_w)} \right]^{\frac{1}{6}} \cdot Re_{r,f}^{0.67} \exp(-5.0\omega_0) \quad 2-2$$

Huang *et al.* (2010a) proposed correlations for condensation heat transfer coefficient which also belong to the same category above. Their experimental data include R410A/Ester Oil RB68EP mixture flow inside 4.8 and 1.6 mm ID and oil concentration range of 0-5%. Their proposed correlations were developed from Haraguchi *et al.* (1994) which covers both wavy-stratified and annular flows. Their correlation considers

condensation heat transfer Nusselt number as the superposition of Nusselt number for forced convection condensation and that for free convection condensation. The correlations were verified within -30 to 20% deviation from their experimental data.

$$Nu = \alpha_{tp.x.o} D / \lambda_L = (Nu_F^2 + Nu_B^2)^{0.5} \quad 2-3$$

$$Nu_F = 0.0152(\phi_V/X_{tt})Re_L^{0.77}(0.33 + 0.83Pr_L^{0.8}) \quad 2-4$$

$$Nu_B = 0.725H(\varepsilon)(Ga_L Pr_L / Ph_L)^{0.25} \quad 2-5$$

Where

$$\phi_V = 1 + 0.5\{G/[gD\rho_V(\rho_L - \rho_V)]^{0.5}\}^{0.75}X_{tt}^{0.35} \quad 2-6$$

$$H(\varepsilon) = \varepsilon + \{10[(1 - \varepsilon)^{0.1} - 1] + 1.7 \times 10^{-4}Re_{LO}\}\varepsilon^{0.5}(1 - \varepsilon^{0.5}) \quad 2-7$$

The lubricant presence in the condenser takes important effect in the pressure drop increase. Cremaschi (2004) reported up to 30% increase in the pressure drop for 5% oil mass fraction in the condenser compared to oil-free condition. The author tested two commonly used refrigerant-oil pairs, namely R134a and R410A with mineral and POE lubricants. Similar effects also presented by Shao and Granryd (1995) for R134a/oil mixture which reported of 20% increase of pressure drop when oil was present. The increase of oil concentration also induces higher pressure drop in the condenser mainly

due to the influence of higher oil viscosity to the mixture properties. In addition, the thicker oil film at higher oil concentration also reduces flow area hence increases pressure drop. Pressure drop increases during condensation of refrigerant-oil mixture were found to be less severe compared to that of evaporation. It was related to the increasing mixture viscosity which induces higher shear stress increase during stratified flow pattern in the condenser than annular flow pattern predominantly found during evaporation (Tichy *et al.*, 1986). The pressure drop increases were reported to be less severe as mass flux increases (Schlager, 1988; Cremaschi, 2004). It is interesting to note here that several researchers had reported unusual decrease of pressure drop during condensation (Schlager, 1988; Eckels *et al.*, 1993; Zürcher *et al.*, 1998). An explanation based on flow state was offered by (Shen and Groll, 2005). The authors applied Lockhart-Martinelli (1949) pressure drop correlation to R134a/oil mixture obtained from Zürcher *et al.* (1998) and plotted the frictional pressure drop versus quality for different oil concentrations. They found sharp decrease of frictional pressure drop at high quality and the change was more for higher oil concentration. The explanation for this phenomenon was possibly due to the oil presence increases the mixture viscosity so significantly at higher quality, causing changes of flow state from turbulent to laminar. Hence higher oil concentrations tend to induce more laminar flow earlier, causing a decrease of pressure drop.

As for condensation heat transfer, models to predict frictional pressure drop of refrigerant-oil mixture during condensation have been developed based on several approaches. The first approach is to introduce a penalty factor (*PF*) to correct two-phase frictional pressure drop of pure refrigerant and apply it to refrigerant-oil mixture

(Schlager *et al.*, 1990; Eckels *et al.*, 1993). Huang *et al.* (2010b) conducted comparison of PF correlations based on Müller-Steinhagen and Heck (1986) as pure refrigerant frictional pressure drop correlation. Another approach for calculating condensation pressure drop is to consider refrigerant-oil mixture properties as the input parameters. Zürcher *et al.* (1998) developed correlation for two-phase multiplier used in Friedel (1979) which account for refrigerant-oil mixture's viscosity. Choi *et al.* (1999) developed correlation for refrigerant-oil mixture based on Pierre (1964) with modified friction factor.

$$f_N = 0.00506 Re_{fo}^{0.0951} K_f^{0.1554} \quad 2-8$$

where K_f is two-phase number. For refrigerant-oil mixture, the Reynolds number for liquid only was replaced by that of mixture by considering local mixture viscosity from Yokozeki (1994).

Huang *et al.* (2010b) proposed condensation pressure drop of R410A/oil mixture which also consider mixture viscosity. The authors modified Martinelli parameter used in two-phase multiplier by considering pure R410A for vapor phase properties and R410A/oil mixture for liquid phase. The friction factor for vapor single-phase flow recommended by Jung and Radermacher (1989) was used.

$$X_{tt} = \left(\frac{1 - x_{r,o}}{x_{r,o}} \right)^{0.9} \left(\frac{\rho_{r,v}}{\rho_{r,o,L}} \right)^{0.5} \left(\frac{\mu_{r,o,L}}{\mu_{r,v}} \right)^{0.1} \quad 2-9$$

$$f_V = 0.046Re_V^{-0.20} \quad 2-10$$

The applicable ranges are: inside tube diameter from 1.6 mm to 4.18 mm, mass fluxes from 200 to 600 kg/m²s and oil mass fraction from 0 to 5%.

2.3 Effect of Lubricant during Refrigerant Evaporation

The second objective of this research is focused on flow boiling evaporation of refrigerant-oil mixture in microchannel evaporator. The evaporator is the most sensitive component for lubricant presence in refrigeration system. In the evaporator, the oil is accumulated at the end of the evaporator. While the lubricant does not significantly affect the heat transfer capacity of the condenser, it greatly reduces heat transfer capacity of the evaporator. Lottin et al. (2003;2003) reported heat transfer capacity degradation of evaporator in the range of 20-35% using different correlation with 5% OMF. The pressure drop increases due to oil presence were reported by Cremaschi (2004) up to 20% with 8% oil mass fraction in the evaporator.

Lottin et al. (2003;2003) performed numerical analysis of R410A and POE mixture in the refrigeration system. They reported no significant degradation of overall system performance for oil concentration below 0.5%. However the COP can decrease to 18.9% with 5% oil concentration by weight in the system. Experimental study of oil retention in air conditioning system was performed by Cremaschi *et al.* (2005) which includes commonly used refrigerants-oil mixture, i.e. R22/MO, R410/MO, R410/POE, R134a/POE, and R134a/PAG. Oil retention was measured in the suction line, and fin-and-tube evaporator and condenser. The effect of the oil to the overall performance was reported for R22/MO where increased oil mass fraction from 0 to 9%, decreased the COP

and cooling capacity of 9 and 7%, respectively. Extension of the work was reported by (Radermacher *et al.*, 2006) where a model for oil retention in the suction line and evaporator was developed and verified. Several researchers have reported an increase of pool boiling heat transfer coefficient at low oil concentration and decrease it at higher concentration (Monde and Hahne, 1987;Memory *et al.*, 1995).

As described earlier, the lubricant properties, which modify refrigerant-oil mixture properties, play important roles in the heat transfer degradation. Collier and Thome (1994) suggested that the flow boiling heat transfer coefficient is affected by: an increase of nucleate boiling contribution, a decrease in convective boiling contribution due to high local viscosity, and adverse effect of mass transport during evaporation processes. Shen and Groll (2005) suggested similar explanations due to foaming, increased wetted surface: due to the increased mixture viscosity and surface tension, there should be no doubt that the oil solution accelerates the formation of annular flow and enhanced nucleate boiling as described above.

The most prominent flow boiling heat transfer model which has been used widely is the superposition model of Chen (1963). The model suggested that the flow boiling heat transfer mechanism was governed by nucleate boiling and convective evaporation contributions. The nucleate boiling contribution was obtained from Foster-Zuber (1974) pool boiling correlation and was considered to be suppressed with suppression factor S . The suppression factor was defined as the ratio of mean superheat to the wall superheat temperature. The convective evaporation was calculated by Dittus-Boelter (1930) equation for single-phase liquid turbulent convection inside tube. The convective

contribution was corrected by factor F , a convection multiplier as a function of Martinelli parameter.

Another model which has been applied for conventional channels is asymptotic model of nucleate boiling heat transfer (h_{NcB}) and convective heat transfer (h_c) contribution in the form of:

$$h_{TP} = \left[(h_{NcB})^n + (h_c)^n \right]^{1/n} \quad 2-11$$

The value of n was defined as 2 by (Kutateladze, 1961) using power law method, while Steiner and Taborek (1992) used $n=3$. On one of the method presented in Collier and Thome (1994), Gnielinski (1976) correlation was used to obtain h_c and (Gorenflo, 1993) type of relationship for h_{NcB} .

Kandlikar (1990) proposed set of empirical correlations for heat transfer prediction inside horizontal and vertical tubes from extensive database of 24 experimental investigations. The model utilized non-dimensional convection and boiling number and introduced a fluid-dependent parameter F_{fl} . For the application in mini and microchannel, the correlations were modified in Kandlikar and Steinke (2003) considering laminar flow occurred in small diameter channels due to the small hydraulic diameter and low mass flux commonly employed in microchannels applications. The all-liquid flow Nusselt number used in their correlation was given by:

$$Nu_{lo} = \frac{h_{lo} \cdot D_h}{k_l} = C \quad 2-12$$

where C is dependent on the channel geometry and the wall thermal boundary condition, for example, for circular channel under constant heat flux and constant temperature boundary condition, the value of C were defined as 4.36 and 3.66 respectively.

Kattan (1998) proposed a flow pattern-based heat transfer prediction model for horizontal tubes as follows:

$$h_{TP} = \frac{\theta_{dry} \cdot h_v + (2\pi - \theta_{dry}) h_{wet}}{2\pi} \quad 2-13$$

According to them, flow boiling (h_{wet}) occurs on the wetted tube wall perimeter and vapor-phase forced convection (h_v) occurs on the dry tube wall perimeter represented by dry angle θ_{dry} . The flow boiling heat transfer can take the form of asymptotic model explained earlier and the convective evaporation component is obtained from film flow model and local void fraction of Steiner model. The model was further developed by L Wojtan (2005) by modifying the expression for the dry angle and extending the model for dryout and mist flow regimes.

The models explained above consider the nucleate boiling heat transfer mechanism takes important role in flow boiling heat transfer and suggest this mechanism become more and more important as the channel's diameter decreases as for the case of microchannels. A different view on what mechanism governs the flow boiling heat transfer inside microchannels was proposed by Jacobi and Thome (2002). They suggested that the

transient thin film evaporation in the elongated bubble mode governs the heat transfer in microchannels, instead of nucleate boiling mechanism noted earlier.

Their model was further developed in Thome *et al.* (2004) with three-zone flow boiling model, namely liquid slug, evaporating elongated bubble and vapor slug. The heat transfer mechanism includes liquid convection, vapor convection at the presence of dry zone and thin film evaporation as the main contributions. The model distinct approach considers the transient variation in the local heat transfer coefficient during sequential and cyclic passage, in opposite of the all-regime empirical models. Ribatski *et al.* (2006) made comparison of extensive experimental data from 17 different studies of which most of them were performed in the test section with hydraulic diameter between 200 μm to 3 mm. Their results reported the three-zone model as the most accurate models, although with 50% of mean absolute error and only predicted 45% of the data within $\pm 30\%$ error band. So far the model only covers heat transfer coefficient prediction in the elongated bubble regimes (slug flow) in circular channels; hence further research are needed to extent for other flow regimes and channels geometries to develop a comprehensive phenomenology-based heat transfer coefficient prediction model.

Different trends of local heat transfer coefficient versus vapor quality and the effects of mass flux and heat flux in flow boiling inside microchannels have been reported until date. Analysis by Agostini and Thome (2005) on 13 studies concluded that at low to medium vapor qualities, the heat transfer coefficient increase with the heat flux and decrease or relatively constant with respect to vapor quality. At the higher vapor quality, the heat transfer coefficient decreases sharply with vapor quality and independence on heat flux or mass flux. From the literatures studied, there are always positive effects of

heat flux to the heat transfer coefficient, except at high vapor quality, while the mass flux effect varies from no effect, an increasing effect or a decreasing effect.

One of the drawbacks in flow boiling inside microchannels is its higher pressure drop due to friction increase compared to larger diameter channels. It is essential to develop two-phase pressure drop models since the pressure drop, together with void fraction, are the most important aspects of two-phase flow. In addition, the model is the basic element for the design of microchannels heat exchanger devices. Collier and Thome (1994) described two main approaches to model frictional pressure drop in two-phase flow inside tubes, namely homogenous model and separated-flow model. The homogenous model has been used in various forms in the steam generation, petroleum and refrigeration industries for a considerable time. The model considers the two-phase flow as a single phase possessing mean fluid properties. The two-phase mean viscosity used to determine two-phase frictional factor can be obtained from one of the correlations by McAdams (1954), A. Cicchitti (1960) or Dukler (1964).

The separated flow model considers the phases to be artificially segregated into liquid and vapor stream. The simplest approach for this model suggests each stream flows at a mean velocity. Lockhart-Martinelli (1949) developed separated-flow model which proposed an empirical approach to determine the two-phase frictional multipliers Φ^2 as a function of parameter X, where,

$$X^2 = \frac{\left(\frac{dp}{dz} F\right)_l}{\left(\frac{dp}{dz} F\right)_v} \quad 2-14$$

$$\phi^2 = 1 + \frac{C}{X} + \frac{1}{X^2} \quad 2-15$$

The value of C is a constant which depends on flow characteristic of each phase. For the two-phase flow in microchannels, the value of C would be 5 because liquid and gas flows are in laminar conditions. Mishima and Hibiki (1996), using data of air-water two-phase flow inside circular and rectangular channels with hydraulic diameter range of 1-4mm, have proposed a correlation for C:

$$C = 2 \left(1 - e^{-0.319D_h} \right) \quad 2-16$$

Kawahara *et al.* (2002) suggested the value of C=0.24 for their two-phase flow of de-ionized water and nitrogen inside a 100µm diameter microchannel.

Pressure drop in multi-microchannels showed fluctuations due to flow instabilities in the upstream section as addressed in Bergles and Kandlikar (2005). These instabilities may results in flow reversals (vapor back flow) which significantly affect the local pressure drop. The instabilities were classified into upstream compressible volume instability and excursive instability. The former instability is an oscillating flow which may lead to CHF, occurred when there is a significant compressible volume at the upstream of the heated test section. In two-phase flow inside microchannels the compressible volume may be caused by an entrained bubble, flexible hose or large volume of removed gases from liquid flow. The excursive instability, also called fundamental static instability, occurred in flow boiling inside microchannels due to unique pressure drop characteristics

of boiling channels. Both instabilities can be reduced by utilizing throttle valve prior to the test sections even though this would require higher pressure drop and fabrication considerations.

Recently, Ribatski *et al.* (2006) compared 12 well-known frictional pressure drop models of various channel diameters with experimental data from 9 different authors of which including data from mini and microchannels experiments. According to them, model proposed by Müller-Steinhagen and Heck (1986), which were developed for conventional channels, showed the best results with 53.1% data were predicted and mean absolute deviation of 31.3%. The second best results were shown by homogenous model which utilizing two-phase viscosity suggested by A. Cicchitti (1960) together with the model proposed by Mishima and Hibiki (1996). They also found that for vapor qualities higher than 0.6, all models showed poor prediction results. Their analyses indicated that the existing models cannot predict the pressure drop characteristic in flow boiling microchannels with reliable results. Furthermore, the models failed to capture the effects of flow patterns transitions in microchannels on the pressure drop results.

2.4 Oil Retention Models

This section summarizes previous strategy to model oil retention in heat exchangers and the limitations with respect to microchannel heat exchanger. One of the remarkable work on modeling heat exchangers was presented by Jiang (2003). The author used a segment-by-segment approach within each tube. This made the model able to account for two-dimensional non-uniformity of air distribution across the exchanger, to address the significant change of properties and heat transfer coefficients. It was able to consider the

two-phase regime and heterogeneous refrigerant flow patterns through a tube too. The effectiveness-NTU method for cross-flow configuration was also used for combined heat and mass transfer problems under dehumidification, by defining equivalent thermal resistance and heat capacity. So the air-to-refrigerant heat transfer and the refrigerant pressure drop are calculated for each individual segment. On the refrigerant side, each segment is provided with an inlet enthalpy, an inlet pressure, and a mass flow rate. The predicted conditions at the outlet of the segment are passed as input for the adjacent section until the entire refrigerant circuitry was completed. On the air side, the inlet air temperature was provided for each segment.

The work by Schwentker (2005) improved the previous model including the effects of the oil on heat exchangers and the development of a specific model for plate tube heat exchangers. He included correlations developed specifically for refrigerant-oil mixtures to calculate heat transfer coefficients and pressure drop, and he calculated oil retention in heat exchangers with the use of correlations for the void fraction.

A phenomenological model for oil retention in fin-and-tube heat exchangers was developed in Cremaschi (2004). The oil retention was predicted within the refrigerant circuitry of suction line, the fin-and-tube evaporators, and condensers for refrigerants R22, R410A and R134a and lubricant mineral oil, polyolester and polyalkyl glycol pairs. Their results indicated that the oil retention was at the highest at suction line due to high liquid film viscosity of refrigerant-oil mixture and low inertia force of the refrigerant vapor. The authors also suggested that the higher mass flux and smaller diameter reduce the amount of oil retention. The lubricant property, i.e. higher viscosity found to increase

oil retention. Finally, the solubility and miscibility of the pairs also found to has effect on the oil retention.

Cremaschi (2005) and Radermacher *et al.* (2006) compared void fraction correlations of Lockhart-Martinelli, (1949), CISE-Premoli *et al.* (1971), Chisholm (1972) and Turner and Wallis (1965) to be used in his oil retention model. Although all aforementioned correlations were developed for pure fluid, the authors include refrigerant-oil mixture property, i.e. viscosity and surface tension to account for the influence of the oil. The authors indicated that CISE correlation gives the best prediction of oil retention. The authors also introduced mixture property corrections to account for refrigerant-oil pair miscibility. Their model for evaporator and condenser were verified within 21 and 23% relative errors, respectively. Similar method was applied by Choi *et al.* (2009) in their numerical model of oil retention in heat exchangers. Both results are able to predict the trends of the oil mass fraction effect to oil retention. Lee (2003) conducted oil retention modeling and experiments of carbon dioxide air conditioning system. His model was able to predict oil retention in the suction line, evaporator and condenser within $\pm 20\%$ of its experimental data. Void fraction correlation from Hughmark (1962) and Premoli *et al.* (1971) were found to give the best prediction. For application in microchannel heat exchangers, void fraction correlation suggested by Kawaharat *et al.* (2002) seems to be a promising candidate, given that the liquid property should be corrected to account for oil influence.

$$\alpha = \frac{0.03\beta^{0.5}}{1 - 0.97\beta^{0.5}} \quad 2-17$$

Where

$$\beta = j_G / (j_G + j_L) \quad 2-18$$

Diaz et al. (2011) proposed mathematical model for R134a-ester oil inside 3.22 mm diameter tube which consider three flow regimes along the tube, namely single phase liquid, bubbly and foam flow regions. A void fraction based on homogenous flow was used for bubbly flow. The authors divided foam flow region into foam deformation and plug flow regions and assumed slip velocity to calculate mixture mass flow rate. Their model for mass flow rate of the refrigerant-oil mixture was verified using experimental data from Castro et al. (2009) with maximum error of 21%.

Works on the oil effects on refrigerant distribution in microchannel heat exchanger were recently reported by Li and Hrnjak (2013) with the focus on evaporator. The authors proposed a model for the refrigerant distribution, which was affected by the oil in circulation through the evaporator. The refrigerant distributions were reported to be worse as the oil mass fraction increased up to 3%. However more uniform distribution were observed at higher oil mass fraction. Further studies by the same authors include model and experiments for oil retention in automotive air conditioning system that had a microchannel condenser (Jin and Hrnjak, 2013;2014). The model, which used a thermodynamic approach originally proposed by Thome (1995), was able to predict the oil retention in microchannel condenser within 15% of error with respect to the

measurements. The authors suggested that the lubricant was separated from the flow in the condenser header and started to accumulate in the bottom of the channels.

2.5 Oil Retention Experimental Methodology

A brief summary of available literatures on experimental methodology to measure oil retention in heat exchangers is presented next. In order to determine the oil retention volume, one option might be to measure the thickness of the oil film created during annular flow on the interior wall of the refrigerant tubes. Shedd and Newell (1998) proposed a non-intrusive, automated, optical film thickness measurement technique to be used with a wide range of fluids and flow configurations. Later, Bai and Newell (2002), Shedd and Newell (2004) and Schubring et al. (2009) used a similar approach to describe the characteristics of annular two-phase viscous flow of air and water or air and 300 SUS Alkybenzene oil. Extensive experimental flow visualization in horizontal and vertical pipes was required and the oil film thicknesses were correlated with the oil mass flow rates, vapor velocity and pipe diameter. Shear stress correlations were developed and verified with the experimental data. Unfortunately this technique requires optical access to the refrigerant flow and it might not be feasible for the small tubes in microchannel heat exchangers. The flow regime during refrigerant condensation in the actual air conditioning applications of the microchannel heat exchanger is mostly annular and the oil film thickness is generally not uniform along the heat exchanger refrigerant path. Oil retention is affected by the flow pattern of the refrigerant-oil mixture because the magnitude of the forces exerted on the fluid element depends on the type of motion of the

fluid, relative interfacial surface area between the two phases, and velocity slip ratio between gas and liquid phases.

Crevaschi et al. (2005) measured the oil retention in fin-and-tube heat exchangers of air conditioning and refrigeration systems. In the study, oil retention was measured for both evaporators and condensers at different refrigerant mass flow. An increase of OMF promoted a drastic change of oil mass accumulated in the heat exchangers. The authors reported that an increased OMF up to 5 wt%, the mass of oil held up in the evaporator and suction line was about 25% of the total mass of oil initially charged into the compressor for R410A/POE case. The corresponding scenario for R134a/POE was 15% of the oil initially charged into the compressor was held up in the evaporator and suction line and an additional 15% was retained in the condenser. Clearly the oil retention was depended on the OMF, which should be chosen as one of the control variables during the measurement of oil retention for the oil retention research.

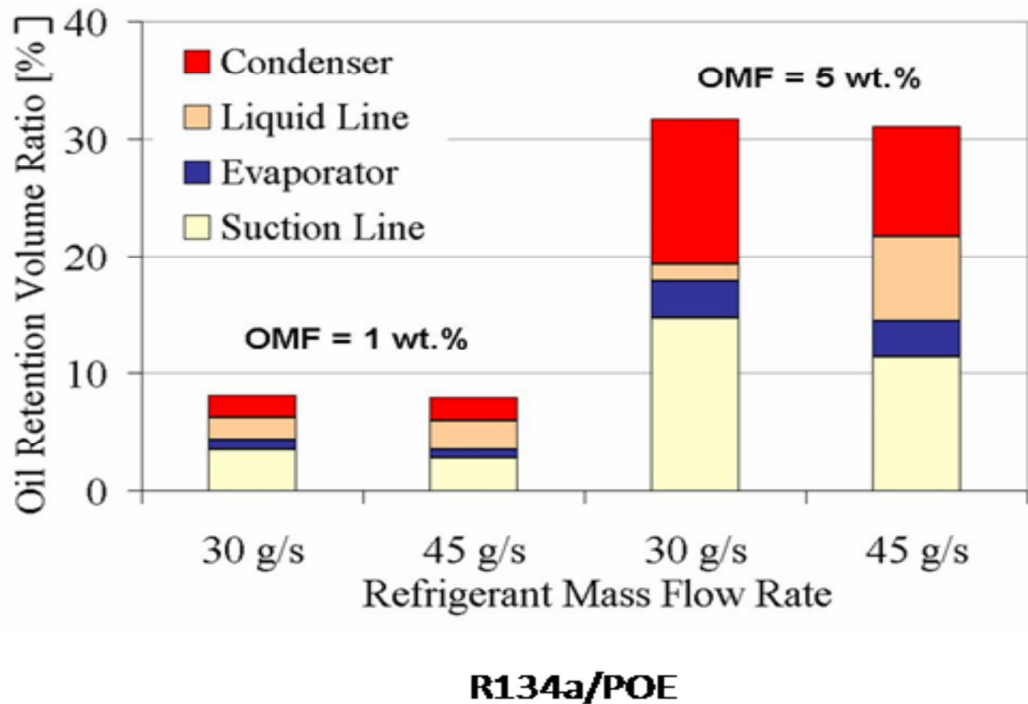


Figure 2.1: Example of oil retention volume, expressed in percentage of oil volume charged inside the compressor, in components of an R134a/POE refrigeration system (reprinted, by permission, from Cremaschi (2004))

Figure 2.1 presents the oil retention in each component as a percentage of the total oil volume initially charged into the compressor from Cremaschi (2004). One could observe that OMF and refrigerant flow rate are still the controlling variables for oil retention. There is an additional interesting fact that could be learned from the data provided in the figure. While the system experienced a large amount of oil retention in the suction line, a certain amount of oil retention was also found in the condenser. Overall the fin-and-tube evaporator had a small amount of oil retention, that is, only a few percentages with respect to the oil volume charged into the compressor. Since the proposed research focuses on microchannel heat exchangers used as condensers and evaporators,

Figure 2.1 provides order of magnitude estimation for the maximum amount of oil retention that we would expect in microchannel heat exchangers. The proposed test apparatus should be able to measure to this level of accuracy to satisfy the objectives of the research. Considering that microchannel heat exchangers have between 30 to 50% lesser internal volume than fin-and-tube heat exchangers with similar heat exchange capacity, the bars in the above figure clearly indicate that weighing the entire coil to detect the presence of oil is not a viable option for microchannel heat exchangers. If we consider this approach for a moment we can quickly conclude that we will end up with the technical challenge of measuring few grams of oil residual inside a coil that might weigh several kilograms. Both uncertainty of the weight measurements as well as repeatability of the oil retention measurements will be significantly compromised due to (i) the fact that the heat exchanger must be physically disassembled from the rest of the system before it can be weighted, (ii) refrigerant must be recovered from the heat exchanger before the weight measurements could take place and during the refrigerant recovery phase some unknown amount of oil might be carried out from the heat exchanger and migrate with the refrigerant; (iii) the accuracy and hysteresis of HVAC&R laboratory scales might be simply too high to meet the requirements. For these reasons measuring the oil retention using the difference of the weights between the dry coil and the coil with residual oil in it was considered an incompatible approach with the objectives.

CHAPTER III

3 Experimental methodology

3.1 Introduction

The oil retention experiments were conducted using pump-boiler type closed loop refrigeration system in which the refrigerant was circulated by using a gear pump. Oil was injected in the refrigeration loop by using a variable frequency drive (VFD)-controlled gear pump and the oil was injected at two locations, namely the inlet and the outlet of the microchannel heat exchanger (referred to as test section in this dissertation). To calculate the oil retention in the microchannel heat exchanger, the oil injection flow rate injected at the inlet and outlet of the test section and the time that the oil was observed in the sight glass installed downstream the microchannel heat exchanger for each injection were measured. The amount of oil retention in each test was calculated from numerical integration of the oil injection flow rate over the corresponding time. The amount of the oil retention at the microchannel heat exchanger was obtained from the difference between oil retained during oil injection at the inlet and the outlet of the microchannel heat exchanger. Preliminary tests of both oil separators were performed to determine the amount of oil-bypassing the oil separators by using the refrigerant sampling method specified by the ASHRAE Standard 41.4 (1996).

During the period for the oil injection at the inlet of the test section, the heat transfer capacity and the refrigerant-side pressure drop of the microchannel heat exchanger were measured. The heat transfer capacity was experimentally measured from the air side of the heat exchanger. Calibration tests were performed for the same system running with only refrigerant at the same flow rates and saturation pressure at the inlet of the microchannel. The results were then used as baseline data of heat transfer capacity and pressure drop of the test section when no oil was present in the system, i.e., in oil free conditions. The heat transfer rate and pressure drop during the tests with oil were then compared to that of the corresponding baseline data. Because the baseline data in oil free conditions and the experimental data with oil shared same total mixture flow rate, i.e. the refrigerant flow rate for the baseline data was equal to the mixture (refrigerant plus oil) flow rate for the experiments with oil. Same saturation pressure, same inlet refrigerant temperature, and same air side inlet temperature and velocity were maintained between the experiments with oil and the reference baseline tests without oil. The results of the comparison provided heat transfer factors and pressure drop factors that isolated the effect of oil on the heat transfer rate and pressure drop of the microchannel heat exchanger.

3.2 Microchannel Heat Exchangers

The study used two different louvered-fin aluminum microchannel heat exchangers; one type for the condenser and one type for the evaporator. All heat exchangers were commercially available and they were used in commercially available heat pump systems. The following section describes the heat exchangers and how they were installed in the air tunnel of the experimental test apparatus.

3.2.1 Microchannel Condenser That Was Tested in the Research

The test section in the condenser tests was a 2-pass, 1.2 x 0.9 m (48 x 36 inch) aluminum louvered-fin type heat exchanger. A schematic figure is given in Figure 3.1. Each microchannel tube had four rectangular ports with a hydraulic diameter of 0.07 inch (1.7 mm). The manufacturer data of the heat exchanger were not available, and the measurements were conducted at OSU research laboratory and they were summarized in Table 3-1. The internal volume of the condenser was about 2,436 cm³ (that is, 2.4 liters or 149 inch³) and it was calculated based on the outside envelope dimensions and an estimated wall thickness for the headers. The microchannel tube internal volume was calculated by measuring the port internal diameter and the number of ports in each microchannel tube. These measurements were taken from two tubes at the top and bottom of the condenser, which served to hold the fins but were open, that is, not connected to the inlet and outlet vertical headers. We assumed that the internal geometry of these two tubes was representative of the internal geometry for all microchannel tubes of the condenser. This assumption was reasonable because (i) typically the same type of tubes are brazed altogether with the fins during a stage of the manufacturing process of a microchannel condenser and (ii) the tubes visually appeared to be of the same type, same dimensions, and of the same material.

The two passes sections of the heat exchanger were determined by using infrared camera picture of the inlet header during preliminary tests. As expected for a condenser, the first pass had higher number of tubes than the second pass due to the presence of vapor phase at the beginning of condensation. With reference to Figure 3.1, the numbers of tubes on each pass were 69 for the condenser section at the top and 32 for the subcooler section at

the bottom. The manufacturer did not provide the internal dimensions of the microchannel heat exchanger used in the test section. The dimensions were estimated for analyzing the geometry effects and for modeling. The exact position of the partition inside the header was not known but it was found by using an infrared image of the header, as depicted in Figure 3.2. The superheated temperature of the refrigerant vapor in the first pass can be easily differentiated at the partition from the saturated temperature of the two-phase refrigerant at the outlet of the second pass.

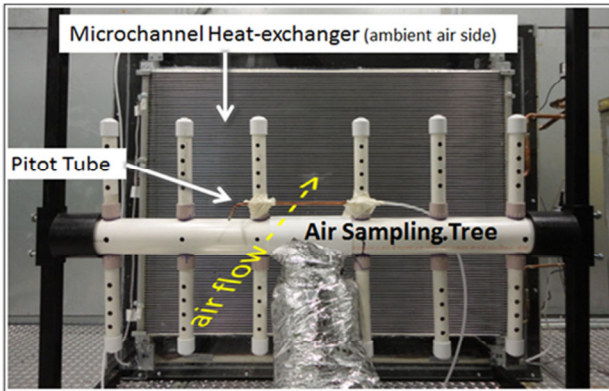


Figure 3.1: Schematic of the microchannel condenser tested in the research

Table 3-1 Dimensions of the microchannel condenser that was tested in the present study

Description	Measurement*
Coil length (L)	48 in. (1.22 m)
Coil height (H)	35.7 in. (0.90 m)
Number of tubes in the first pass	69
Number of tubes in the second pass	32
Tube and Fin Material	Aluminum
Fin Type	Louvered
Number of refrigerant passes	Two (condenser top & subcooler bottom)
Outer diameter of each header	1.18 in. (30 mm)
Total height of each header	35 in. (0.89 m)
Height of the condenser inlet header, H_c	~23.8 in (0.605 m)
Height of the subcooler outlet header, H_s	~11.2 in (0.285 m)
Distance of the inlet copper tube from the bottom of the coil	21.25 in. (0.54 m)
Outer diameter of the inlet copper tube.	5/8 in. (15.88 mm)
Distance of the outlet copper tube and the bottom of the coil	1.5 in. (38.1 mm)
Outer diameter of the outlet copper tube	3/8 in. (9.53 mm)
Number of ports (microchannels) in each tube	4
Hydraulic diameter of each port in the tube	~0.067 in. (1.7 mm)
Aspect ratio of each port in the tube (width/height)	6.125
Tube depth in the direction of air flow, t_d	1. in (25.5 mm)
Microchannel tube spacing, space between adjacent tubes, t_s	0.291 in. (7.4 mm)
Microchannel tube thickness, t_t	0.055 in. (1.4 mm)
Fin density or pitch	~18 fin per inch
Fin spacing, free space between adjacent fins	~0.05 in. (1.4 mm)
Fin thickness	~0.002 in. (0.07 mm)
number of louvers on the fin	18
Louver length	~0.252 in. (6.4 mm)
louver height from the fin plane	~0.008 in. (0.2 mm)
Louver pitch	0.889 louvers per mm
Louver angle measured from fin plane	~30°
Total internal volume of the condenser	2,436 cm ³ (149 inch ³)

*Note: The dimensions of the microchannel heat exchanger sample were not provided by the manufacturer. The dimensions were estimated by conducting a limited number of measurements on the sample at Oklahoma State University Research Laboratory.



Actual photo of the front side of the microchannel condenser installed inside OSU psychrometric chamber

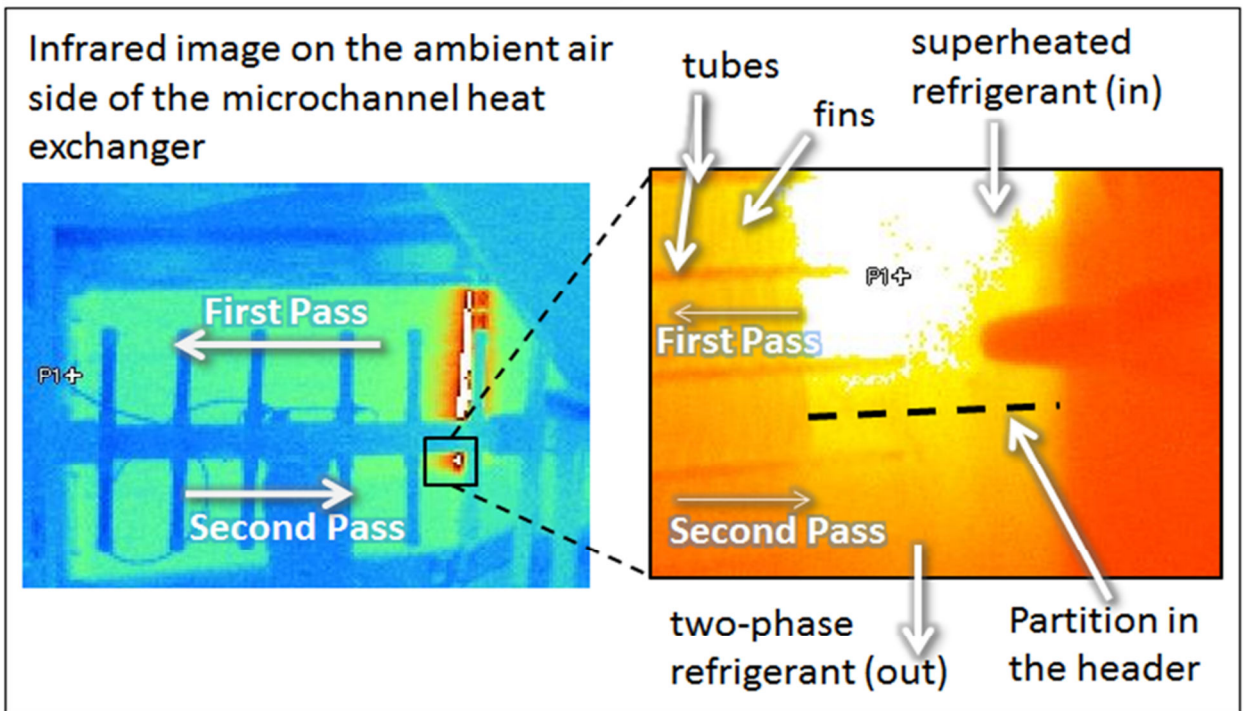


Figure 3.2: Use of an infrared image to locate the partition inside the header of the microchannel condenser (Deokar, 2013)

3.2.2 Microchannel Evaporator That Was Tested in the Present Study

A louvered-fin aluminum microchannel heat exchanger was experimentally tested as evaporator and it is referred throughout this paper to as evaporator A. Evaporator A was a single pass heat exchanger as shown schematically in Figure 3.3. The evaporator was installed in a cross flow configuration relative to the air flow direction. The dimensions of the evaporator are given in Table 3-2.

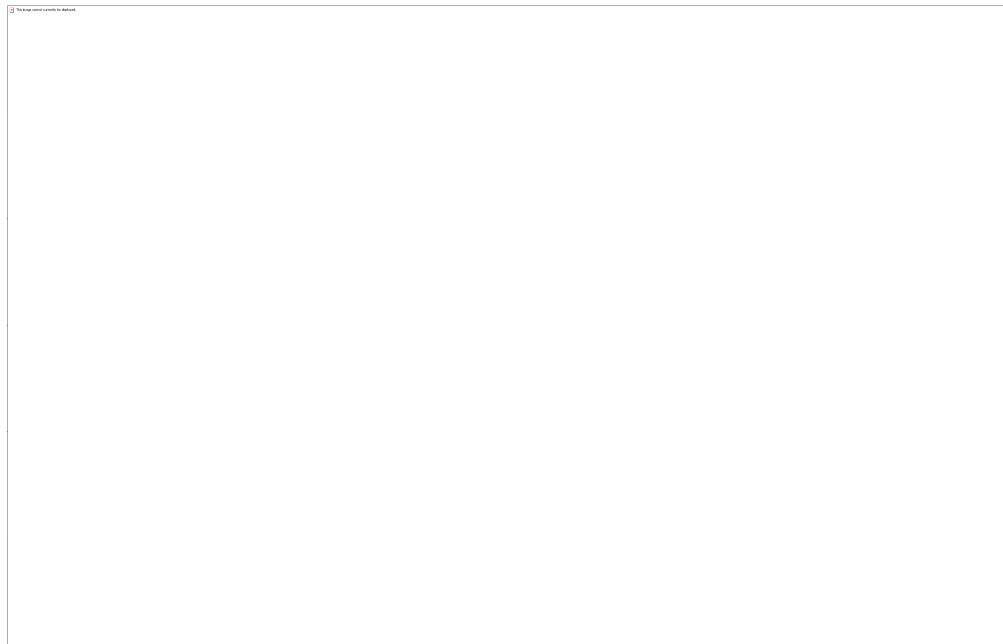


Figure 3.3: Microchannel evaporator A: (top) actual picture of the first heat exchanger, A, tested in the present study and (bottom) schematic of the heat exchanger A with refrigerant flow direction during the evaporator tests

Table 3-2 Dimensions of the Microchannel Heat Exchanger-Evaporator That Was Tested in the Present Study

Parameter	Evaporator A*
Material	Aluminium
Fin type	Louvered
Number of tube	98
Height (H)	0.438 m (17.2 in)
Width (W)	0.884 m (34.8 in)
Number of slab / passes	1
Sectional cross flow area of one entire tube (A_{flow})	12.6 mm ² (0.020 in ²)
Wetted perimeter in one entire tube (P_{wet})	50.72 mm (2.00 in)
Hydraulic diameter of one entire tube (D_h)	1.4 mm(0.055 in)
Microchannel tube height	1.4 mm (0.055 in)
Microchannel tube depth, in the direction of air flow, or depth of one microchannel heat exchanger slab	25.4 mm (1.00 in)
Microchannel tube spacing, space between adjacent tubes	7.44 mm (0.29)
Microchannel tube thickness	0.35 mm (0.014 in)
Fin Pitch	0.79 fin/mm (20 fpi)
Fin Height	7.44 mm (0.29 in)
Fin Type	Louvered
number of louvers on the fin	16
Louver length	6 mm (0.236 in)
louver height from the fin plane	0.2 mm (0.008 in)
Louver pitch	0.89 n.louv./mm (22.6 n.louv./in)
Louver angle measured from fin plane	30 deg.

Inlet header diameter (measured as envelope diameter)	31.75 mm (1.25 in)
Outlet header diameter (measured as envelope diameter)	31.75 mm (1.25 in)
Total internal volume of the heat exchanger	1,890 cm ³ (115 in ³)

*Note: The dimensions of the microchannel heat exchanger sample were not provided by the manufacturers. The dimensions were estimated by conducting a limited number of measurements on the sample at Oklahoma State University Research Laboratory.

#the sectional cross flow area, A_{flow} , and the wetted perimeter, P_{wet} , for one entire tube were provided by the manufacturer of this microchannel heat exchanger. The hydraulic diameters for microchannel evaporators were calculated as $D_h = 4 A_{\text{flow}}/P_{\text{wet}}$.

3.3 Experimental Setup

The microchannel heat exchangers were installed inside a thermally controlled enclosure and the inlet air psychrometric conditions were regulated by the large-scale climate control psychrometric chamber (Cremaschi and Lee, 2008). Pressure transducers and inline thermocouples were installed to monitor the refrigerant conditions along the test section and a dedicated differential pressure transducer was used to measure the refrigerant side pressure drop. The heat transfer capacities of the microchannel heat exchangers were measured from the air side heat transfer and the air flow rate measured and calculated according to ANSI/ASHRAE 41.2 Standard (1987). Heat balance tests were conducted when the refrigerant outlet was in subcooled condition for the condenser tests and in superheated vapor conditions for the evaporator tests. The error of heat transfer capacities measured from the refrigerant side and the air side were within $\pm 5\%$.

3.3.1 Psychrometric chamber used to control the inlet air streams

For the present study a large-scale psychrometric chamber (shown in Figure 3.4) was used to control the temperature, humidity, and velocity of the air entering the microchannel heat exchangers during the oil retention experiments. The psychrometric facility consisted of two adjacent air conditioned rooms that were controlled over a wide range of psychrometric conditions with and without a live thermal load in it; one room artificially reproduced the outdoor climate conditions and it was used for the present study.

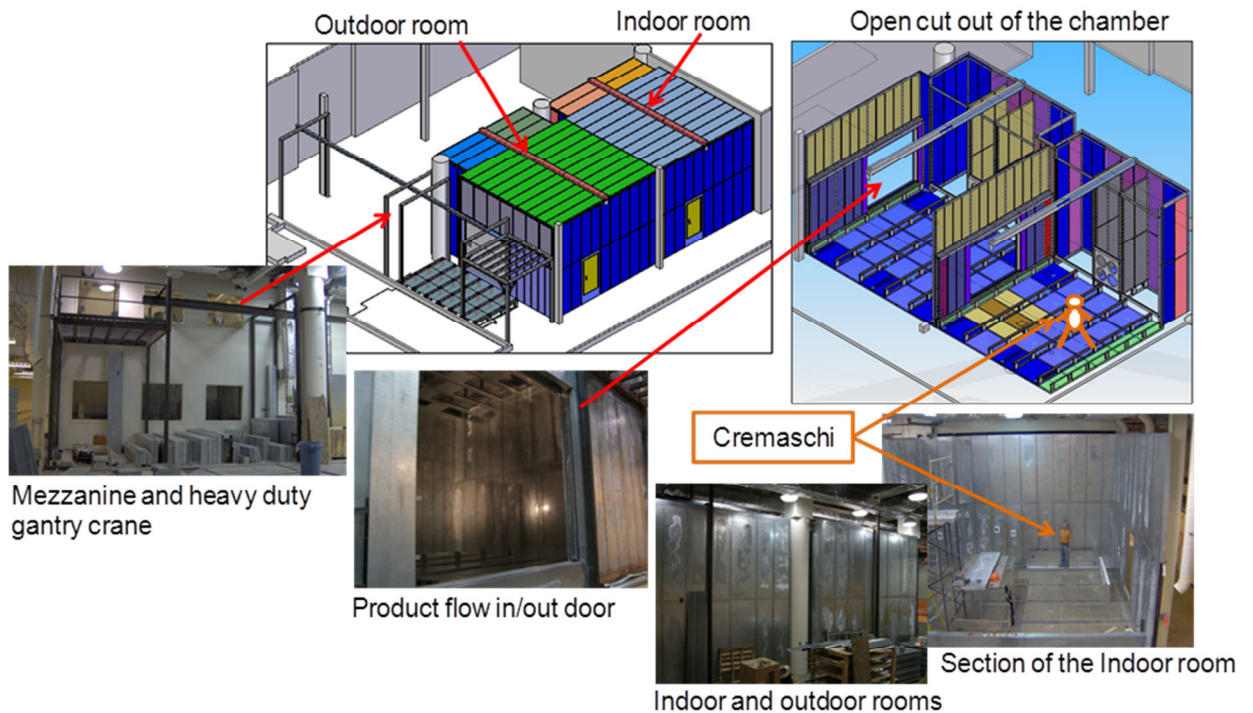


Figure 3.4: Psychrometric chamber at Oklahoma State University (Deokar, 2013)

The climate control psychrometric chamber, was fairly large with sufficient space to accommodate the microchannel heat exchangers for air conditioning, coolers, or refrigeration systems. The temperature range of the room was from 10°F to 130°F (-12°

to 54°C), and the relative humidity range was from 10% up to 95% R.H. In the chamber, air was first conditioned to the desired psychrometric states and then circulated in the rooms through an under-floor plenum displacement ventilation system. Our previous findings confirmed uniform temperature and velocity in the room, which had dimensions of about 20 ft by 21 ft floor area and 16 ft ceiling height (6 m x 6.4m floor area and 5 m ceiling height). More details about the facility design, construction, and specifications can be found in Cremaschi and Lee (2008).

The chamber was fully operational with a total of 256 thermocouples, 32 high accuracy RTDs, and 96 analog inputs (voltage and/or current). All sensors were sampled at a rate of 2 seconds and the data were processed in real time. To maintain the facility at the desired set points, adjustments were made automatically by using 192 analog outputs that controlled different electric motors, heaters, variable frequency drives, mixing valves, and pumps.

The psychrometric chamber allowed controlling the air flow conditions independently from the refrigeration side conditions. The refrigeration system serving the test section was build outside the chamber, in a large indoor high bay area of a basement of an air conditioned building. The temperature of the high bay area was fairly constant throughout the year thus the errors due to electrical noise from the sensor output signals and due to temperature variations of the electronics was minimized. Two refrigerant pipelines connected the test set up with the microchannel heat exchangers inside the chamber, as shown in Figure 3.5, and more in detail in Figure 3.8 for the condenser tests and in Figure 3.11 for the evaporator tests.

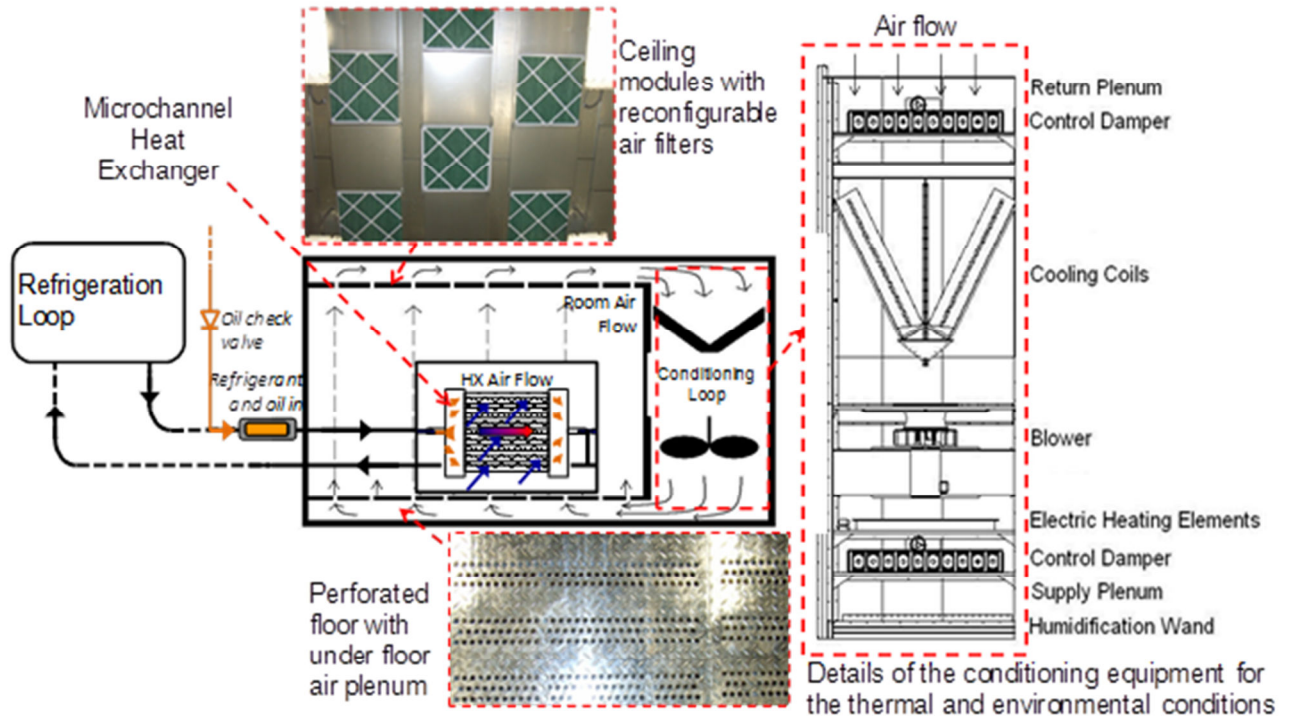


Figure 3.5: Layout of the oil retention test set up in the large scale psychrometric chamber (Deokar, 2013)

The psychrometric room was designed so that a slow motion of the air was produced with air ascending in the room from a perforated floor. The displacement ventilation system of the chamber consisted of a conditioning loop, an under floor air plenum supply, and a set of adjustable ceiling filters. Air was circulated through the conditioning loop first by using variable speed fans. The air flow rate was adjusted with the fans and a set of electro-mechanical dampers were used to adjust the supply air to the room. With reference to Figure 3.5 the first process the air goes through once inside the conditioning loop was cooling and dehumidification through water-to-air cooling coils. The coils' surface temperature and capacity was controlled by a variable speed pump, electronic mixing valves and bypass valves. After being cooled and dehumidified, the air stream

was guided to a series of electric resistance heating coils, which raised the air temperature up to the required ambient room temperature for the tests. The electric resistance heaters allowed for temperature control and an immediate response time.

3.3.2 Oil Retention Measurements in the Microchannel Condenser

Initially a test apparatus was designed and constructed based on a vapor compression cycle, that is, with a compressor. However, it was changed later to a pump-boiler cycle by replacing the compressor with a gear pump and by adopting a low temperature chiller to liquefying the refrigerant before entering the pump. The pump-boiler test apparatus provided greater flexibility to control the mass flux, pressure, and degree of superheat at the inlet of the condenser or at the outlet of the evaporators when oil was introduced in the microchannel heat exchangers. This high degree of control of the refrigerant side operating parameters during the experiments was key in order to identify and isolate the effects of oil retention on the heat transfer rate and refrigerant side pressure drop. In other words, the pump allowed to conduct initial tests without oil and to conduct tests with oil at the same total mass flux, saturation pressure, and degree of superheat. Even small variations of these three parameters could potentially skew the experimental results and need to be accounted for eliminating potential systematic errors during the data reduction and analysis. In addition, the oil management with the vapor compression based test set up was very difficult to achieve because the balance of oil between the heat exchangers and the compressor was depended on pressure differentials. Controlling mass flux, saturation pressure, and degree of superheat while simultaneously adjusting for the pressure differentials in the test apparatus was not feasible in our laboratory. In time, the oil introduced in the heat exchangers during the experiments tended to gradually and

slowly accumulate in the compressor and during shutoff and startup periods the compressor either was flooded with oil or run dry for several minutes. Both scenarios led to compressor mechanical failure. The pump boiler test set up eliminated this issue and a gear pump was able to manage the oil and control the refrigerant side operating parameters at the same time of the actual heat transfer experiments. However, it should be emphasized in here that the pump boiler test set up required additional auxiliary equipment to cover the range of testing conditions of the present study. This equipment will be described later in the manuscript. While an in depth description of the original vapor compressor based test set up is out of the scope of the present study, a brief summary about its limitations and weakness is reported next to document the lessons learned during the first part of this research.

3.3.2.1 Brief description of the initial vapor compression based test apparatus

In the initial vapor compression based test apparatus there were two main circuits within which the oil circulated. A detailed description of the system was discussed in Deokar (2013). The first circuit for the oil flow consisted of the test section, which consisted of the port for oil injection, the microchannel heat exchanger, the expansion valve, the evaporator, and oil separators of the oil extraction device. Oil was released to this circuit at the injection port and extracted from this circuit at the extraction device. The second loop for the oil flow consisted of a compressor, a discharge oil separator (oil separator no. 2 in Figure 3.6), and the oil return line to the compressor suction. The schematic of the initial (compressor-based) test facility is shown in Figure 3.6. A scroll type compressor is component (1). An auxiliary condenser (3) was placed in parallel with the test section, that is, with the microchannel heat exchanger. The metering valves (9-a) and (9-b)

enabled different mass flow rates through the microchannel heat exchanger by redirecting some flow through the auxiliary condenser. The pressure transducers and inline thermocouples monitored the refrigerant conditions, and a differential pressure transducer measured the pressure drop across the microchannel heat exchanger during the oil retention tests. The liquid refrigerant from both condensers then expanded in one expansion valve (component (8)) before going to the evaporator (component no. (7)). The refrigerant oil separator (2) was used at the discharge of the compressor to prevent the entrained oil droplets in the refrigerant from leaving the compressor and flowing to the test section. A metered amount of oil was either injected upstream (port-A) or downstream (port-B) of the microchannel heat exchanger using appropriate valves (10-a) and (10-b). The oil extraction device was used to separate the oil from the vapor refrigerant and for measuring the oil volume. The device used an oil tank with vertical sight glass and two custom made helical and coalescent oil separators in which the oil floating valves were removed. The volume of oil extracted by the oil extraction device into the tank was then measured using the graded sight glass tube and, initially for redundancy, an electric oil level capacitance probe sensor.

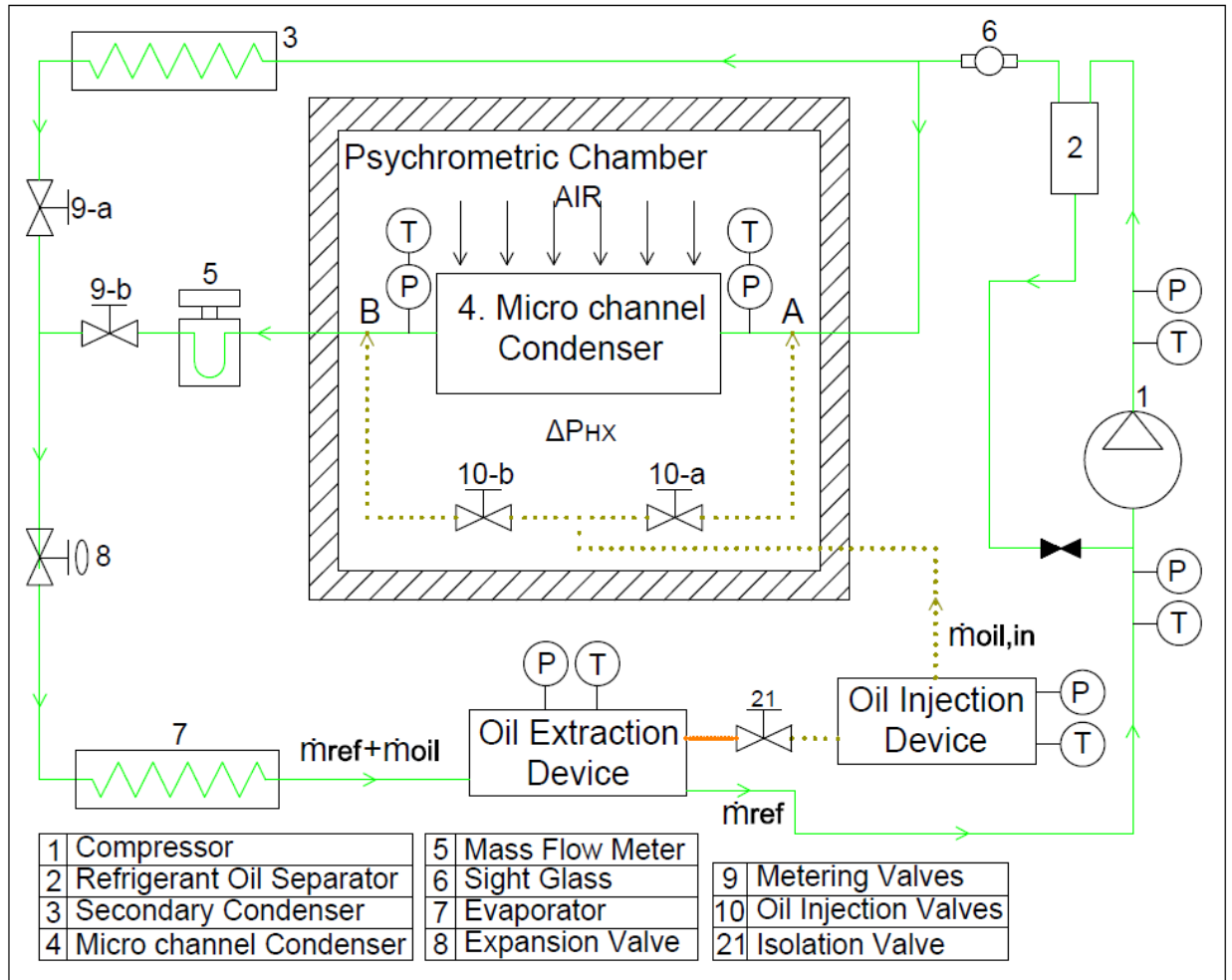


Figure 3.6: Schematic of the initial compressor based test facility designed and constructed for the research – later it was modified and upgraded to a pump boiler based test facility (Deokar, 2013)

The oil was metered to the test section through the injection port from the oil reservoir and by using an oil injection gear pump. Some of the oil was retained in the microchannel condenser and in the evaporator downstream the condenser. Then oil was extracted at the oil separator, which was a coalescent oil separator, and the oil was transferred to the oil level tank. In the process of oil extraction, the oil separator did not extract 100 percent of the incoming oil because even if it had close to 100 percent efficiency, the oil separator was not ideal. Thus, the oil that slowly escaped the oil separator was potentially retained

in the accumulator installed on the suction line of the compressor. In the compressor circuit, an unknown amount of oil was lost by the scroll compressor, along with the discharged refrigerant and it was (at least theoretically) trapped and separated by the discharge oil separator that consisted of a helical and coalescent oil separators installed in series along the direction of the refrigerant flow. Again, the process of oil separation at the discharge oil separators was not ideal and an unknown, small but not measured amount of oil escaped the discharge oil separators and it circulated to the microchannel heat exchangers under testing. In simple words, the compressor acted as component that systematically introduced an unknown, uncontrolled, and potentially unstable amount of oil into the microchannel heat exchangers that were to be tested for oil retention. We were not able to eliminate this systematic error by using the compressor based experimental apparatus and only a pump based experimental apparatus was able to eliminate this source of uncertainty for the oil mass fraction circulating inside the microchannel heat exchangers during the heat transfer experiments.

Figure 3.7 shows an example of the refrigerant side operating conditions during an oil retention tests and the main thermodynamic state points of the refrigerant are plotted on a $P-h$ diagram. The cycles in the figure is for $OMF = 0$ wt.% (that is, no oil in the test apparatus) and the figure shows two cycles overlapping: the one in solid red line, which is the cycle performed by the refrigerant in the pump boiler test apparatus, and the one in dashed green line, which is the cycle performed by the refrigerant in the compressor based test apparatus. The difference between the maximum and minimum pressures observed was 235 psi (1620.3 kPa). The fluid in the compressor based cycle experienced

a large pressure drop in the expansion valve in addition to the minor pressure losses in the heat exchangers and pipelines.

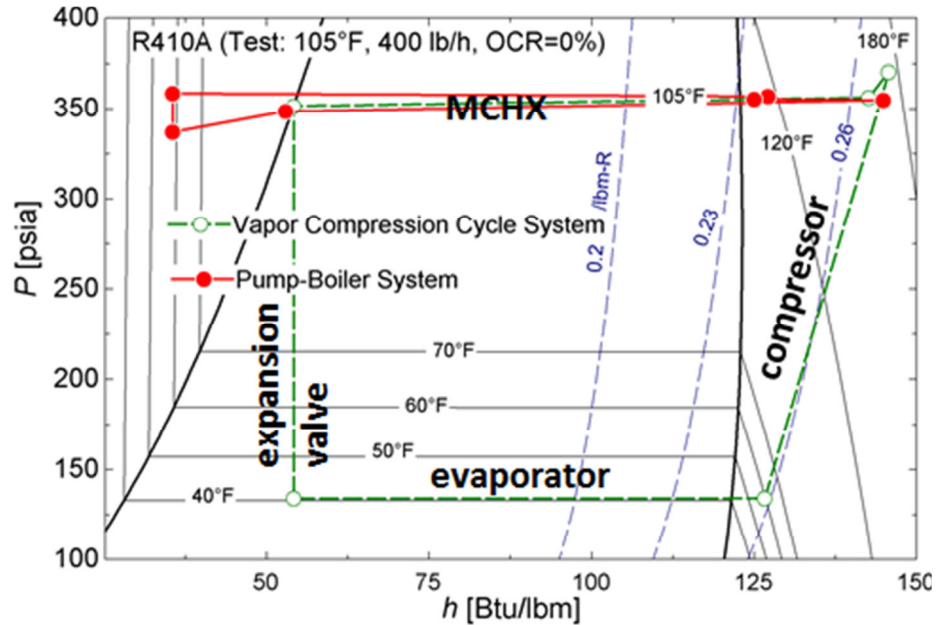


Figure 3.7: P-h diagram of Vapor Compression cycle and Pump-Boiler systems (Deokar, 2013)

In the vapor compression cycle based test apparatus there were two main additional issues associated with the control of the refrigerant operating parameters during the tests and the simultaneous oil management between compressor, (which needed its own lubrication at all times), and the rest of the components of the test apparatus. As previously mentioned, one circuit for the flow of oil consisted of the test section, that is, the port for oil injection (port-A or port-B), the microchannel heat exchanger, the expansion valve, the evaporator, and the oil separator 2 of the oil extraction device. The second oil flow circuit consisted of the compressor and the its discharge oil separator (oil separator 1) and the oil return line to the compressor suction in which an adjustable oil metering valve was installed. An oil sight glass was also installed next to the compressor

housing and directly connected to the compressor housing to visually monitor the oil level inside the compressor. Unfortunately, it was not possible to completely eliminate oil traveling from one circuit to the other. While an unknown amount of oil that traveled to the test section could potentially result in a systematic error for determining the actual OMF in the microchannel heat exchangers under experimental investigation, a lack of oil or too much oil in the compressor caused mechanical failure. During the first year of the current study and after few tests with microchannel condensers, three compressors experienced mechanical failure and, upon further investigation, the failure of the compressors were due to severe bearings wear. After reaching steady state conditions, typical symptoms of imminent compressor failures were identified as (a) compressor current suddenly increased by over 50%; (b) compressor discharge temperature suddenly increased by about 50°F (27.2°C) without any external perturbation to the test setup; and/or (c) the oil level in the sight glass installed next to the compressor decreased below minimum level for proper lubrication. These symptoms occurred after several hours of run and, in one case, after only few hours of operation of the compressors in our test apparatus. It should be noted in here that the compressors were always run within their envelope operating design conditions specified by the manufacturer. Once a compressor stopped, any POE oil recovered from the compressor housing appeared dark in color, with small (but visible) metal particles in it. We opened one compressor and took a closer look at its interior and we observed that its bearings were visibly wear out. These observations indicated that oil that was originally charged inside the compressor, was carried over with the refrigerant outside the compressor housing at some point in time during the experiments. The compressor then run without lubricant in it for a certain

period until ultimately failed. Because the compressors were used in a non-conventional vapor compression system having multiple auxiliary components in parallel configurations and having long lines and multiple intermediate valves, any attempts to compensate for oil escaping the compressor was not successful in our compressor based test apparatus. In addition, it was not possible to isolate and quantify the uncertainty in the OMF due to the amount of oil that instantaneously travelled (and could be potentially retained!) to the microchannel condensers. Thus, we decided to switch to a pump boiler based test set up in order to eliminate the issues of contamination of the compressor oil in the test section and to control the refrigerant side parameters during the oil retention tests and the heat transfer experiments. The pump boiler loop was successfully utilized for testing the condenser and the evaporators and it is described in the next section.

3.3.2.2 Pump-boiler based test apparatus

The schematic of the pump-boiler loop of the experimental setup for the oil retention measurements in microchannel condenser is shown in Figure 3.8. The experimental setup included three main systems, namely a refrigeration loop, an oil injection system and an oil extraction system. A laboratory small-scale pump-driven refrigerant loop was constructed to control the refrigerant saturation temperature and the refrigerant flow rate to the test section. From the pump, the refrigerant flowed through a Coriolis mass flow meter and then it was directed to tube-in-tube evaporator coils to achieve superheated vapor conditions at the inlet of the oil separators. The refrigerant should be in superheated condition to allow the oil separation from the refrigerant and oil mixture at

the oil separators. The evaporator coils were water-heated heat exchangers in which hot water was supplied from a large hot water tank. From the evaporator coils the refrigerant circulated through the refrigerant line to the oil separators. The refrigerant was then directed to a plate heat exchanger that worked as superheater to control the degree of superheat of the refrigerant entering the test section. From the test section, the refrigerant mixture was circulated through a large plate-type heat exchanger acting as post-condenser and subcooler. At the outlet of the subcooler, the refrigerant was liquid and it was fed back to the pump. The required system pressure and temperature were controlled to the steady-state conditions before each injection test by regulating the temperatures and flow rates of the water in the evaporator coils and of the air stream entering the condenser. In addition, a hydraulic accumulator was installed in the refrigerant line to stabilize the pressure during the oil injection and extraction processes.

The oil injection system consisted of an oil reservoir and a gear pump. Before the injection, the oil inside the reservoir was heated by an electric flexible band heater to adjust the temperature of the oil close to the temperature of the refrigerant entering the test section. Refrigerant vapor, taken at high pressure, was used to pressurize the oil at the top of the oil reservoir and to assist the oil pump during the injection of the oil into the test section. The temperature and pressure of the oil reservoir were measured to determine the solubility of refrigerant in the oil that was released to the test section. This solubility was also experimentally measured with random periodic samples taken from the oil reservoir and analyzed according to the ASHRAE Standard 41.4 (1996). From the oil reservoir, oil was metered into the test section using a variable speed gear pump coupled by a variable-frequency drive. Additional fine tuning of the oil flow was

provided by a bypass metering valve. A Coriolis mass flow meter was used to measure the injected oil mass flow rate. When the oil was released to the test section, it formed a mixture with refrigerant and circulated in the refrigerant loop through the plate-type heat exchanger, refrigerant pump, and the evaporator coils. Then the oil entered the oil separators where it was separated from the refrigerant stream and extracted from the refrigerant loop.

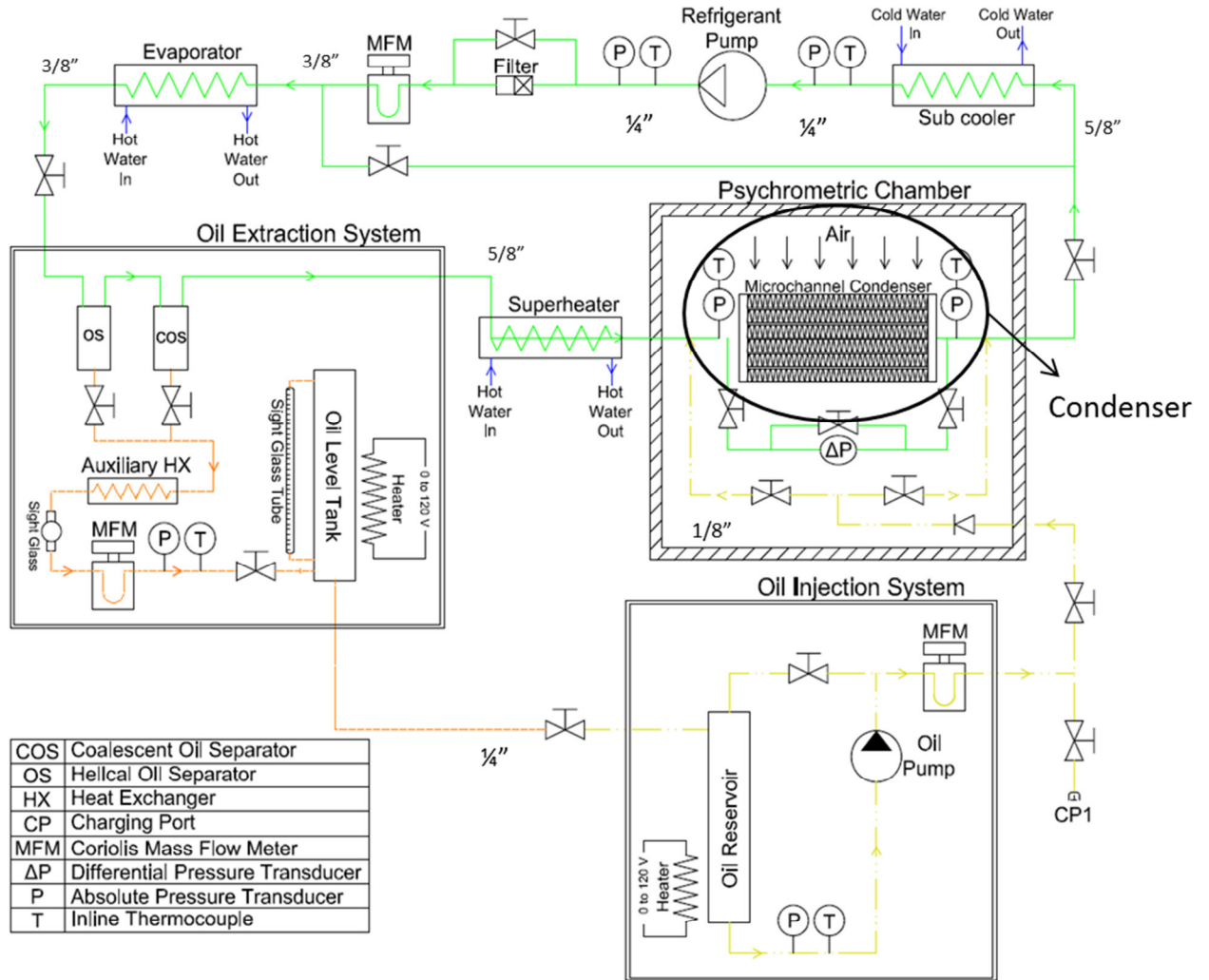


Figure 3.8: Schematic of the experimental setup for condenser tests (modified from Deokar (2013))

The oil extraction system consisted of two customized refrigerant oil separators that were placed in series, a mass flow meter and oil tanks as depicted in Figure 3.9. The first oil separator was a helical-type separator of large capacity and it separated the main oil stream from the refrigerant flow. A second oil separator was a coalescence-type separator installed downstream to remove all residual oil, if present. Both oil separators originally had internal floating valves in the oil compartment but the valves were removed to promote stable and continuous flow of the oil that was extracted from the refrigerant

loop. A sight glass was mounted in the oil line of the oil separators to visually observe the extracted oil flow. A special refrigerant dye was mixed with the oil to help the detection of the oil and visualization of the flow. An auxiliary heat exchanger was installed after the sight glass to further subcool the refrigerant dissolved in the extracted oil. This subcooler improved the stability of the measurements of the mass flow rate for the extracted oil, which were done by using a Coriolis mass flow meter. The extracted oil were then stored in two oil tanks equipped with level sight glass indicators. During the injection tests, as the extracted oil filled the tanks, the refrigerant dissolved in the oil was continuously vented out and the refrigerant vapor was redirected through a series of pressure-equalization lines to the inlet of the auxiliary evaporator coils. The pressure equalization lines were critical to ensure that there was not any back pressure build up inside the oil tanks. Thus, the oil flow extracted from the oil separators continuously flowed down to the oil tanks because the back pressure inside the oil tanks was controlled to below the pressure inside the oil separators.

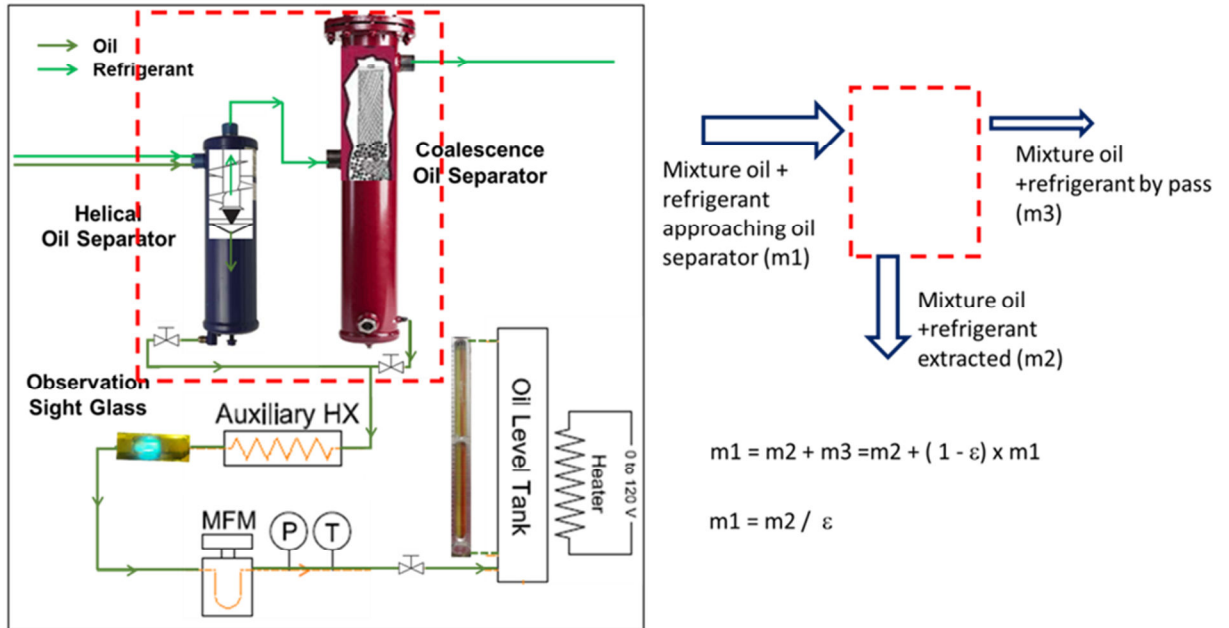


Figure 3.9: Oil extraction system (left) and mass balance at the oil extractor (right, the oil extractor consisted of the two oil separators connected in series, as indicated inside the red dashed square on the left side of the figure)

The mass balance of the oil separators depicted in Figure 3.9 can be expressed as:

$$\dot{m}_1 = \dot{m}_2 + \dot{m}_3 \quad 3-1$$

Where,

\dot{m}_1 = mass flow rate of refrigerant and oil mixture approaching oil separators (lb/hr)

\dot{m}_2 = mass flow rate of refrigerant and oil mixture extracted from oil separators (lb/hr)

\dot{m}_3 = mass flow rate of refrigerant and oil mixture bypassing oil separators (lb/hr)

The extraction efficiency, ϵ , represents the ratio of the extracted over the entering mass of the refrigerant and oil mixture in oil separators, that is,

$$\varepsilon = \frac{\dot{m}_2}{\dot{m}_1} \quad 3-2$$

The efficiency was determined through a series of preliminary tests on the oil separators in which the entering mixture had oil mass fraction ranging from 1 to 5 wt.% and it circulated through the oil separators at various pressures and flow rates. The oil concentration in the exiting mixture was measured by using the ASHRAE Standard 41.4 (ASHRAE, 1996) during these preliminary experiments and the efficiency of the oil separators, estimated by using Eq. 4-2, ranged from 95 to 99%. ε was depended on the concentration of oil in the mixture entering the separators and it decreased to 95% if the OMF was 1 wt.% or below. The oil separators efficiency was also checked periodically during the tests to confirm that no oil (or that a very small but known amount of oil) was bypassing the oil separators. Even when small, the mass of the oil bypassing the oil separator was accounted for with the oil separator extraction efficiency by substituting equation 3-2 into 3-1 and it resulted as follows:

$$\dot{m}_3 = (1 - \varepsilon) \times \dot{m}_1 \quad 3-3$$

The oil retention experiments were conducted by using this pump-boiler type loop, in which the refrigerant was circulated by a gear pump. As previously mentioned, oil was injected in the refrigerant loop by using a variable speed gear pump and the oil was purposely injected at two locations, namely the inlet and the outlet of the microchannel condenser (referred to as test section in this manuscript). The principle of the oil retention measurement procedure is illustrated in Figure 3.10. The amount of oil injected and extracted in the figure was measured from the injection and extraction mass flow rates.

The amount of refrigerant dissolved in the oil was taken into account based on solubility data from Cavestri and Schafer (2000) for given pressures and temperatures measured in the oil reservoir. At the time t_0 , oil was released to the inlet of the microchannel heat exchanger. The oil flowed through the test section and reached the oil separators where it was extracted from the system. The extracted oil was visually detected at the oil line sight glass at time t_1 and, at the same time, a regular step up increase of the oil flow rate measured from the Coriolis flow meter installed at the bottom of the oil separators in Figure 3.9 was recorded. The injection and extraction flow rates became stable and steady at time t_2 . It should be noted that refrigerant was also present in the liquid mixture flow that was extracted from the refrigerant loop at the oil separators location because both refrigerants R410A and R134a are soluble in POE oil. The solubility of the refrigerant in the oil was account for in order to calculate the net amount of POE oil present in the extracted oil rich liquid mixture of POE oil and refrigerant. It should be also emphasized that the extractor efficiency of separation was considered in order to obtain the total amount of oil that entered the oil extractor. From time t_2 to time t_3 , the average difference between the oil mas injected and the oil mass extracted resulted in the oil mass that was held up in the microchannel condenser plus all connecting pipelines downstream the test section and in between the injection port and the oil separators, M_a . With reference to Figure 3.10, the amount of oil M_a was measured from the time integral of two oil flow rates as follows:

$$M_a[\text{lb}_m] = \int_{t_0}^{t_3} \dot{m}_{injected@inlet\ port} dt - \int_{t_0}^{t_3} \dot{m}_{extracted@oil\ separators} dt \quad 3-4$$

A similar procedure was then conducted for the injection test at outlet port of the test section, and the mass of oil retained in the pipelines downstream the test section was measured by using the time integral shown in Equation 3-5:

$$M_b [lb_m] = \int_{t'_0}^{t'_3} \dot{m}_{injected@outlet\ port} dt - \int_{t'_0}^{t'_3} \dot{m}_{extracted@oil\ separators} dt \quad 3-5$$

Where the symbols t'_0 and t'_3 indicates the new times at which the oil was released to the outlet port of the test section and at which the flow rate became stable and steady for the injection test at the outlet port of the test section. The average difference between the oil mass injected and the oil mass extracted during the injection test at the outlet port of the test section was the oil mass retained in the connecting pipelines between outlet injection port and the oil separators, M_b . The difference between the two amounts of oil masses resulted in the oil mass that was retained in the test section, $M_{oil,retention}$, that is:

$$\text{Oil retention mass in the test section} = \text{Oil retention mass in the test section plus in the downstream pipeline} - \text{Oil retention mass in the downstream pipeline}$$

Or, according to the variables defined in Eq. 3-4 and 3-5, it yielded

$$M_{oil,retention} [lb_m] = M_a [lb_m] - M_b [lb_m] \quad 3-6$$

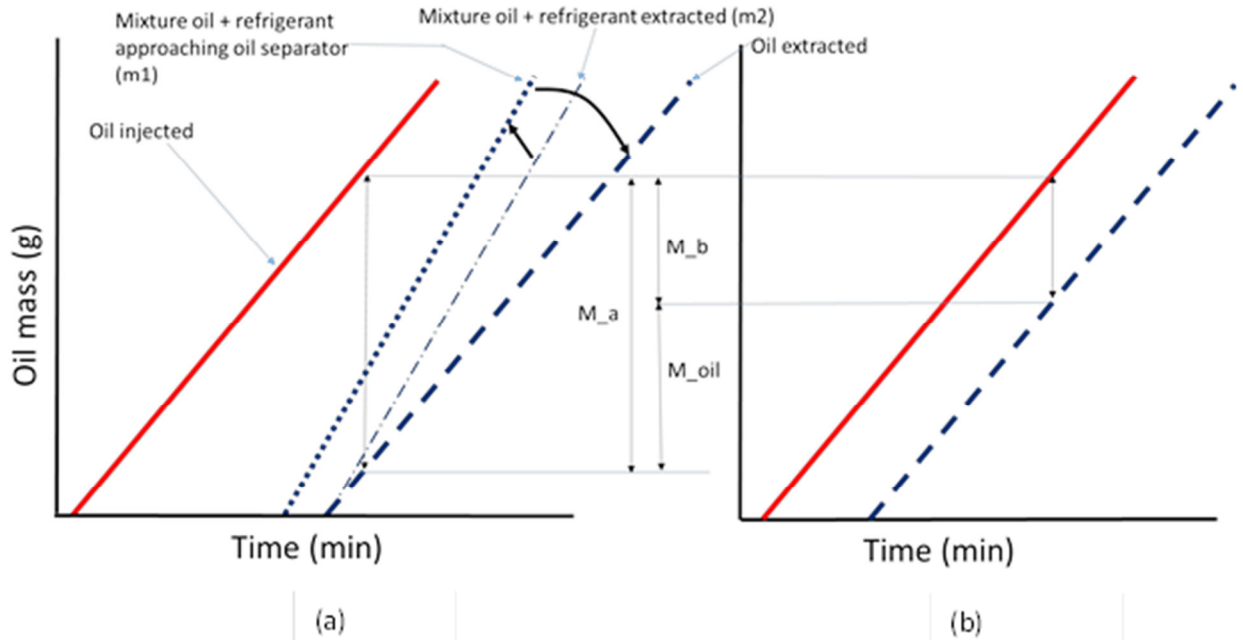


Figure 3.10: Oil retention calculation: (a) injection at inlet of MCHX; (b) injection at outlet of MCHX

At the end of each test, the system was flushed by running the refrigerant loop without oil for at least an hour and by collecting the residual oil in the oil extraction device. During this flushing cycle, the refrigerant in the test section was controlled to near saturated liquid conditions and the liquid refrigerant in the entire test section mixed with the residual oil. Since refrigerants R410A and R134a were soluble and completely miscible with POE oil when they were in liquid phase, the liquid refrigerant gradually picked up the oil and cleaned the main microchannel tubes of the test section. Two sight glasses were installed before and after the oil separators to detect the presence of any residual oil in the refrigerant loop during the flushing cycles. To facilitate the oil detection in the sight glasses, even when oil was in small traces, a fluorescent dye was added to the oil. When traces of oil were present in the refrigerant loop, the flow at the sight glasses appeared of yellow color with respect to transparent color when no oil was present inside the loop. The flushing cycles were run until no traces of oil were visually observed at the sight glasses of the refrigerant loop. When clear flow was confirmed, the assumption was that all oil retained in the test section was removed. However, small amounts of oil might have been present inside the headers of the test sections, where local

oil and liquid traps and local stagnation flows might have occurred during the flushing cycles. These small amounts of oil, if present, did not exit the microchannel heat exchangers under testing but they also did not affect the heat transfer rates and the refrigerant-side pressure drops. In other words, the flushing procedure was successful in cleaning all the significant residual oil held up in the test section because the initial heat transfer capacities and refrigerant-side pressure drops of the microchannel heat exchangers were restored after each flushing cycle. Thus, if oil was still present inside the test section after each flushing cycle, it had an effect on the heat transfer rate and pressure drops that was below the sensitivity of the present test apparatus.

The main advantages of the technique used in the present work to measure oil retention in microchannel type condensers and evaporators can be summarized as follows:

- (i) it had good repeatability because it did not require any opening of the system, any disassembly of the test section, and any recovering of the refrigerant after each test;
- (ii) it had good accuracy because it did not require any weighting of the test section or sampling of the oil and it was based on a fairly simple mass conservation law;
- (iii) it allowed testing condensers and evaporators operating in conditions that were close to those of the actual applications; in other words it allowed testing of the microchannel heat exchangers operating in conditions similar to the ones that the heat exchangers experienced when they were part of real life air conditioning and refrigeration systems.
- (iv) it isolated and quantified the net effect of oil retention on the heat transfer capacities and pressure drops by measuring directly the heat transfer rates and pressure drops of the microchannel heat exchangers with and without oil and

at the same flows and pressures; the fact that a controlled amount of oil was metered to the heat exchanger improved the confidence on how much oil was present inside the test section at any instant of time during the tests.

3.3.3 Oil Retention Measurement in Microchannel Evaporator

The oil retention in microchannel evaporator was measured for two different refrigerant and oil mixtures. Refrigerant R410A and POE oil mixture was used to study microchannel evaporators in air conditioning applications while refrigerant R134a and POE oil mixture was used to investigate microchannel evaporators for AC systems, water/wine coolers vending machines applications of refrigeration systems. All the test conditions carried out for the microchannel evaporator are given in Table 3-4, from test number 7 to 15. Experiments were carried out for saturation temperatures at and above freezing point of water i.e. 32° F (0° C).

The pump-boiler based test apparatus used to experimentally measured the oil retention, heat transfer rate, and pressure drop of microchannel condensers was modified to accommodate similar tests for microchannel evaporators. This section provides an overview of the modifications of the test apparatus used for measuring oil retention, and the effects of oil on pressure drop, and heat transfer capacity in microchannel evaporators. As before, the experimental setup consisted of four main sections as follows:

1. Pump-boiler refrigerant side loop (also referred in this paper to as “refrigerant loop”),
2. Air flow loop,
3. Oil loop, which consisted of the oil injection and oil extraction devices,
4. All remaining auxiliary hydronic systems used to control the test parameters and the test setup operating conditions.

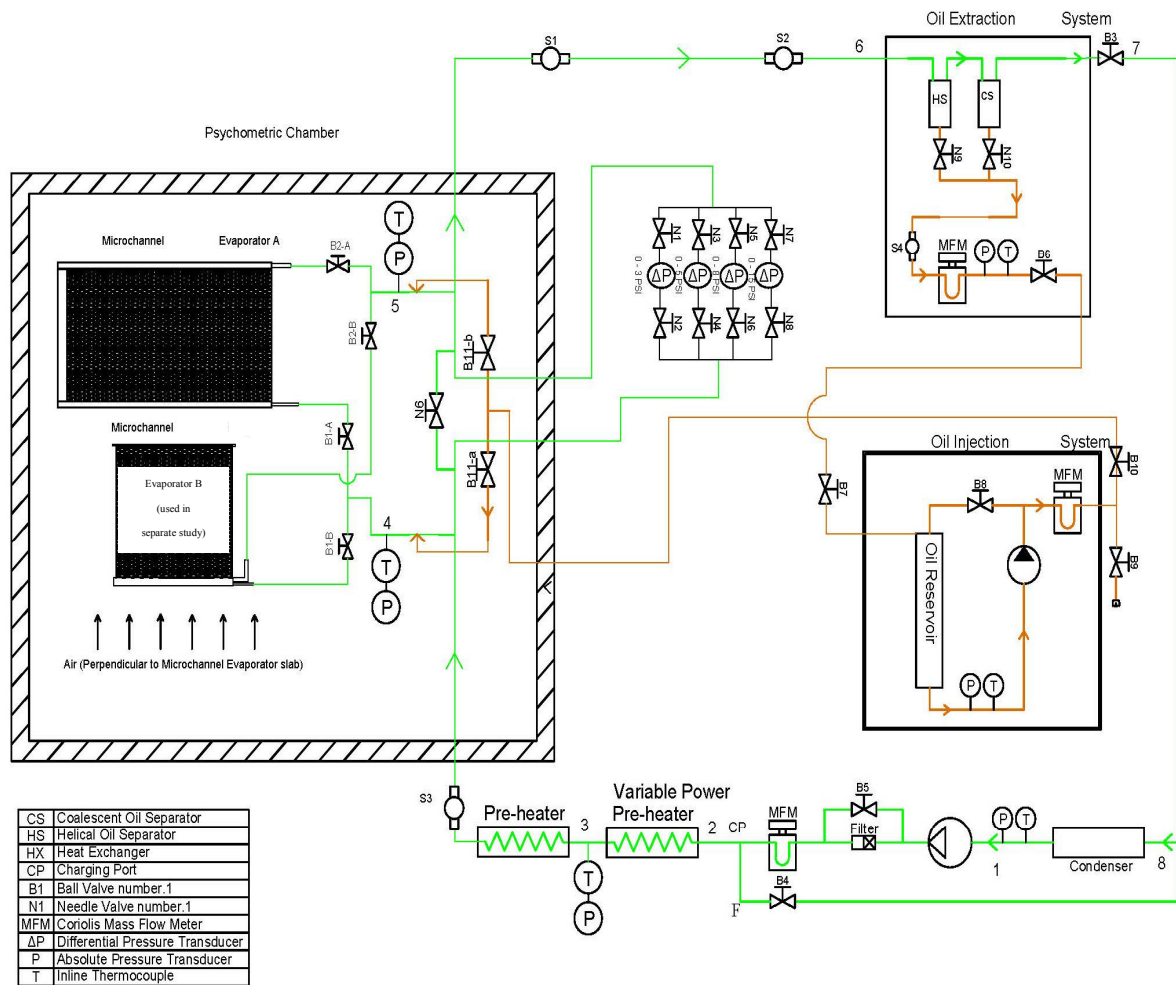


Figure 3.11: Schematic of the pump-boiler based experimental setup used in the evaporator oil retention tests

The schematic of the pump-boiler based test setup for the oil retention measurements in microchannel evaporators is shown in Figure 3.11. The refrigerant pump-boiler loop system, oil injection loop and oil extraction device were similar to that of the condenser tests but with some minor modifications. For the microchannel evaporator tests, a series of electric tape heaters were installed along the refrigerant pipelines before the microchannel evaporators. These heaters controlled the degree of subcooling of the liquid

refrigerant at the inlet of the evaporator. Furthermore, to guarantee sub-cooled liquid refrigerant at the inlet of the gear pump, a large plate-heat exchanger, labeled as condenser in the figure 4.8, was installed after the test evaporators. A low temperature chiller was used to cool the refrigerant to below saturation temperature before it entered the refrigerant gear pump. Liquid refrigerant from the pump was circulated to a Coriolis mass flow meter and then was heated slightly with a series of electric heaters in a preheater. With reference to Figure 3.11, the preheater had two sections: the first section was a variable electric power heater from point 2 to 3 and the second section was a constant electric power heater from 3 to s3. Both heaters were made of smooth copper tube with electric tape heaters wrapped around them. The first heater section had electric tape heaters that were controlled by a variable transformer in order to adjust the heat transfer rate to refrigerant flow. In the variable power heater, the liquid refrigerant was heated up to about 5 to 10 degree of subcooling and at the exit of the first variable power preheater, pressure and temperature of the liquid refrigerant were measured in order to determine its enthalpy. Then, in the second heater, the refrigerant liquid was heated to near saturation liquid temperature, that is, to slightly subcooled liquid state with only 1 to 2°F (0.5 to 1°C) of subcooling at the inlet of the test microchannel evaporators. The second heater in the preheater section was very well insulated and the electric power was measured during the tests by using a voltmeter. Thus, from the inlet enthalpy in state 3, mass flow rate, and heat transfer rate measured from the second section of the preheater, the refrigerant inlet conditions at the inlet of the test section were experimentally determined. The refrigerant at the inlet was slightly subcooled liquid with temperature of 1 to 2°F (0.5 to 1°C) below the thermodynamic refrigerant saturation temperature of

evaporation. This meant that refrigerant near to saturated liquid state entered the microchannel evaporators. This approach was intentionally chosen to promote uniform distribution of the refrigerant among the vertical microchannel tubes in the test evaporators. A sight glass (component s3 in Figure 3.11) was installed between the second preheater and the inlet of test section to visually confirm the liquid phase of the refrigerant at the inlet of the test evaporators.

In the test section, the refrigerant evaporated in the microchannel tubes and exited as superheated vapor. The degree of superheat at the outlet of the evaporators was controlled to 11 to 15°F (6 to 8°C) by adjusting the air temperature of the air flow entering the heat exchanger and the refrigerant flow rate. The test section was installed inside a psychrometric chamber, which controlled the inlet air temperature, humidity, and air speed. Two sight glasses, referred as to components S1 and S2 in Figure 3.11, were installed along the refrigerant pipelines downstream the test section. Since refrigerant was in vapor phase in this part of the loop, these two sight glasses were used to visually detect the instant at which oil arrived to the sight glasses. This technique was used to determine the oil retention in the test evaporators. Then, the refrigerant vapor and oil mixture was directed to the oil separators in the oil extraction device. In this component, oil was separated from the refrigerant vapor and it was collected in the oil reservoir. The refrigerant vapor was circulated to the condenser and cooled down to subcooled liquid before it was recirculated back to the refrigerant gear pump. Both the oil injection and extraction devices were similar to the one used in the condenser oil retention tests. However, the methodology to determine the oil retention volume was slightly different, as discussed next.

3.3.3.1 Pump-boiler loop for the evaporators tests

The schematic of the pump-boiler loop for the oil retention measurements in microchannel evaporator series is shown in Figure 3.11 as light green solid line loop.

This section provides an overview of the pump-boiler system that was used for the tests. With reference to Figure 3.12, subcooled liquid refrigerant from condenser was fed into pump suction. The pump (component 1 in Figure 3.12) used in this system was same as the one used in condenser tests. The pump suction pressure and temperature (before component 1 in Figure 3.12) showed how much subcool was at pump suction. The liquid refrigerant at the pump suction had over 10°F (~5°C) of sub-cooling in order to prevent cavitation of gear pump. From the refrigerant pump, the refrigerant circulated to a Coriolis mass flow meter and then was directed to the preheaters. The actual image in Figure 3.12 shows the positioning of condenser, pump, mass flow meter, and the direction of refrigerant flow.

Figure 3.12: Section of pump boiler loop from exit of oil separators until preheater tubes (Deokar, 2013)

Figure 3.13: Variable power preheater and constant power preheater tube heat exchangers of the pump boiler loop

The subcooled refrigerant from the pump was heated in preheater tube (from point 2 to S3 in Figure 3.11) to near saturated liquid conditions. The preheater consisted of three electrical tape heaters installed around the refrigerant pipelines (from point 3 to S3 in Figure 3.11). The first electrical tape heater (from point 2 to 3 in Figure 3.11) was coupled with variable AC transformer (VARIAC). Constant power supplies were connected to the second and third electrical tape heaters (from point 3 to S3 in Figure 3.11). The power supply to the first electrical tape heater varied from 0 to 500 Watts using the VARIAC, which was manually adjusted to control the temperature of the refrigerant at the test section inlet. The second and third electrical tape heaters were of constant power of 300 Watts each. The temperature and pressure readings (indicated with the symbols T and P at point 3 in Figure 3.11) indicated how much subcooled the liquid refrigerant was in this location of the refrigerant loop. This helped to estimate how much power supply was needed to bring the subcooled liquid refrigerant in 3 to near saturated liquid conditions at the inlet of the test section.

Figure 3.14 shows how one of the electrical tape heaters of preheater was installed on refrigerant pipelines before entering the test section. The second and third electrical tape heater (from point 3 to 3s in Figure 3.11) was heavily insulated with fiberglass insulation. The component 8 in Figure 3.13 shows the exterior of fiberglass insulation on preheater. This insulation guaranteed that most of the heat from electrical tape heater was directed into the liquid refrigerant circulating inside the pipelines.

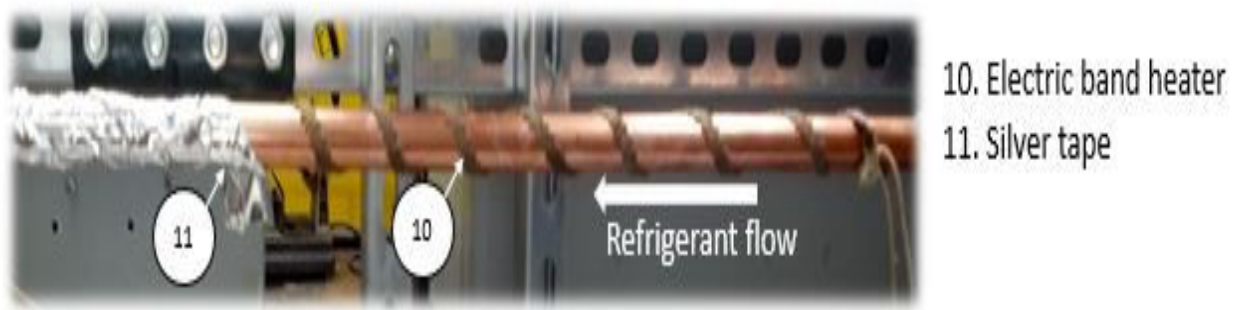


Figure 3.14: Example of an electric heater wrapped around a refrigerant copper tube and used as preheater for the evaporator tests

In order to measure the pressure drop across the test section, the inlet and outlet of the test section were connected to the differential pressure transducer bank that was located outside the psychrometric chamber. With reference to Figure 3.11 and Figure 3.15 the differential pressure bank consisted four differential pressure transducers connected in parallel to each other. Each differential pressure transducer had different range from each other. Table 4-3 shows the range of each differential pressure transducer in the bank. The proper differential pressure transducer was selected and connected in parallel with the test section based on the actual pressure drop measured during the experiments. For example, after having reached the test conditions but before commencing the test, the actual pressure drop was measured with the differential pressure transducer DP4. If the actual pressure drop in the test section was about 0.8 psid, the DP4 was close and isolated and DP1 was opened and put in parallel to the test section. Then, DP1 was used during the recording period of the experiment.

Table 3-3: Range of the differential pressure transducers used in the experimental setup

Differential Pressure Transducer	Pressure differential range
DP1	0 to 20 kPa (0 to 3 psid)
DP2	20 to 34.5 kPa (3 to 5 psid)
DP3	34.5 to 55.2 kPa (5 to 8 psid)
DP4	55.2 to 103 kPa (8 to 15 psid)

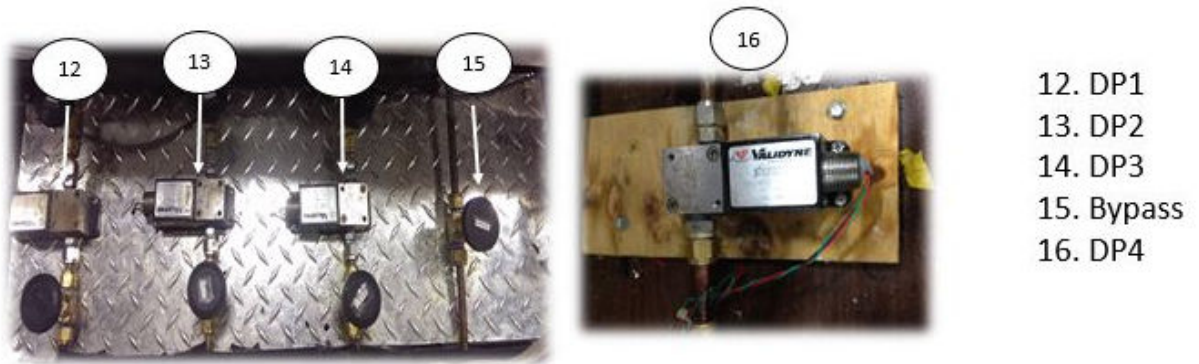


Figure 3.15: The four differential pressure transducers installed in parallel and used in the evaporator tests

The inlet of test section was connected two absolute pressure transducers. One pressure transducer at point 4 in Figure 3.11 had 0 to 500 psia range. The second absolute pressure transducer had a range from 0-150 psia and it had higher precision and sensitivity than the first one. This transducer was installed outside the chamber and it was connected to inlet of the microchannel test evaporators by using a long pressure line made by port ¼ inch diameter copper tubing. This high precision pressure transducer was used in order to improve the accuracy of the measurements of the inlet absolute pressure.

During the oil injection tests in microchannel evaporator A, the ball valve B1-A and B2-A (see between points 4 to 5 in Figure 3.11) were opened and ball valves B1-B and B2-B were closed. This configuration directed the refrigerant flow to the microchannel test evaporator A. As the refrigerant entered the test section, it evaporated in the microchannel tubes and exited as superheated vapor. The superheated refrigerant from test section outlet exited the psychrometric chamber and entered the oil separators. There were two sight glasses S1 and S2 installed before oil separators (indicated with the symbols S1 and S2 in Figure 3.11). The actual photo in Figure 3.16 shows the position of sight glass S1 and sight glass S2 with respect to oil separators. The sight glasses S1 and S2 were used as visual aid to see when refrigerant and oil mixture layer first appears in those sight glasses. In the oil separators oil was separated from the refrigerant vapor. After that the refrigerant from oil separator entered the condenser (see points 7 to 8 in Figure 3.11). The condenser was a large plate-heat exchanger used to cool refrigerant below its saturation temperature. The condenser was served with a glycol solution (Dynalene HC-40) from a low temperature chiller, and more details on the low temperature chiller are presented in section 3.5.2.

Figure 3.16: Photo of the position of sight glass S1 and sight glass S2 with respect to oil separators (the sight glasses S1 and S2 were used as visual aid to see when refrigerant and oil mixture layer first appears in those sight glasses).

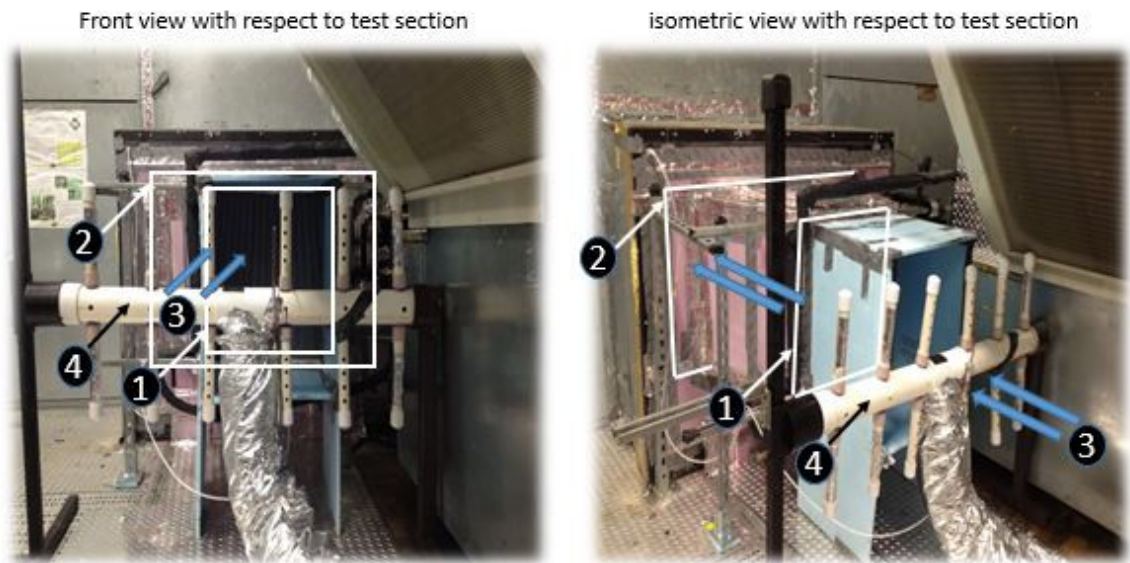
3.3.3.2 Air flow loop

After the completion of condenser tests, the air flow loop was slightly modified for the evaporator tests. An additional dehumidification system was used to further remove the moisture from the air stream entering the microchannel test evaporator. Lowering the air dew point temperature was critical to prevent frost formation when the saturation temperature of the refrigerant inside the microchannel test evaporator was at 32°F (0°C). This was achieved by controlling the air dew point temperature of the entering air stream to below the refrigerant saturation temperature inside the microchannel test evaporator. Thus, the temperature of the heat transfer surfaces (both fins and microchannel tubes) of

the evaporator was above the air dew point temperature and condensation and frosting of the fins were eliminated. We refer to this condition as dry fins testing condition because during the oil retention experiments, the latent loads of the evaporators, if any present, were very small compared to the measured sensible load of the evaporators.

3.3.3.2.1 Air flow loop for tests of the microchannel evaporators

The air flow loop for medium temperature series was similar to that used for microchannel condenser tests.



1. Microchannel Evaporator B (used in separate study)
2. Microchannel Evaporator A
3. Air direction
4. Air sampling device

Figure 3.17: Test sections and Air sampling device in front of test section

With reference to Figure 3.17, the air entered microchannel evaporators via a small tunnel in front of microchannel evaporator. The air was sampled before the microchannel evaporators through a mechanical air sampling probe. The sampled air dry bulb and wet bulb temperatures were measured by using RTDs in a standard dry/wet bulb probe device.

Air entered into the slabs of an isolated microchannel heat exchanger (referred as evaporator B, used in separate study) and then entered into intermediate tunnel between it and microchannel evaporator A (between 1 and 2 in Figure 3.17). As air passes through the evaporator A (test section), the temperature of air decreases. The temperature of the air after the test section was measured using thermocouples and the mechanical sampling dry bulb probe. Figure 3.18 shows 5 out of 20 thermocouples that were installed at the outlet of the evaporators. Thermocouples were installed on a plastic thin wire forming grid of 5 rows and 5 columns and they were used to measure the local temperature of the air exiting the microchannel evaporator A.

Figure 3.18: Thermocouple grid arrangement during Evaporator A installation

3.3.3.3 Oil injection and extraction systems

The oil injection system for the tests on the microchannel evaporators was similar as that used in condenser tests. The experimental equipment used for oil extraction system was the same as that of the microchannel condenser tests. The oil collection method that was used for oil retention measurement in condenser test was not feasible in the evaporator tests. During the injection of oil in evaporator tests it was observed that there was not enough free flow of oil after the oil extractors. This was observed through sight glass that was located at the bottom of the oil extractors (see sight glass S4 in Figure 3.11) and the flow meter located below the oil separators (see MFM located below the HS and CS in Figure 3.11). In other words, there was not enough pressure difference to drive the oil

from the oil separators to the oil reservoir of the oil extractor system when the test section functioned as microchannel evaporator. This meant that measuring the flow rate of the extracted oil from the refrigerant loop was not possible for the microchannel evaporator tests. More specifically $\dot{m}_{extracted@oil\ separators}$ in Equations 3-4 and 3-5 was either zero or fluctuating too much to be reliable. An alternative method was developed to estimate the oil retention in the microchannel evaporators. This alternative method was verified for condenser tests and it provided equivalent results of oil retention (as it will be presented later in the manuscript). The alternative method to measure oil retention in microchannel evaporators is described in detail next.

3.3.3.4 Oil retention measuring methodology for the microchannel evaporator tests

The methodology to measure the oil retention for the microchannel evaporator tests is explained briefly in this section. Liquid refrigerant from the pump was directed to a Coriolis mass flow meter and then flowed to the preheater tubes. In the preheater, the refrigerant was heated to near saturation conditions before entering the microchannel test evaporator.

Figure 3.19: Infrared Image of microchannel evaporator A for one medium temperature test; this image indicates refrigerant flowing vertically from bottom to top of the heat exchanger and fairly uniform refrigerant flow distribution

The refrigerant inlet conditions were controlled at near saturated liquid conditions with the aim to promote uniform distribution of refrigerant and of the refrigerant and oil mixture. Infrared thermal images of the microchannel evaporator A were taken to confirm that the distribution was uniform. An example is shown in Figure 3.19, in which the color appears uniform along the horizontal sections. The liquid refrigerant entered at the bottom (dark blue color in Figure 3.19), evaporated in the vertical microchannel tubes, and exited as superheated vapor refrigerant at the top. Two sight glasses (indicated by the symbols S1 and S2 in Figure 3.11) were installed at the outlet of the test section. The refrigerant vapor circulated toward the oil separators in the oil extraction device.

From the outlet of the oil separators, the refrigerant circulated to the condenser and was brought to subcooled liquid conditions before it circulated back to the gear pump.

After achieving the required mass flow rate of refrigerant and test condition in pump boiler system, oil was injected at the inlet port of the test section by opening ball valve B10 (component B10 in Figure 3.11). The time ' t_0 ' is noted when injection of the oil was started. During the oil injection at the inlet of the test section, the oil mixed with refrigerant and flowed through the test section and proceeded to the outlet and then passed through the sight glasses (see again S1 and S2 in Figure 3.11). As the oil was released to the test section, the oil filled the test section and connecting pipelines until it reached the sight glass S1. A liquid film layer of lubricant appeared clearly visible at the walls of the sight glass S1. During each test for the evaporators, the sight glasses S1 and S2 were monitored by using video recordings of the flow. These videos helped to measure the time at which the oil was first observed on each sight glass.

Figure 3.20 shows an example of a measurement of the time at which the oil reached the sight glass. At the top image, the sight glass was clear and only refrigerant vapor was present. In the center image, a first drop of oil appeared at the inlet of the sight glass. When a first complete layer of oil covered the sight glass S1 the time t_1 was recorded. This was the scenario in the bottom image of Figure 3.20. Similarly, the time t_2 was noted when a first layer of oil was observed to cover completely the sight glass S2. After oil was detected in both sight glasses S1 and S2, oil was continuously metered to the test section for additional 15 minutes to record the effect of oil on heat transfer rate and refrigerant-side pressure drop. After completion of one test, the test section was cleaned by circulating liquid refrigerant, which collected the residual oil in the test section and

connecting pipelines between test section and the oil separators. The cleaning procedure used in microchannel evaporator tests was similar to the cleaning procedure used for the condenser tests and described in section 3.3.2.

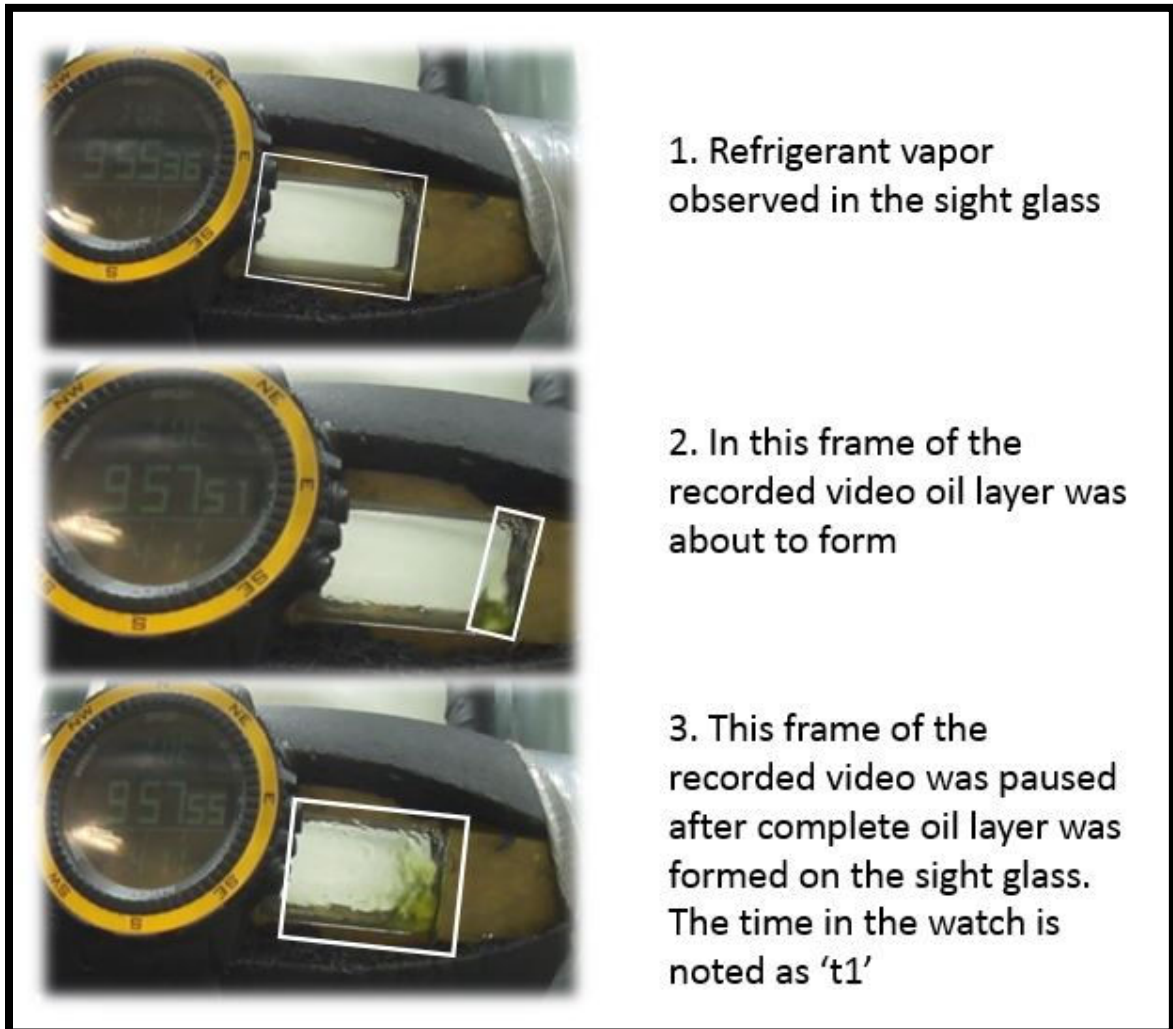


Figure 3.20: Examples of a measurement of the time at which the oil reached the sight glass; a digital chronometer was video recorded next to the sight glass to synchronize the data (the uncertainty of the measured time was of max 2 seconds)

After circulating the liquid refrigerant for about 1 hour, the oil residual was stored in a tank and the test section was ready for next test. The above procedure was carried out for

OMF of 0.5 wt.%, 1 wt.%, 3 wt.%, and 5 wt.%. A similar procedure was repeated when the oil was metered at the outlet of the test section but the OMFs were 0.5 wt.%, 0.8 wt.%, 1 wt.%, 2.5 wt.%, 3 wt.%, and 5 wt.%.

After completion of each test, the time it took the oil to travel from the sight glass S1 to the sight glass S2 was recorded: $\Delta t_{in}=t_{1,in}-t_{2,in}$ was defined as time it took the oil to travel from the sight glass S1 to the sight glass S2 when the oil was injected at the inlet of the test section and $\Delta t_{out}=t_{1,out}-t_{2,out}$ S1 when the oil was injected at the outlet of the test section. For same OMF and mass flow rate, $\Delta t_{in}=\Delta t_{out}$ but our experiments showed that for the same OMF, Δt_{in} was greater than Δt_{out} . In other words, oil travelled from S1 to S2 with slightly lower velocity when the oil was injected at the inlet of the test section compared to when the oil was injected at the outlet of the test section. For estimation of the oil retention in the test section, the conditions downstream the test section during the injection tests at the outlet of the test section were corrected to replicate the conditions downstream the test section during the injection tests at the inlet of the test section. These conditions included controlling the same temperature, pressure, refrigerant mass flux and same oil velocity. When the outlet conditions were the same between inlet and outlet injection tests, then the oil retention in the test section was measured by taking the difference between two oil masses. The following example clarifies the procedure used to estimate the oil retention for one test.

After completion of a test series, Δt_{in} and Δt_{out} were measured as function of OMF as shown in Figure 3.21. In this example, it was observed that Δt_{in} were greater than Δt_{out} and a correction was needed. If OMF was equal to 2.4 wt.% then Δt_{out} was 70 seconds

while Δt_{in} was 80 seconds. Δt_{in} became 70 seconds if the OMF was slightly higher, that is, of 2.8 wt.%. Therefore when oil was injected at the inlet of the test section with OMF of 2.8 wt.%, then the oil travelled in the pipeline downstream the test section with the same velocity of when the oil was injected at the outlet of the test section with OMF of 2.4 wt.%. Now that we found the two OMFs for which the flow conditions in the pipeline downstream the test section were the same, we calculate the oil retention as follow:

$$\begin{array}{l} \text{Oil retention mass in} \\ \text{test section} \end{array} = \begin{array}{l} \text{Oil retention mass in test} \\ \text{section plus in the pipeline} \end{array} - \begin{array}{l} \text{Oil retention mass in the} \\ \text{pipeline} \end{array}$$

That is,

$$OR_{mass@OMF=2.8wt\%} = Ma_{@OMF=2.8wt\%@inlet} - Mb_{@OMF=2.4wt\%@outlet}$$

Where

$$Ma_{(@OMF=2.8wt\%@inlet)} = \int_{t_{0,in}}^{t_{1,in}} \dot{m}_{oil,injected@inlet} dt = 275.0 \text{ grams}$$

and

$$Mb_{(@OMF=2.4wt\%@outlet)} = \int_{t_{0,out}}^{t_{1,out}} \dot{m}_{oil,injected@outlet} dt = 98.6 \text{ grams}$$

And where $\dot{m}_{oil,injected} = \frac{\dot{m}_{oil,injection}}{(1+S)}$ is the mass flow rate of oil injected at the inlet and at the outlet by subtracting the amount of refrigerant dissolved in the oil. The time $t_{0,in}$ and $t_{0,out}$ are the times at which the oil was first released to the inlet and outlet of the

test section. The time $t_{1,in}$ and $t_{1,out}$ are the times at which the oil was detected at the sight glass S1 for oil injection at the inlet and outlet of the test section. The final oil retention mass is

$$OR_{mass@OMF=2.8wt.}\% = 275.0 \quad - \quad 98.6 \text{ grams} = 176.4 \text{ grams}$$

And the oil retention volume was calculated with the following equation:

$$OR_{volume@OMF=2.8wt.}\% = \frac{OR_{mass@OMF=2.8wt.}\%}{\rho_{oil@68^{\circ}F}} = \frac{176.4 \text{ grams}}{0.980 \text{ gram/cm}^3} = 180 \text{ cm}^3$$

Where ρ_{oil} was the density of the oil at reference temperature of 68 °F (20 °C). The oil retention inside the microchannel evaporator A is normalized with respect to the total internal volume of the heat exchanger, that is,

$$ORV_{N,@OMF=2.8wt.}\% = \frac{OR_{volume@OMF=2.8wt.}\%}{V_{total,Evap A}} = \frac{180 \text{ cm}^3}{1,890 \text{ cm}^3} = 0.095 \text{ or } 9.5\%$$

In summary, for this example, if the OMF in the evaporator A is 2.8 wt.% then the oil occupies 9.5 percent of the total internal volume of the heat exchanger.

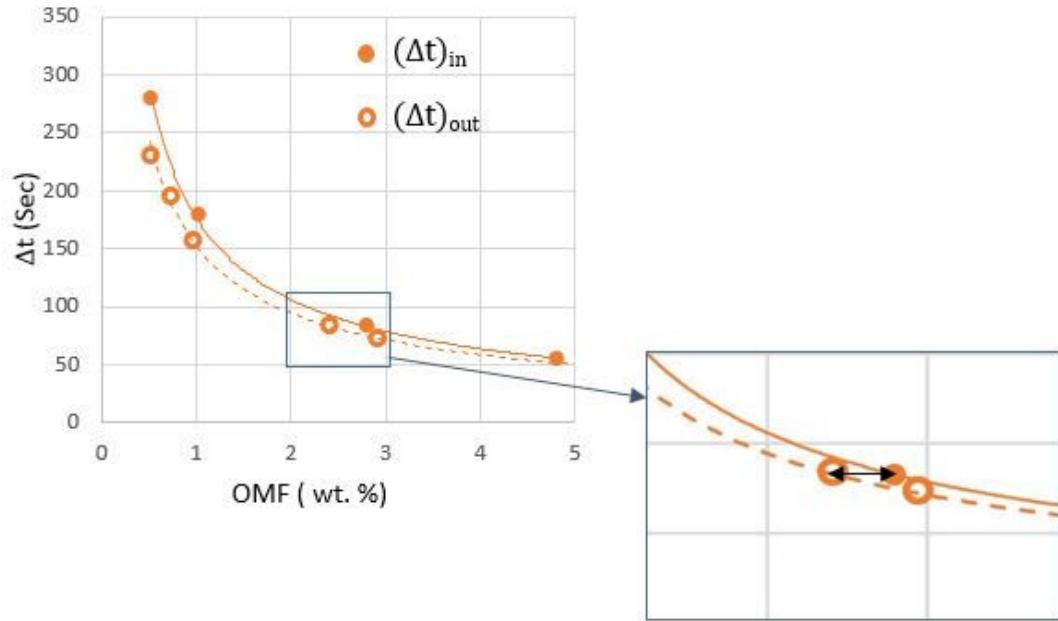
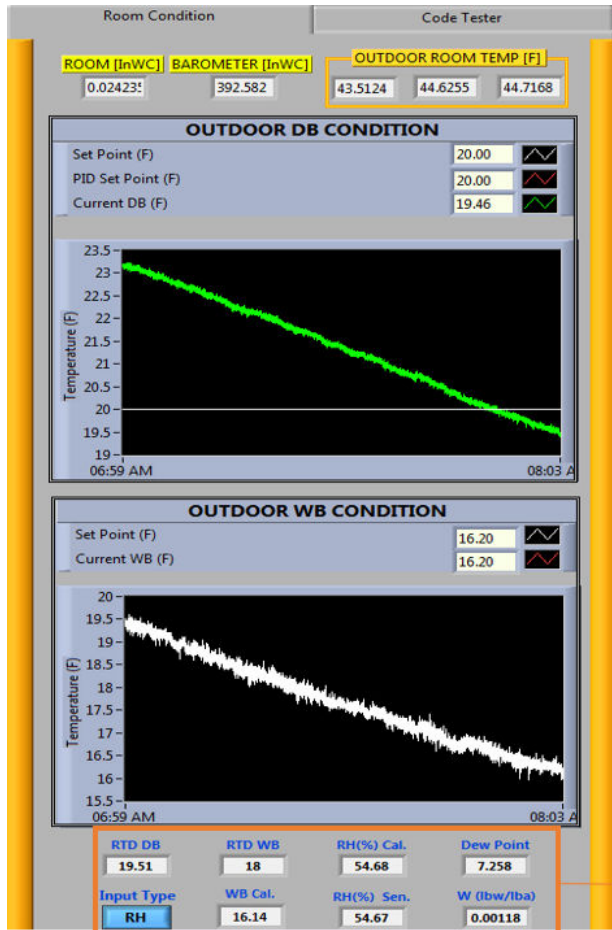


Figure 3.21: Example of time for the oil to travel along the pipeline versus OMF

Figure 3.22: Mass of oil measured when injected at the outlet of the test section ($M_{(OMF\%@outlet)}$) versus OMF and for two locations of the fight glasses.

3.3.3.5 Heat transfer experiments with dry fin tests conditions

Dry fin tests conditions were defined as when the moisture in the air did not condensate or did not frost on the microchannel evaporators air-side heat transfer surfaces during the period of the experiments. During the heat transfer experiments, the microchannel evaporators were tested in dry fin tests conditions. The dew point temperature of the entering air stream was lower than the refrigerant saturation temperature inside the evaporators. Figure 3.23 shows an example of the measurements of dry bulb temperature, wet bulb temperature and relative humidity (sensor) of air entering the test section. Dew point temperature was calculated using dry bulb and wet bulb temperatures for above freezing wet bulb temperature and the dry bulb temperature and relative humidity for below freezing wet bulb temperature.



Various Notation for information of air entering Microchannel Evaporator

1. RTD DB – RTD Dry Bulb temperature (°F)
2. RTD WB – RTD Wey Bulb temperature (°F)
3. RH(%) Cal. – Relative humidity calculated from Wet bulb and dry bulb (RTDs)
4. RH(%) Sen. – Relative humidity measured from sensor
5. WB cal. – Wet bulb calculated using RTD DB and RH(%) Sen.
6. Dew Point : Dew point of air entering microchannel calculated from RTD DB and RH(%) Sen.

Figure 3.23: Screenshot of the Labview graphic interface DAQ displaying the psychrometric conditions of the air at the inlet of microchannel evaporator

Figure 3.24 shows an example in which frost formation accidentally occurred on the fins of microchannel evaporator A during an experiment. For this case, the saturation temperature of the refrigerant R410A in test section was 32°F (0°C). Since the experiments were conducted at constant blower speed, a gradual but continuous decrease of the air flow rate was symptomatic that frost might have been occurred. The air side air flow rate was continuously monitored live during the experiments by using a Labview graphic interface DAQ for the air flow rate, shown in Figure 3.25. The pressure

difference across the nozzle, ΔP_{Nozzle} , was proportional to air flow rate across the evaporators. If frost formed on the fins, then the air flow rate decreased and any variation of the airflow rate was indicated by a decrease in the measured instantaneous ΔP_{Nozzle} . The decrease in ΔP_{Nozzle} was used as used an indicator that frost started to accumulate on the test section. If frost formation occurred, then the test was interrupted and a defrost cycle was initiated. In order to defrost the microchannel, the saturation temperature of refrigerant in microchannel evaporator A was raised higher than 40° F and the setup was run overnight with warm air that melted the frost. Then the test was repeated.

Figure 3.24: Example of a case in which frost formation on the microchannel evaporator A occurred during the experiments (the test was interrupted, the evaporator was defrosted, and then the test was repeated in frost-less conditions)

Figure 3.25: Display of the Labview graphic interface DAQ for the air blower and for the flow nozzles used to measure the air flow rate during the heat transfer experiments

3.3.4 Verification that the Two Methods Adopted in the Present Work for Measuring Oil Retention in the Microchannel Heat Exchangers Provided the Same Experimental Data

As discussed in the previous sections, the oil retention inside condenser tests described in section 3.3.2 were performed by measuring the extracted oil flow rate from the oil separators. This method required that pressure difference was established between the oil separators and oil reservoir through a complex network of pipelines, metering valves, and pressure equalization lines (see Figure 3.8). In the evaporator tests, it was not practical to establish a similar pressure difference because the evaporator outlet, i.e, the oil separator inlet, was already close to the lowest pressure point of the pump boiler loop. In the

evaporator tests, the pressure difference between the oil separator and the pump suction was not enough to drive the oil down from the oil separator into the oil level reservoir. Therefore, the measurement of the oil retention was based on the sight glasses and visual observation and timing method of the oil flow, when testing the microchannel heat exchangers in evaporator mode. Several tests were conducted to verify that two methods were equivalent and provided the same oil retention data within the experimental uncertainty. This section explains these verification tests.

First, it is important to emphasize that the efficiency of the oil separators of the pump boiler loop was not affected whether the test section was a condenser or an evaporator. Figure 3.26 and Figure 3.27 showed the thermodynamic state points of the refrigerant cycle in the pump-boiler test set up of the present work. The state points are plotted on P-h diagrams and each component of the cycle is indicated in plots. For example, the gear pump operated in the liquid mixture phase on the left side of the P-h diagrams for both condenser tests in Figure 3.26 and evaporator tests in Figure 3.27. The oil separators run on the far right location of the P-h diagrams, that is, in the superheated regions of the refrigerant and oil mixture. In other words, for both condenser and evaporator tests, the condition of oil and refrigerant mixture at the inlet of oil separators was always superheated vapor phase and the oil separation process inside the oil separators was similar between the condenser tests and the evaporator tests.

Figure 3.26: P-h diagram and corresponding components for condenser tests

Figure 3.27: P-h diagram and corresponding components for evaporator tests

Second, the equivalence of the oil retention volume measurements by using the collection of oil method in the oil level reservoir and the oil flow visual observation and timing method were performed for condenser tests and the results are shown in Figure 3.28. The data in this figure were obtained for refrigerant R410A at saturation temperature of 105°F (41°C) for OMF of 1.6 and 4.5 wt.%. The results showed that the oil retention volume normalized, ORV_N , for both methods were in good agreement and the two methods provide equivalent oil retention results. The ORV_N for the oil flow visual observation and timing method was slightly lower for both OMFs but the difference of ORV_N values of 0.004 and 0.006 was well within the experimental uncertainty for ORV_N , which was ± 0.01 and it is indicated by the error bars in Figure 3.28. These results provided some confidence that the oil flow visual observation and timing method was accurate enough to be used in the condenser tests. Because the oil separation process shared similar characteristics between the condenser and evaporator tests, we assumed that the relation of the ORV_N s between the two methods were valid for the evaporator tests.

Figure 3.28: Comparison between oil retention measurements in the condenser by using the two equivalent experimental techniques of the research.

3.4 Test Conditions and flow rates for the condenser and evaporators tests

The test conditions were selected based on typical applications for the refrigerants R410A and R134a in air conditioning systems and for refrigerant R134a in vending machines, water/wine coolers of a refrigeration systems. The saturation temperatures for the condenser tests were from 85 to 130°F (29 to 54°C) while for the evaporators tests, the saturation temperature varied from 32 to 48°F (0 to 9°C). Flow rates and OMFs are summarized in Table 3-4 below.


Table 3-4 Test matrix for typical air conditioning and refrigeration systems



Test No.	Saturation Temp. [°F] (°C)	Refrigerant & Oil	Refrigerant Flow Rate [lb _m /hr] (g/s)	Oil Mass Fraction [wt.%]	Component function / application
1	130 (54)	R410A/POE	600 (75)	0 0.5 1 3 5	Condenser AC unit
2	105 (41)	R410A/POE	400 (50)		
3	85 (29)	R410A/POE			
4	130 (54)	R134a/POE	450 (57)	0 0.5 1 3 5	Condenser / refrigeration condensing unit
5	105 (41)	R134a/POE	250 (31)		
6	95 (35)	R134a/POE			
7	48 (9)	R410A/POE	360 (45)	0 0.5 1 3 5	Evaporator A AC unit
8	38 (3.3)	R410A/POE	200 (25)		
9	32 (0)	R410A/POE			
10	48 (9)	R134a/POE		0 0.5 1 3 5	Evaporator A AC units, vending machines, water/wine coolers
11	38 (3.3)	R134a/POE	200 (25)		
12	33 (0.5)	R134a/POE			

3.5 Further Details of the Equipment and Instrumentation of the Experimental Facility

Table 3-5 provides a brief description of the main equipment and sensors used for the research. A state-of-the-art data acquisition system from National Instrument with Labview Real Time Controller was used for monitoring the tests, plotting, and recording the data. A designed pump-driven refrigeration system was used to control the saturation temperature of the refrigerant to the test section. A large variable speed fans was used to control the flow rate across the test section and for setting the environmental conditions during the tests. The heat transfer capacity was measured from the refrigerant side (primary method) and from the air side (secondary method) for redundancy. The main sensors are also shown on the right column of Table 3-5.

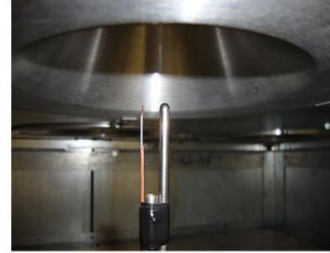
Table 3-5 Main equipment and sensors of the psychrometric chamber used in this study

Equipment	Sensors
Process Control and Data Acquisition System (DAQ) (National Instruments PXI controller platform)	Dry and Wet-bulb temperature probes inside chamber 

Equipment	Sensors
Labview and Real Time Controller	<p data-bbox="1008 365 1487 596">Dry-bulb and wet-bulb RDTs for air side measurements Dry bulb and wet bulb temperatures are measured according to ASHRAE standard 37 (ASHRAE, 1988)</p> 
Variable Speed Fan with VFD control	<p data-bbox="1013 890 1479 984">Hot wire anemometer for local velocity measurements</p> 
3 tons capacity water cooled heat pump unit. This unit will be used as auxiliary systems for outdoor room temperature below 40 °F	Air Pressure Transducers

5 tons capacity air cooled heat pump unit. This unit will be used as auxiliary systems to dehumidify the inlet air to the microchannel evaporator at low temperature tests

Air flow nozzle with RTD at the inlet of the nozzle. This calibrated nozzle measures the air flow rate according to ASHRAE standard 41.2 (ASHRAE, 1987)



3.5.1 Air Tunnel Apparatus

The microchannel heat exchanger is placed inside the psychrometric chamber, while the remaining components in the test setup are installed outside the chamber. This section describes the position of the microchannel heat exchanger inside the chamber, the instrumentation, and the fluid lines to the microchannel heat exchanger using images for clarity and emphasis.

Figure 3.29: Air flow loop inside the psychrometric chamber at Oklahoma State University (Deokar, 2013)

The primary method for measuring the capacity of the coil was to measure the heat transfer rate from the air-side of the heat exchanger. This air-side heat transfer rate is

calculated by measuring the air flow rate and the temperature difference of the air stream across the heat exchanger. A set of flow nozzles was used to measure the air flow rate and it was positioned downstream the heat exchanger as shown in the schematic of Figure 3.29. Two probes were used to measure the average air dry bulb temperature entering and exiting the heat exchanger. Figure 3.30 shows the side of the microchannel heat exchanger exposed to the ambient air.

Figure 3.30: Front side of the microchannel heat exchanger exposed to the ambient air (air flow direction is entering the heat exchanger as indicated by the yellow dashed arrow (Deokar, 2013))

The position of the microchannel heat exchanger in the duct (having a chamber approach) is such that it has the same face velocity of air over its entire slab. Figure 3.31 is the image, as seen from inside the duct, of the air supply side of the microchannel heat exchanger. A set of thermocouples was installed downstream to measure the air

distribution as show in the schematic of Figure 3.31 labelled as thermocouples grid row. The grid consisted of 18 welded thermocouples on the air supply side and was placed 1 in. away from the microchannel heat exchanger slab. The grid has 4 horizontal rows; starting from the top each row has 4, 5, 5, and 4 thermocouples.

Figure 3.31: Back side (in the direction of the air flow) of the microchannel heat exchanger (air flow direction is exiting the heat exchanger moving toward the fan (Deokar, 2013))

Because of space limitation the oil, liquid, and vapor lines entered the chamber through its wall, travelled inside the air supply duct, and emerge from the inner left wall of the duct as seen in Figure 3.32 upon which they were connected to the microchannel heat exchanger's header. The figure also shows the fluid lines coming out of the duct on the air (ambient) side and connecting to the microchannel heat exchanger. The connecting

lines inside the air supply duct are insulated to prevent their thermal interference with the air supply.

Figure 3.32 also shows the position of the inline thermocouple and the pressure transducer on the refrigerant vapor supply line and the refrigerant liquid (or two-phase) return line. The differential pressure transducer connected between the supply and return lines measures the pressure drop inside the microchannel heat exchanger. In the event of excess pressure drop across the supply and return lines, the ball valves in series with the differential pressure transducer are closed to isolate the transducer. The differential pressure transducer can also be protected by opening the needle valve, which is parallel to it, causing the pressure on both the sides of the transducer's diaphragm to balance and prevent its failure.

Figure 3.32: Instrumentation and configuration of refrigerant and oil lines connecting the microchannel heat exchanger

The air side condition entering the microchannel heat exchanger was monitored using air sampling devices. The sampling devices on the two sides of the microchannel heat exchanger, one exposed to the ambient air and the other on the side exposed to the supply air, were constructed according to ANSI/ASHRAE Standard 41.1(2013). The following section gives the description of the components of the sampling device and how they work.

The sampling trees shown in Figure 3.30 and Figure 3.31 were similar in construction. Each sampling tree was constructed of a horizontal 4 in. (10.16 cm) diameter PVC pipe, the ends were capped, and the center was connected to a flexible duct. The horizontal PVC pipe has 12 vertical branches made of 1.5 in. (3.81 cm) diameter PVC pipes. Holes drilled into the branches face the air flow. The construction of the tree helps to mechanically collect small samples of air (collected through these holes) over a large region, mix them in the central horizontal PVC pipe, and then transport the mixture further through the flexible duct.

A flexible duct carries the sampled air from the sampling tree to the relative humidity measurement probe. Further, the sampled air gets carried through a long PVC pipe to the dry bulb and wet bulb temperature-measuring RTDs. The long PVC pipe assists in having a fully developed flow before the air reaches the temperature sensors. The wet bulb probe has its own water reservoir in which its wick is dipped. A separate tank (seen in the top left corner of in-line centrifugal fan/blower helps to overcome the pressure drop in the 4 in. diameter flexible duct and the long PVC pipe from the sampling tree to the dry and wet bulb RTDs, inducing a sufficient air flow velocity of around 1000 ft/min (5 m/s) over the temperature sensors. The in-line centrifugal fan/blower from Suncourt Inc. Centrax (Model #TF104-CRD 4") has a capacity to have a flow rate of 200 cfm at least resistance. The flow rate at the temperature sensors is measured using a differential pressure transducer and a Pitot tube during the calibration phase. The blower then returns the sampled air back to the main airstream (on the downstream side of the sampling tree).

The sampling devices on the two sides of the microchannel heat exchanger, one exposed to the ambient air and the other on the side exposed to the supply air, were constructed

according to ANSI/ASHRAE Standard 41.1(2013). Each sampling tree was constructed of a horizontal 4 in. (10.16 cm) diameter PVC pipe, the ends were capped, and the center was connected to a flexible duct. The horizontal PVC pipe has 12 vertical branches made of 1.5 in. (3.81 cm) diameter PVC pipes. Holes drilled into the branches face the air flow. The construction of the tree helps to mechanically collect small samples of air (collected through these holes) over a large region, mix them in the central horizontal PVC pipe, and then transport the mixture further through the flexible duct. In-line centrifugal fan/blower helps to overcome the pressure drop in the 4 in. diameter flexible duct and the long PVC pipe from the sampling tree to the dry and wet bulb RTDs, inducing a sufficient air flow velocity of around 1000 ft/min (around 5 m/s) over the temperature sensors. The in-line centrifugal fan/blower from Suncourt Inc. Centrax (Model #TF104-CRD 4") has a capacity to have a flow rate of 200 cfm at least resistance. The flow rate at the temperature sensors is measured using a differential pressure transducer and a Pitot tube during the calibration phase. The blower then returns the sampled air back to the main airstream (on the downstream side of the sampling tree).

3.5.2 Chiller and Secondary Coolant Loop

The chiller loop is utilized to provide cooling to the airflow loop. The overall schematic of chiller loop can be seen in Figure 4.16 with blue solid line. As seen in the figure, the chiller loop is directly connected to the low temperature chiller. The model number of this chiller is CPCW-12LT/TC2-1-9X2 manufactured by Cooling Technology Inc. This low temperature chiller supplies up to 2.0 tons capacity with leaving temperature of -31.67°C (-25°F). The secondary coolant used by this chiller is Dynalene HC 40, while R404A refrigerant is used in the refrigerant side of the chiller. The chiller is equipped

with recirculating pump that supply up to 6 to 8 gpm with pressure rise between 25 to 30 psi (172.4 to 206.8 kPa). This chiller is equipped with integrated temperature controller which can be used to set and control the leaving fluid temperature.

This chiller is directly connected to refrigeration coil used to provide cooling to the air in the airflow loop. Additionally, one plate frame heat exchanger is installed in the chiller loop. This plate frame heat exchanger is used to exchange heat between the refrigerant in the chiller loop and the heat sink loop.

Figure 3.33: Chiller and heat sink loop

3.6 Instrumentation and Data Acquisition System

The oil retention measurement test facility utilized multiple sensors to measure the temperatures, pressures, mass or volume flow rates and other properties of air, refrigerant and oil. These sensors are discussed in brief in the following sections. These sensors were connected to National Instruments Data Acquisition (NI-DAQ) system with Real Time Labview Graphic Software Interface. The readings from the sensors were displayed, plotted, and recorded every 2 seconds. An example of the Labview graphic interface during one oil retention experiment is shown in Figure 3.34.

Figure 3.34: Labview control and graphic interface for oil retention tests

The graphic interface consisted of two screens: the control screen (top image in Figure 3.34) was used to provide the inputs to both the air side and refrigerant side control parameters of the test facility. The display screen (bottom image in Figure 3.34) plotted

all the readings from the sensors with time, which allowed us to identify stable and quasi steady state conditions of the test apparatus before starting the actual oil retention test.

The instrumentation and main equipment used in the test setup for the oil retention test apparatus are listed in Table 3-6, which provides manufacturer, model, and a short description of the specification and functionality of each component.

Table 3-6 Specification of the components used in the oil retention tests

Component	Manufacturer [Model]	Specifications and description of use
Ball Valves, Gate Valves, PVC pipes, Copper pipes and tubes, and fittings	Grainger Inc., Lowe's, McMaster-Carr, Locke Supply Co, United Refrigeration Inc.	Refrigeration system and Hydronic system (water side of the sub cooler, auxiliary heat exchanger and the evaporators).
Bladder Accumulator	McMaster-Carr [59595K12]	Capacity of 1 gallon; used to stabilize the flow of the refrigerant in the Pump-Boiler System.
Centrifugal pump	Taco [1400 – 50 –A]	Input: 230 V, 60 Hz, 1 phase, 2.4 A, 3450 rpm; used to provide necessary head at the sub cooler and the superheater's inline heater.
Check valve	McMaster-Carr [7775K12,7768K14]	One is used on the oil injection line and the other on the pressure equalization line.

Coalescent Separator	Temprite [925R]	Separates up to 0.05 microns particles, height: 28.6 in. (0.73 m), diameter: 4 in. (10.2 cm). The bottom 16.4 in. (41.6 cm) serves as a reservoir, which has sight glass for monitoring purpose. Internal float valve absent.
Compressor's oil level indicator	McMaster-Carr [1106K27]	Designed for maximum pressure of 290 psi, 9 in. in length; connected at the bottom of the compressor to check its oil/lubricant level.
DAQ wire	Olympic Wire and Cable Corp. [2824]	Multi-conductor 24 AWG cable; used to connect the sensors to the DAQ system.
Expansion Tank	Bell and Gosset [HFT- 15]	It has a total volume of 3 gallons and an acceptance volume of 1 gallon, the shell and diaphragm are made up of carbon steel and heavy duty butyl rubber respectively. It is pre charged to 12 psi, designed to handle 100 psi and 240°F, weight is 5 lbs.

Flow Switch - water flow circuits	Mcdonnell & Miller [FS6-3/4]	Allows minimum flow rate of 0.12 gpm and maximum flow rate of 2.5 gpm.
Gear Pump Motor	Baldor.Reliance Super-E motors [CEM3545]	Input: 230/460 V, 2.8/1.4 A, 60 Hz, 3 phase, usage: 0.75 kW, 1 hp, 3450 rpm; used for refrigeration and injection gear pumps
Helical separator	Henry Technologies Inc. [S-5188]	Designed for 10 cfm for 10 tons refrigeration capacity, height: 19 in. (48.3 cm), diameter: 4 in. (10.2 cm). Internal float valve absent.
High Temperature Heater Tapes	OMEGA Engineering Inc. [FWH171-060]	Input: 120 V, usage: 624 W with 5.2 W/in ² , resists up to 900 °F (480 °C); used to heat the oil-refrigerant mixture in the oil reservoir and the oil level tank.
High-Pressure Safety Valves	McMaster-Carr [5825T21]	The brass safety valve is placed after the refrigerant gear pump (not shown in any figures), and is designed to relieve the pressure from the system if it exceeds 500 psig (34.5 bar).

Inline Water Heater	Chromalox [NWHSRG 06-024PE1]	Heating capacity of 2 KW, 480V, 1 phase, INCOLOY® Sheath Element; used on the hot water loop having the refrigerant superheater.
Injection Gear Pump	Micropump	
Injection Oil Reservoir (Blue Tank), Oil Reservoir #1	Emerson Climate Technologies [AOR-4]	Capacity: 4 gallon (15.1 L), 2.5 ft. (0.88 m) tall; stores the oil to be injected using the injection gear pump.
In-Line Centrifugal Fan	Suncourt inc. Centrax [TF104-CRD 4"]	Input: 120 V, 0.53 A, 60 Hz, 1 phase, usage: 60 W, 4 in. (10.2 cm) air inlet and outlet, 200 cfm, in-line centrifugal fan; used as a fan/blower on the air sampling device.
Needle Valve 1/4"	Parker Hannifin Corp. [4A-V4LR-B]	Opens 10% per 1/2 turn - total 5.125 turns; used on the pressure equalization and the oil injection lines.
Needle Valve 3/8"	Parker Hannifin Corp. [6A-V6LR-B]	Opens 10% per 1/2 turn - total 5.5 turns; used for refrigerant mass flow rate control.

Oil Level Tank/Cylinder	Swagelok [304L-HDF8-1GAL]	Capacity: 1 gallon (3.79 L); oil level tank is made up of two of these cylinders.
Oil Reservoir #2	Parker Hannifin Corp. Sporlan Division [POR-3]	Capacity: 3 gallon (11.4 L), stores the oil separated from the vapor refrigerant and then supply it back to the suction line of the compressor.
Plate Heat Exchanger	GEA [GB400L-14]	14 plates, heat transfer area of 16 ft ² , and minimum heat transfer capacity of 15750 Btu/h
Refrigerant Filter-Dryer	Parker Hannifin Corp. Sporlan Division [C-032]	Size of 3 in ³ , removes moisture, dirt, acid, and sludge; initially was used on the refrigerant liquid line, then was transferred on oil line to filter it.
Refrigerant Filter-Dryer	Parker Hannifin Corp. Sporlan Division [C-083-S-HH 3/8]	Size of 8 in ³ , removes moisture, dirt, acid, and sludge; used after the refrigerant gear pump.
Refrigeration Gear Pump	Micropump [GC-M25.JVS]	0.48 gallon/1000-rev (1.82 ml/rev), maximum differential pressure: 125 psi (862 kPa)

Remote gas bulb control thermostat	Honeywell [L4008A]	Control thermostat with high temperature limit of 150°F (66°C); used on the Vapor Compression cycle system.
Scroll Compressor	Copeland [ZF15K4E-PFV]	Used on the Vapor Compression cycle system.
Service Manifold	Ritchie Engineering Co., Inc. YELLOW JACKET product division [Series 41]	Used to charge and recover the refrigerant from the system.
Sight glass	McMaster-Carr [1138K64]	Pipe size - 1/2 in; used to monitor the oil-refrigerant extraction at the oil separators, and also to ensure that liquid refrigerant enters the refrigerant gear pump (not shown in any figures)
Sight Glass Tube/ Level Indicator	McMaster-Carr [1106K76]	Designed for maximum pressure of 240 psi, viewing glass of 18 in. length; it is graduated and connected to oil level tank to measure the volume of the extracted oil-refrigerant mixture.

Suction Line Accumulator	Grainger Inc. [6AXD3]	Placed on the suction line to prevent any liquid refrigerant to enter the compressor.
Suction line Filter-Dryer	Parker Hannifin Corp. Sporlan Division Catch-All [C-417-S-T-HH]	Separates moisture, dirt, acid, sludge doing to the compressor
Variable frequency Drive	Baldor Electric Company [VS1SP21-1B]	Input: 230 V, 4.2 A, 60 Hz, 3 phase, usage: 0.75 kW, 1hp; Configured for the motors of the refrigerant gear pump and the injection gear pump.
Variable Transformer	Superior Electric [3PN116C]	Input: 120 V, 50/60 Hz, 1 phase, 1.4 KVA, output: 0 - 120V; variac for the heater tapes.

3.6.1 Temperature Measurements

The temperature sensors on the air side were resistance temperature detector-type (RTD). RTD works based on the effect of temperature on the electrical resistance of material, in this case, platinum. Platinum is chosen in place of nickel or copper on account of its inertness, and also because its temperature and resistance relation is repeatable over a large temperature ranges. In this study, RTDs were used to measure dry and wet bulb temperatures at the inlet and outlet of the air flow across microchannel heat exchanger. It

was also used to measure the temperature of air at the inlet other nozzle bank ($T_{N,i}$). The specification is listed in Table 3-7.

Table 3-7 Specifications of Resistance Temperature Detectors

Item	Item Specification
Model	P-M-1/3-1/8-6-0-T-3
Type	Pt100
Range	-148 to 752°F (-100 to 400°C)
Accuracy	Accuracy 1/3 DIN (-50 ±0.18°C, 0 ±0.1°C, 100 ±0.27°C); ±0.1°F (±0.05°C) after calibration.
Description	100 Ω at 0°C; temperature coefficient of resistance = 0.00385 Ω/Ω/°C; 6" length, 1/8" diameter
Manufacturer	Omega Engineering, Inc.

A thermocouple (TC) works on the principle of the thermoelectric effect, more precisely the Seebeck effect; where a junction (TC) of two dissimilar metals produces voltage when there is a temperature difference between the junction and the voltmeter. The voltage generated across the TC is then calibrated with the help of a reference cold junction to produce an accurate temperature reading. Thermocouples are used on air side, oil side and refrigeration side. The specifications of the TCs are shown in Table 3-8.

Table 3-8 Specifications of the Thermocouples

Item	Item Specification
Type	T-type
Model: Inline Thermocouple	TMQSS-125G-6
Model: Thermocouple Wire	TT-T-24-SLE-1000, the wire needs to be welded.
Range	-40 to 130°F (-40 to 54°C)
Accuracy	±0.5°F (0.3°C); ±0.1°F (±0.05°C) after calibration.
Manufacturer	Omega Engineering, Inc.

Inline thermocouples are installed to measure the temperatures at the refrigerant gear pump inlet ($T_{pump,i}$), the microchannel condenser inlet ($T_{mchx,i}$), the microchannel condenser outlet ($T_{mchx,o}$), and the evaporator outlet ($T_{evap,o}$). They are also used to measure the temperature of the extracted oil-refrigerant mixture from the oil extraction device ($T_{oil-ref,o}$), and the temperature of the injected oil-refrigerant mixture ($T_{oil-ref,i}$). These inline thermocouples are placed in the stream of oil and refrigerant using compression fittings to prevent any possible leaks.

A grid of 18 welded TCs is used on the air supply side of the microchannel heat exchanger. This grid helps in calculating the heat transfer to the air on selected sections of the microchannel heat exchanger slab. A TC is also placed at the inlet of the nozzle in parallel with the RTD, for cross-referencing.

Several welded TCs are attached to external surfaces of the copper fluid line at particular locations where the measurement of temperature is required. The attachment is done with

a layer of thermal grease between the tip of a welded TC and the surface to reduce the contact resistance. The readings from these surface TCs are not used in the data analysis but they help to provide a better and more predictive control over the system. For example, the TCs used to measure the water temperatures in and out of the secondary condenser/sub cooler helped the system operator maintain a definite refrigerant subcooling at the gear pump inlet, or, the measurement of hot water temperatures at the evaporator helped in maintaining the superheat and the pressure of the system. TCs also help in activating the shut-off limits of the pumps; a two-phase flow or no flow will shut down the pump, preventing further damage. A welded TC is attached to the fin of the microchannel heat exchanger when capturing the infrared images in order to calibrate the camera.

Calibration of the TCs and the RTDs is done in a temperature bath with reference to a NIST (National Institute of Standards and Technology) traceable thermometer having an accuracy of $\delta T_a = \pm 0.36^\circ\text{F}$ ($\pm 0.2^\circ\text{C}$). The software by National Instruments, Measurement & Automation Explorer (MAX) is used along with the NI-DAQ to record the data points at a sampling rate of 1 millisecond (1 kHz) during the calibration. These TCs and RTDs are calibrated to an uncertainty of $\delta T_b = \pm 0.05^\circ\text{F}$ ($\pm 0.03^\circ\text{C}$) with respect to the thermometer. Adding the errors in the thermometer and the calibrated TCs or RTDs in quadrature (Taylor 1996), gives the net error or uncertainty δT of 0.36°F ($\pm 0.2^\circ\text{C}$) in temperature measurements. Temperature measurements using the RTDs and TCs followed and exceeded the ANSI/ASHRAE Standard 41.1 (2013).

3.6.2 Oil and Refrigerant Pressure Measurements

Absolute pressure transducers are installed to measure the pressures at the refrigerant gear pump inlet ($P_{pump,i}$), the microchannel condenser inlet ($P_{mchx,i}$), the microchannel condenser outlet ($P_{mchx,o}$), and the evaporator outlet ($P_{evap,o}$). They are also used to measure the pressure of the extracted oil-refrigerant mixture between the oil extraction device and the oil level tank ($P_{oil+ref,o}$), and to measure pressure of the injected oil-refrigerant mixture ($P_{oil+ref,i}$) using the transducer at the oil reservoir. The specifications of the absolute pressure transducer are shown in Table 3-9. The absolute pressure transducers measuring the refrigerant's vapor pressures at the evaporator outlet and at the oil separators have a sufficient draft of air flowing over them to prevent a high temperature at their circuitry that might damage the sensor or drift the readings. For refrigerant and oil lines having less than 5/8 in. (15.8 mm) outer diameter, the tubing to the pressure transducers is of the same size, while for higher diameter copper lines, the tubing are kept as small as possible to avoid turbulence at the sensor, which could measure total pressure instead of static pressure. Bourdon tube gauges are also used at the oil level tank and the oil reservoir to visually check the pressures while controlling it through the needle valves on the pressure equalization lines. All the pressure measurements on the refrigerant, oil, and air side are done according to ANSI/ASHRAE Standard 41.3 (2014).

Table 3-9 Specifications of the Absolute Pressure Transducers

Item	Item Specification
Model	206
Pressure Range	7 to 500 psia (50 to 3450 kPa)
Accuracy	± 0.65 psi (± 4.5 kPa)
Output	24 VDC Nominal
Excitation	0-5 VDC
Manufacturer	Setra System, Inc.

A differential pressure transducer was placed between the inlet and the outlet lines connecting the microchannel heat exchanger slab. It measures the pressure drop experienced by the refrigerant or the oil-refrigerant mixture when flowing through the resisting ports of the micro-channels. Figure 3.32 shows the position of the transducer. The specifications of the differential pressure transducer are shown in Table 3-10.

Table 3-10 Specifications of the Differential Pressure Transducers

Item	Item Specification
Model	P55D-4-N-4-40-S-4-A
Pressure Range	8 to 12.5 psi (55 to 86 kPa), actually it can measure 0 psi.
Accuracy	$\pm 0.25\%$ of full scale; ± 0.03 psi
Output	4 to 20 mA
Excitation	9-55 VDC
Manufacturer	Validyne Engineering

3.6.3 Air Humidity Measurements

The relative humidity (ϕ or RH) values of the ambient air and the air supplied by the microchannel heat exchanger are measured and then used along with the dry bulb temperatures to determine the density of the air flowing across the heat exchanger. The specifications are shown in Table 3-11.

Table 3-11 Specifications of the Relative Humidity Sensors

Item	Item Specification
Model	HX71-MA
Operating temperature range	-13 to 185°F (-25 to 85°C)
Accuracy	$\pm 3.5\%$ from $\phi = 15\%$ to $\phi = 85\%$; $\pm 4\%$ below $\phi = 15\%$; and $\pm 4\%$ above $\phi = 85\%$ when measured at 73.4°F (23°C).
Manufacturer	Omega Engineering, Inc.

3.6.4 Air Flow Measurements

The airflow nozzles are arranged in parallel at the nozzle bank to have a pressure drop in the airflow path. Pressure drop measurements are used to calculate the air flow rates (*CFM*). This *CFM* value is then used for the air side calculations, to check the heat balance with the refrigerant side calculations. All the air flow measurements are done according to the ANSI/ASHRAE Standard 41.2 (1987). The specifications of the nozzles are shown in Table 3-12.

Table 3-12 Specifications of the Air flow Nozzles

Item	Item Specification
Model	Elliptical nozzle
Metal	Aluminum
Bore Diameter	8" (203 mm), 7" (178 mm), and 0.5" (12.7 mm)
Operating range	150 to 2,000 cfm (0.07 to 1 m ³ /s)
Accuracy	±0.4% of flow rate (using Setra 264 pressure transducer and precise calculation of uncertainty propagation); Tightest Tolerance ±0.001" (±0.0254 mm) = error in bore diameter.
Manufacturer	Helander Metal Spinning Company

Very low differential pressure measurement of air was performed by an unidirectional differential pressure transducers, 2641-003WD, measure the air pressure drop across the nozzle bank ($\Delta P_{air,N}$, $\Delta P2$) and the microchannel heat exchanger ($\Delta P_{air,mchx}$, $\Delta P1$), while 2641-2R5WD measures the static pressure of the Psychrometric test room ($P_{air,amb}$, $P1$) in which the microchannel heat exchanger is placed. The bidirectional differential pressure transducer, 2641-1R5WB, measures the static pressure before the nozzle bank ($P_{air,N,i}$, $P2$). The specifications are shown in Table 3-13. Simple Pitot tubes are used to measure the pressure inside the air ducts; they are either purchased or constructed from small size copper tubes. As recommended, these Pitot tubes have holes of 1/16 in. (1.6 mm) diameter perpendicular to the direction of the air flow.

Table 3-13 Specifications of the Very Low Differential Pressure Transducers

Item	Item Specification
Model	264
Manufacturer	Setra System, Inc.
1.) Unidirectional Transducer	2641-003WD
Pressure Range	0 to 3 in. W.C. (0 to 747 Pa)
Accuracy	±0.25% of full scale; ±0.0075 in. W.C.
Output	24 VDC Nominal
Excitation	0-5 VDC
2.) Unidirectional Transducer	2641-2R5WD
Pressure Range	0 to 2.5 in. W.C. (0 to 623 Pa)
Accuracy	±0.25% of full scale; ±0.00625 in. W.C.
Output	0-5 VDC Nominal
Excitation	9-30 VDC
3.) Bidirectional Transducer	2641-1R5WB
Pressure Range	±1.5 in. W.C. (±373 Pa)
Accuracy	±0.25% of full scale; ±0.0075 in. W.C.
Output	24 VDC Nominal
Excitation	0-5 VDC

3.6.5 Oil Volume Measurements

As described in the previous sections, in order to measure the oil retention volume in the test section, the amount of oil mass injected at the inlet of the test section and extracted at the outlet of the test section must be measured first. The oil mass balance provide the oil mass that was retained in the test section and in the connecting pipeline. By taking out the oil retained in the pipeline downstream the test section, which is measured in the same manner with the pipeline being the only component present between injection and extraction ports, the oil retained in the test section is determined. While the amount of oil mass injected at the inlet of the test section (or at the inlet of the downstream pipeline) was simple to measure by using a Coriolis mass flow meter, that is, the oil mass injected was the result from the time integration of the mass flow rate of oil pushed to the injection port from the oil gear pump, measuring the amount of oil extracted at the outlet of the test section (also the outlet of the downstream pipeline) was not a trivial task and it requires some more explanation.

First, the liquid mixture extracted was not only oil but rather a mixture of oil and liquid refrigerant. The oil and refrigerant mixture from the oil separators circulated to a second Coriolis mass flow meter (referred to as “extraction flow meter”) and then it was stored in the oil level tank only if enough pressure differential was established to drive such flow. However, the pressure differential could not be too high as to divert the main stream of refrigerant vapor to the extraction flow meter because it would skew the measurements of the flow rate of liquid mixture present at the outlet of the test section. It should be emphasized here that we refer to liquid mixture because refrigerant is soluble in POE oil and thus the liquid collected at the extractor consists of POE oil and of

refrigerant dissolved in it. A set of pressure balancing lines and multiple metering valves were installed to regulate the pressure gradient across the extraction flow meter. Oil tanks were installed downstream to this flow meter, and they had an oil level sensor in order to measure the volume of liquid mixture that was stored inside the tanks. During condenser tests, the volume of mixture in the oil level tank was measured by using a custom made graduated sight glass tube installed next to the tanks and connected in parallel. An additional electric capacitance level probe was used to confirm the readings from the sight glass at regular time intervals. Both the sight glass and the electric capacitance probe measured the rate of volume increase of the mixture in the tank, or in other words, the rate of liquid mixture extracted at the outlet of the test section over time. The temperature and the pressure of the extracted mixture were measured so that density and the solubility of the mixture were estimated. Thus, once how much refrigerant dissolved in the extracted mixture was known, the actual mass of oil extracted was calculated.

The oil level tank consisted of two steel cylinders and a copper tube connected in parallel configuration. Both the steel cylinders had a volume of about 1 gallon (3.7 liters). Two 18 inches (~46cm) long sight glass tubes were marked every 5 mL and 20 mL, respectively and they were staggered vertically in order to provide about 36 inches (92 cm) of graduated level scale for the mixture stored in the tanks. The sight glasses were installed in parallel to a vertical copper tube of 0.75 inch inner diameter, which was used when the oil extracted rate was very low in order to augment the sensitivity of the oil level measurements. The oil level tanks were opened to the oil loop only when the oil extracted rate was high in order to extend the time of the test. For this case, the rate of accumulation of the mixture in the tanks was high and the vertical copper tube was not

sufficient to collect all the liquid mixture. Both sight glass and capacitive level sensor were calibrated in-situ in preliminary tests by pouring a known amount of oil from at the top. While the sight glass level sensor provided the volume of liquid stored inside the tanks independently from the nature and type of the liquid, the capacitive level probe was affected by the presence of refrigerant dissolved in the oil. Often the dielectric constant of the extracted liquid mixture and the presence of flash vapor inside the tanks skewed the measurements of volume when looking at the output from the capacitive electric level probe sensor. For this reason, the sight glass level sensor was a preferred approach. Figure xx shows the detailed schematic of the oil level tank system. One steel cylinder was installed vertically while the second cylinder was slightly tilted. The cylinders were staggered in the vertical direction and a set of manual shut off valves were used to open or isolate each cylinder to/from the system. This configuration helped the sensitivity of the measurements of volume of mixture that was stored in the tanks. If the rate of mixture extraction was high or for long periods of time, both cylinders were opened to the system. The mixture reached the vertical cylinder first and, only after it exceeded the cylinder capacity, it started to fill the tilted cylinder, too. If the rate of mixture extraction was low, both cylinders were isolated and not used during the tests. Only the vertical copper tube was used to measure the volume of mixture extracted from the oil separator during the tests. Figure xx shows the calibration curve of the oil level tank, which was used to measure the volume of liquid mixture extracted. The calibration process involved pouring a known amount of volume of oil in the tank and marking the oil level every 5.0 mL on a graduated scale next to the sight glasses.

The oil level tanks were used in preliminary tests conducted with the vapor compression based test apparatus. With this apparatus, the extraction flow meter was a redundant method to verify the amount of liquid mixture extracted from the oil separator. However, for the pump-boiler test apparatus, there was not sufficient pressure gradient to drive the liquid mixture flow to the extraction flow meter and to the oil level tanks for long period of time. As liquid accumulated inside the tanks, the pressure inside them rose and the flow of extracted mixture stopped. Thus, for the pump-boiler test apparatus, refrigerant vapor was taken out from the top of the oil level tanks to an empty refrigerant cylinder. The rate was slow but continuous in order to control the pressure of the tanks downstream the extraction flow meter and thus to provide a minimum pressure gradient across the extraction flow meter to circulate (and measure the flow rate of) the extracted liquid mixture. At the same time, refrigerant was slowly pumped in to the refrigerant loop to conserve the total mass of refrigerant in the system. This approach successfully controlled the pressure gradient across the extraction flow meter without disturbing or interfering with the main refrigerant loop operating conditions. The time integration of the flow rate from the extraction flow meter provided the cumulative amount of liquid mass that was extracted from the oil separator.

Figure 3.35: Calibration curve for the oil level tank to measure the volume of oil extracted during initial test setup (Deokar, 2013)

The mass flow rate of the refrigerant (\dot{m}_{ref}), the injected oil-refrigerant mixture ($\dot{m}_{oil-ref,inj}$), and the extracted oil-refrigerant mixture ($\dot{m}_{oil-ref,ext}$) are measured using the Coriolis flow meter. The mass of the oil injected at the microchannel heat exchanger ($m_{oil,in}$) is measured by integrating the value of the mass flow rate of injected oil with the time-period of the test. The Coriolis meter can be used to measure either liquid or gas mass flow rate, but it is only employed to measure liquid mass flow rates. The specifications for the mass flow meters are shown in Table 3-14 and Table 3-15, respectively. The mass flow meter CMF025 is placed between the refrigerant gear pump

and the evaporator to measure the pumped refrigerant mass flow rate. One mass flow meter CMF010M is placed at the oil outlet/drain of the oil separator to measure the extracted oil-refrigerant mixture, while the other is placed after the injection gear pump on the injection line to measure the injected oil-refrigerant mixture's mass flow rate.

Table 3-14 Specifications of the Refrigerant Mass Flow Meter

Item	Item Specification
Model	(CMF025) CMF025M319NRAAEZZZ
Type	Coriolis Flow and Density Meter
Transmitter	2700C12BBAEZZZ
Flow rate range	4800 lbm/h (2180 kg/h)
Flow rate accuracy	±0.10% of the flow rate
Zero stability	0.06 lbm/h (0.027 kg/h)
Density range	312 lbm/ft ³ (5000 kg/m ³) or (5 g/cm ³)
Density accuracy	±0.0312 lbm/ft ³ (±0.5 kg/m ³)
Temperature range	300°F (148°C)
Temperature accuracy	±2°F (±1°C)
Output	4 to 20 mA
Pressure rating for sensor	1500 psig (10.4 MPa)
Manufacturer	Micro Motion Inc.

Table 3-15 Specifications of the Oil-Refrigerant Mixture Injection and Extraction Mass Flow Meter

Item	Item Specification
Model	(CMF010M) CMF010M323NRAAEZZZ
Type	Coriolis Flow and Density Meter
Transmitter	2700C12BBAEZZZ
Flow rate range	240 lbm/h (108 kg/h)
Flow rate accuracy	±0.10% of the flow rate
Zero stability	0.0045 lbm/h (0.002 kg/h)
Density range	312 lbm/ft ³ (5000 kg/m ³) or (5 g/cm ³)
Density accuracy	±0.0312 lbm/ft ³ (±0.5 kg/m ³)
Temperature range	300°F (148°C)
Temperature accuracy	±2°F (±1°C)
Output	4 to 20 mA
Pressure rating for sensor	1813 psig (12.6 MPa)
Manufacturer	Micro Motion Inc.

According to the manufacturer, the rated accuracy of the mass flow meter is ±0.10% of the flow rate. But, if the actual flow rate is less than $\frac{\text{zero stability}}{0.001}$, then the accuracy is $\pm \left(\frac{\text{zero stability}}{\text{flow rate}} 100 \right)\%$ of the flow rate. The oil-refrigerant mass flow rate in the system varied from 3 to 20 lbm/h. The $\frac{\text{zero stability}}{0.001} = \frac{0.0045}{0.001} = 4.5$ lbm/h, which means that the flow rate from 3 to 4.5 lbm/h has the uncertainty greater than ±0.10% of the flow rate. If calculated, the uncertainty at 3 lbm/h is ±0.15% of the flow rate. Comparing the

percentage of the net region of 4.5 to 20 lbm/h with the region of 3 to 4.5 lbm/h it will be reasonable to choose the uncertainty as $\pm 0.10\%$ of the flow rate. This is illustrated in Figure 3.36. The refrigerant mass flow rate in the system is always greater than 300 lbm/h, while the $\frac{\text{zero stability}}{0.001} = \frac{0.06}{0.001} = 60$ lbm/h, which is very small compared to the flow rate of the refrigerant in the system. Hence, the uncertainty in the refrigerant flow rate is $\pm 0.10\%$ of the flow rate.

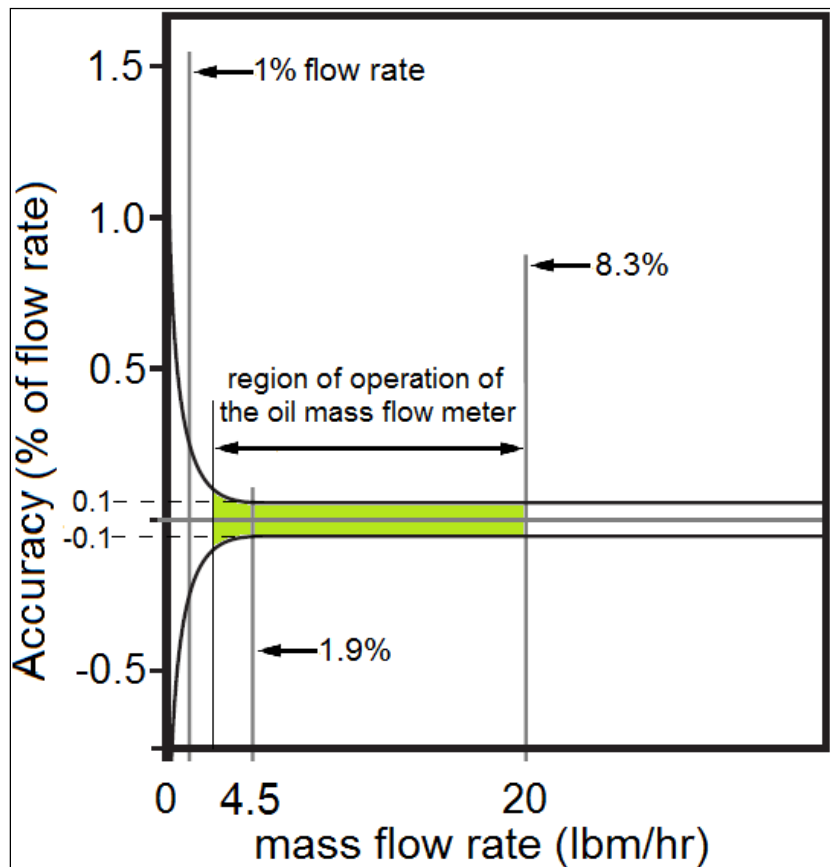


Figure 3.36: Relation between the flow meter accuracy and the mass flow rate

A weighing scale is used to measure the weight of the oil-refrigerant samples collected at the end of each injection test to determine the solubility of the refrigerant in the oil using

the gravimetric method. The specifications of the weighing scale are shown in Table 3-16.

Table 3-16 Specification of the Weighing Scale

Item	Item Specification
Model	SAW-L
Capacity	50 lb (22 kg)
Resolution	0.0005 lb (0.2 g)
Accuracy	$\pm 0.01\%$ of full scale; ± 0.005 lb (± 2.2 g)
Manufacturer	Arlyn scales

CHAPTER IV

4 Data Reduction and Uncertainty Analysis

4.1 Data Reduction

The amount of oil carried over with the refrigerant in the microchannel heat exchanger was referred to as the oil mass fraction (OMF) and it was defined as follows:

$$OMF = \frac{\dot{m}_{oil}}{\dot{m}_{oil} + \dot{m}_{ref}} \times 100 \quad 4-1$$

where \dot{m}_{oil} was the measured flow rate of the oil released to the test section and \dot{m}_{ref} was the measured flow rate of refrigerant in the test setup. Oil was injected at the inlet of the test section with OMF of x wt.%. Once the travel time for the oil to go from S1 to S2 was estimated, the corresponding OMF of $(x - \delta x)$ wt.% for the injection at the outlet of the test section was also found. It should be notice that for the δx was small and for some of the tests it was zero. For these two OMFs identified, the oil travelled in the pipeline downstream the test section with the same velocity. Now that the two OMFs for which the flow conditions in the pipeline downstream the test section were the same were identified, the oil retention was calculated as follow:

$$\begin{array}{l} \text{Oil retention} \\ \text{mass in the test} \\ \text{section} \end{array} = \begin{array}{l} \text{Oil retention mass in the test} \\ \text{section plus in the pipeline} \end{array} - \begin{array}{l} \text{Oil retention mass in} \\ \text{the pipeline} \end{array} \quad 4-2$$

That is,

$$OR_{mass@OMF=x \text{ wt.}\%} = Ma_{@OMF=x \text{ wt.}\%@inlet} - Mb_{@OMF=(x-\delta x) \text{ wt.}\%@outlet} \quad 4-3$$

Where

$$Ma_{(@OMF=x \text{ wt.}\%@inlet)} = \int_{t_{0,in}}^{t_{1,in}} \dot{m}_{oil,injected@inlet} dt = Ma \text{ [grams]} \quad 4-4$$

and

$$Mb_{(@OMF=(x-\delta x) \text{ wt.}\%@outlet)} = \int_{t_{0,out}}^{t_{1,out}} \dot{m}_{oil,injected@outlet} dt = Mb \text{ [grams]} \quad 4-5$$

And where $\dot{m}_{oil,injected} = \frac{\dot{m}_{oil,injection}}{(1+S)}$ was the mass flow rate of oil injected at the inlet

and at the outlet by subtracting the amount of refrigerant dissolved in the oil. The time $t_{0,in}$ and $t_{0,out}$ were the times at which the oil was first released to the inlet and outlet of the test section. The time $t_{1,in}$ and $t_{1,out}$ were the times at which the oil was detected at the sight glass S1 for oil injection at the inlet and outlet of the test section. The final oil retention mass in the test section was calculated as follows:

$$OR_{mass@OMF=x \text{ wt.}\%} \text{ [grams]} = Ma - Mb \quad 4-6$$

And the oil retention volume in the test section was calculated as follows:

$$OR_{volume@OMF=x \text{ wt.}\%} \text{ [cm}^3\text{]} = \frac{OR_{mass@OMF=x \text{ wt.}\%} \text{ [grams]}}{\rho_{oil@68^\circ\text{F}} \text{ [grams/cm}^3\text{]}} \quad 4-7$$

Where ρ_{oil} was the density of the oil at reference temperature of 68 °F (20 °C). The oil retention inside the microchannel heat exchangers was normalized with respect to the total internal volume of the heat exchanger, that is, internal volume of the tubes plus the internal volume of the headers:

$$ORV_{N,@OMF=x\ wt.\%}[-] = \frac{ORvolume_{@OMF=x\ wt.\%}}{V_{total,internal\ volume}} \quad 4-8$$

The ORV_N was a dimensionless number that varied from 0 for the case of no oil retained in the heat exchanger to 1, if the heat exchanger was completely filled up with oil. In the experiments ORV_N varied from 0.01 to 0.15, that is, the oil retained in the heat exchanger ranged from 1 up to 15 percent of the total internal volume of the heat exchanger. An example of the above data reduction procedure was provided in section 3.3.3.4 of this dissertation.

The amount of oil retention in the microchannel heat exchanger offers an additional resistance to refrigerant flow. If the OMF increases, oil retention in the test section increases as well. Consequently the pressure drops depend upon the refrigerant flow rate and on the OMF in the circulating refrigerant-oil mixture (Cremaschi *et al.*, 2005). The oil effect on pressure drop was estimated by measuring the pressure drop in the test section at specific mass flow rates and OMFs. The refrigerant side pressure drop at the measured OMF, $\Delta p_{with\ oil}$ was compared to the corresponding pressure drop across the test section at the same total mass flow rate but with no oil present, $\Delta p_{without\ oil}$. The pressure drop factor (PDF) was used to represent the effect of the oil and it is defined as follows:

$$PDF = \frac{\Delta p_{with\ oil}}{\Delta p_{without\ oil}} \quad 4-9$$

The PDF is a cumulative factor that account for both acceleration and friction pressure drop components e.g. alteration of two-phase flow regime, increase in the liquid phase viscosity and the reduction of the free-flow area available to the refrigerant flow due to the oil retention.

Similarly, the microchannel heat exchanger heat transfer capacity factor, HTF, was calculated based on the heat transfer capacity measured during test with oil and the corresponding operating conditions without oil, as follows:

$$HTF = \frac{\dot{Q}_{air,with\ oil}}{\dot{Q}_{air,without\ oil}} \quad 4-10$$

Where \dot{Q}_{air} is the heat transfer rate measured from the air side of the heat exchanger at given test condition by using the following equation:

$$Q_{air} = \rho_{air} \cdot CFM \cdot 60 \cdot c_p \cdot (T_{air,out} - T_{air,in}) \quad 4-11$$

The volume flow rate of the air, CFM , through the microchannel heat exchanger was calculated from the pressure difference across the flow nozzle in agreement with the ANSI/ASHRAE Standard 41.2 (ASHRAE 1987). The properties of air were estimated by using ASHRAE Handbook – Fundamentals (ASHRAE 2001). The dry bulb temperature of the inlet air ($T_{air,in}$), the dry bulb temperature of the outlet air ($T_{air,out}$) from the microchannel heat exchanger, and the volume flow rate (CFM) were measured. The density of the air (ρ_{air}) was estimated based on the temperature of the air stream at the flow nozzle and the specific heat was $c_p = 0.2405$ Btu/lbm-°F, and it did not change significantly between two pair of tests with and without oil. Since the air flow rate was

also constant between two pair of tests with and without oil, the HTF can be reduced to the following result:

$$HTF \approx \frac{\rho_{air,with\ oil} \cdot (T_{air,out\ with\ oil} - T_{air,in})}{\rho_{air,without\ oil} \cdot (T_{air,without\ oil} - T_{air,in})} \quad 4-12$$

Where the variations in specific heat at constant pressure of the air were neglected because they were small. While Eq. (4-10) is more accurate and it was used in the present study, equation (4-12) shows that the HTF is basically dependent only on temperature measurements. Thus, the experimental uncertainty on the HTF was fairly small.

An example of HTF calculation during the condenser test is given next. The oil-refrigerant mixture was injected upstream of the microchannel heat exchanger at a mass flow rate of $\dot{m}_{oil+ref,inj} = 27 \pm 0.006$ lbm/h. The gravimetric method determines the solubility of this injected mixture as $S = 47.25 \pm 2.18\%$ w/w. The total mass flow rate of the oil-refrigerant mixture at the inlet of the microchannel heat exchanger was $\dot{m}_{ref,test-section} = 395.8 \pm 0.005$ lbm/h. The inlet pressure and superheat temperature measured at the inlet of the microchannel condenser were $P_{mchx,i} = 353.04 \pm 0.65$ psia and $T_{mchx,i} = 111.79 \pm 0.36$ °F, respectively. The heat transfer rate of the microchannel condenser rejected to the air during the injection test causes the temperature of the air to rise and by using equation (4-11) the calculated heat transfer is during this condition is $Q_{with\ oil} = 26,632.02 \pm 1441.37$ Btu/h. The oil-refrigerant fluid pressure drop measured by the differential pressure transducer during the injection test is $\Delta P_{@OCR} = 2.74 \pm 0.03$ psid. Using the mapping data the heat transfer and pressure drop in absence of oil are

interpolated at *same total flow rate and the inlet pressure* as $\dot{Q}_{without\ oil} = 27,215.63 \pm 1441.37$, and $\Delta P_{@OCR=0} = 2.40 \pm 0.03$ psid, respectively. Using equation 4-10, the HTF was calculated as:

$$HTF = \frac{\dot{Q}_{with\ oil}}{\dot{Q}_{without\ oil}} = \frac{26,632}{27,216} = 0.98$$

For the evaporator tests, for series 7, the saturation temperature at Microchannel Evaporator A inlet was controlled to about 48° F, and the mass flow rate was 200 lb/hr. The superheat at microchannel evaporator outlet was controlled to 10° F. An example for the main variables in this case are as follows:

$m_r = 200$ lb_m/hr (Mass flow rate of refrigerant for no oil condition)

$m_{oil} = 10.2$ lb_m/hr (Mass flow rate of oil during injection)

$m_{tot,OMF=5\ wt.\ \%} = m_r + m_{oil} = 210.2$ lb_m/hr (Mass flow rate of refrigerant and oil mixture)

Therefore during oil injection period, the total mass flow rate of the mixture was about 210 lb/hr, the measured heat transfer capacity was $\dot{Q}_{with\ oil} = 16,580$ Btu/hr and the measured refrigerant side pressure drop was $\Delta p_{with\ oil} = 1.023$ psid. Performance mapping tests were conducted at refrigerant mass flow rate of 200 lb_m/hr (referred in this example with the notation “*without oil low*”) and 212 lb_m/hr (referred to as “*without oil high*”) and at the same refrigerant saturation temperature of 48°F, and degree of superheat of refrigerant vapor at the microchannel evaporator A outlet of about 10°F (5.5°C). These performance mapping tests provided four neighboring points for the heat transfer rate ($\dot{Q}_{without\ oil,low} = 18,264$ BTU/hr, $\dot{Q}_{without\ oil,high} = 18,917$ BTU/hr,) and pressure

drop ($\Delta p_{without\ oil,low} = 0.75\ psid$, $\Delta p_{without\ high,low} = 0.9\ psid$) of the microchannel evaporator A when no oil was present and when the refrigerant flow rate ranged from 200 to 212 lb_m/hr. Then, the actual heat transfer rate ($\dot{Q}_{without\ oil} = 18,842\ BTU/hr$) and pressure drop ($\Delta p_{without\ oil} = 0.882\ psid$) for the corresponding baseline case of no oil at the refrigerant flow rate of 210 lb/hr was estimated from linear interpolation between each two pairs of the mapping points (i.e. the two neighboring points for $\dot{Q}_{without\ oil}$ and the two neighboring points for $\Delta p_{without\ oil}$). The HTF and PDF factors resulted as follows:

$$HTF = \frac{\dot{Q}_{with\ oil}}{\dot{Q}_{without\ oil}} = \frac{16,580}{18,842} = 0.88$$

$$PDF = \frac{\Delta p_{with\ oil}}{\Delta p_{without\ oil}} = \frac{1.023}{0.882} = 1.16$$

It should be noted that during the evaporator tests, the absolute pressure varied by less than 3 psia in microchannel evaporator A when oil was injected in the refrigerant loop. This variation was small enough to be neglected for the estimation of $\dot{Q}_{without\ oil}$ and $\Delta p_{without\ oil}$. In other words, for most of the evaporation tests, a linear interpolation was used to calculate $\dot{Q}_{without\ oil}$ and $\Delta p_{without\ oil}$ from two points at different flow rates. The interpolation (or double interpolation) approach eliminated any source of systematic error that could potentially skew the results for HTF and PDF due to the fact that during the experiments the oil slightly altered the pressure and flow rate of the system. With this approach, the effect of oil in the microchannel heat exchanger was isolated in the experimental results and the comparison of heat transfer rate and pressure drop between the case with oil and the case without oil was more meaningful. The HTF and PDF calculated with the data reduction method of the present work were representative of the

degradation of the refrigerant-side heat transfer rate and of the increase of the refrigerant-side pressure drop due to the oil retained in the heat exchangers.

4.2 Uncertainty Analysis

Based on the technical approach described in the previous sections, a preliminary uncertainty analysis was conducted according to the uncertainty propagation method suggested by Taylor and Kuyatt (1994). The accuracies of the main instrumentations used in this study are listed in Table 4-1. These values will be used to calculate the uncertainty of the important parameters based on uncertainty propagation analysis described in the following section.

Table 4-1 Accuracy of the main instrumentation for the study

Sensor	Manufacturer	Model / Type	Nominal range	Accuracy
Refrigerant Mass flow meter	Micromotion	CFM025 Elite series	6 to 19 lb/min (45 to 143 g/s)	±0.1% of reading
Oil Mass flow meter	Micromotion	CFM010 Elite series	0.01 to 0.8 lb/min (0.08 to 6 g/s)	±0.5% of reading if flow <0.04 lb/min; ±0.1% of reading if flow > 0.04 lb/min
Air flow rate	Helander	Elliptical nozzle	150 to 2,000 cfm (0.07 to 1 m ³ /s)	±2.2% of flow rate (using Setra 264 pressure transducer)
Temperature	Omega	T-type	-40 to 130 °F (-40 to 54 °C)	±0.5°F (0.3°C)
High accuracy barometer	Vaisala	PX02	26-32 inHg (88 – 108 kPa)	±0.25% of full scale
Air pressure transducer	Setra	Model 264	0 ~ 3 in WC (0 to 747 Pa)	±0.25% of full scale
Precision Temperature	Omega	RTD (Pt- 100)	-40 to 130 °F (-40 to 54 °C)	±0.2°F (0.1°C)
Refrigerant Saturation Pressure	Setra	Model C206	7 to 500 psia (50 to 3,450 kPa)	±0.65psi (4.5 kPa)
Differential pressure	Validyne	Diaphragm Typer	0 to 50 psi (0 to 350 kPa)	±0.25 psi (1.8 kPa)
Watt Transducer	Omega	OM11	6,800 to 38,000 Btu/hr (2 to 11 kW)	0.2% of reading

4.2.1 Uncertainty Analysis of Microchannel Condenser Tests

The T-type thermocouples and Pt-100 RTD sensors were calibrated in-situ and several times during the experimental campaign. Their accuracy was 0.5 °F (0.3 °C) for the T-type thermocouples and 0.2 °F (0.1 °C) for the RDTs. If the variables of the air side heat transfer rate, that is, ρ_{air} , CFM , $\Delta T_{air} = (T_{air,out} - T_{air,in})$ have random experimental uncertainties of $\delta\rho_{air}$, δCFM , and $\delta\Delta T_{air}$ and these uncertainties are also independent from each other, then the theoretical experimental uncertainty of the heat transfer rate, δQ_{air} , was calculated by using the Taylor series uncertainty propagation equation:

$$\delta Q_{air} = \sqrt{\left[\left(\frac{\partial Q_{air}}{\partial \rho_{air}} \delta \rho_{air} \right)^2 + \left(\frac{\partial Q_{air}}{\partial CFM} \delta CFM \right)^2 + \left(\frac{\partial Q_{air}}{\partial \Delta T_{air}} \delta \Delta T_{air} \right)^2 \right]} \quad 4-13$$

By applying the theory of uncertainty error propagation by Taylor and Kuyatt (1994) to the Heat Transfer Factor (*HTF*) Equation 4-13, gives the Equation 4-14 to calculate the uncertainty δHTF .

$$\begin{aligned} \delta HTF_{-Q_{air}} & \quad 4-14 \\ & = \sqrt{\left[\left(\frac{1}{Q_{air@OMF=0}} \delta Q_{air@OMF} \right)^2 + \left(\frac{-Q_{air@OMF}}{Q_{air@OMF=0}^2} \delta Q_{air@OMF=0} \right)^2 \right]} \end{aligned}$$

The uncertainty above is the uncertainty in *HTF* based on the heat transfer calculation. While calculating the δHTF , the uncertainty $\delta Q_{air@OMF=0}$ was taken to be similar to the experimental uncertainty $\delta Q_{air@OMF}$. This was reasonable because the heat transfer rates

with and without oil were measured by using the same instrumentation and in the same period. The measured values for $Q_{air@OMF=0}$ and $Q_{air@OMF}$ were also close to each other and thus it is logical to assume that $\delta Q_{air@OMF}$ and $\delta Q_{air@OMF=0}$, were also close to each other. Equation 4-14 was simplified to:

$$\delta HTF = \sqrt{\left[\left(HTF \frac{\delta Q_{air}}{Q_{air@OMF}} \right)^2 + \left(HTF^2 \frac{\delta Q_{air}}{Q_{air@OMF}} \right)^2 \right]} \quad 4-15$$

Equation 4-15 simplification leads to Equation 4-16, which expresses the fractional uncertainty of HTF as a function of the fractional uncertainty of $Q_{air@OCR}$.

$$\frac{\delta HTF}{HTF} = \sqrt{1 + HTF^2} \cdot \frac{\delta Q_{air}}{Q_{air@OMF}} \quad 4-16$$

Similar to HTF uncertainty analysis, applying the theory of uncertainty propagation by Taylor and Kuyatt (1994) to the Pressure Drop Factor (PDF) Equation 4-9 gives the Equation 4-17 to calculate the uncertainty on the pressure drop factor, δPDF .

$$\delta PDF = \sqrt{\left[\left(\frac{1}{\Delta P_{@OMF=0}} \delta \Delta P_{@OMF} \right)^2 + \left(\frac{-\Delta P_{@OMF}}{\Delta P_{@OMF=0}^2} \delta \Delta P_{@OMF=0} \right)^2 \right]} \quad 4-17$$

The uncertainty $\delta \Delta P_{@OMF=0}$ of the mapping data and the uncertainty $\delta \Delta P_{@OMF}$ of the pressure drop for tests with $OMF > 0\%$ were same and equal to ± 0.03 psi (according to the specifications of the differential pressure transducer provided by the manufacturer). Equation 4-17 was simplified accordingly to get a new Equation 4-18.

$$\delta PDF = \sqrt{\left[\left(PDF \frac{\delta \Delta P_{@OMF}}{\Delta P_{@OMF}} \right)^2 + \left(PDF^2 \frac{\delta \Delta P_{@OMF}}{\Delta P_{@OMF}} \right)^2 \right]} \quad 4-18$$

The fractional uncertainty of PDF as a function of the fractional uncertainty of $\Delta P_{@OMF}$.

$$\frac{\delta PDF}{PDF} = \sqrt{1 + PDF^2} \cdot \frac{\delta \Delta P_{@OMF}}{\Delta P_{@OMF}} \quad 4-19$$

The uncertainty of oil mass fraction, *OMF* depends on the measured solubility values and it was calculated according to the uncertainty error propagation theory described by Taylor and Kuyatt (1994). For the tests in which $P_{oil\ reservoir} < 365$ psia, the uncertainties in the calculated solubility values increased from $\pm 1\%$ w/w (at 20% w/w) to $\pm 2.7\%$ w/w (at 75% w/w) with a quadratic trend. For tests in which $P_{oil\ reservoir} \approx 495$ psia, the weights of the oil-mixture samples collected in the sampling cylinder were high. This reduced the fractional uncertainties of the weights measured with our laboratory scale and the calculated solubility values had lower experimental uncertainties.

The uncertainties in the solubility values were propagated to the errors in the *OMF*. The errors in the *OMF* also depended on the errors in the measured mass flow rates of the refrigerant and the injected oil-refrigerant mixture. The Coriolis mass flow meters had very good accuracies for the range of flow rates of the present work, which resulted in small uncertainties of the measured mass flow rates. This means that the uncertainties in the solubility dominated the propagation of experimental error for the *OMF*. For this reason, measurements of the solubility values of the injected oil-refrigerant mixture during the tests were used in the present work to estimate the solubility of refrigerant and oil mixture. The theoretical uncertainty errors for the main parameters of the present work are given in

Table 4-2.

Table 4-2 Range and Uncertainty Limits of the Main Variables in Condenser Tests

R410A tests		Range of Data		Uncertainty
Parameter	units	min	max	
$P_{mchx,i}$	psia	269.06	494.60	0.13 %
$T_{mchx,i}$	°F	99.60	134.08	0.36 °F
$\dot{m}_{oil+ref,inj}$	lbm/h	3.60	36.12	0.08 %
$\dot{m}_{oil,inj} + \dot{m}_{ref,mchx}$	lbm/h	350.34	613.20	0.01 %
S	% w/w	21.8	86.0	2.7 %
OMF^*	%	0.46	5.54	0.11 %
$\Delta P_{air,N}$	in W.C.	2.8	3.0	0.25 %
ρ_{air}	lbm/ft ³	0.070	0.073	0.27 %
CFM	cfm	2750	2900	0.55 %
$\Delta T_{air@OCR}$	°F	3.84	12.11	0.51 °F
$\Delta T_{air@OCR=0}$	°F	4.32	12.78	0.51 °F
$Q_{air@OCR}$	Btu/h	11608	33801	4.5 %
$Q_{air@OCR=0}$	Btu/h	13202	35306	4.3 %
$\Delta P_{@OCR}$	psi	2.27	12.64	0.24 %
$\Delta P_{@OCR=0}$	psi	2.19	12.21	0.25 %
$HTF_{-Q_{air}}$	-	0.87	1.11	5.2 %
$HTF_{-\Delta T_{air}}$	-	0.87	1.61	1.9 %
PDF	-	0.85	1.18	1.7 %

4.2.2 Uncertainty Analysis of Microchannel Evaporator Tests

This section discusses further the uncertainty error in OMF, ORV_N , HTF, and PDF for microchannel evaporators tests.

Uncertainty in Oil Mass Fraction (OMF): The sensor and equipment used for the measurements of oil mass flow rate and refrigerant mass flow rate and of solubility of refrigerant in POE oil for microchannel evaporator tests were the same as that of condenser tests. The uncertainty in measurements of oil retention in microchannel evaporators was depended on the oil mass difference at the inlet port and at the outlet port, that is,

$$ORmass_{@OMF=x \text{ wt.}\%} [\text{grams}] = M_a - M_b$$

Where M_a and M_b were total masses of oil described in data reduction section 4.1 and defined specifically by Equations 4-4 and 4-5. Each mass of oil is the result of a time integral of the form

$$M = \int_{t_0}^{t_1} \dot{m}_{oil, injected} dt$$

And using above time integral for inlet and outlet ports of the test section, the oil mass M_a and M_b are obtained.. The uncertainty calculation of oil retention mass includes uncertainty propagation of solubility of the refrigerant dissolved in the oil. The uncertainty of oil mass retention also involves the human operator error in estimating the time t_0 and t_1 of the above time integral of the flow rate. In a conservative way, based on our experience we estimated the human operator error in detecting the time at which the oil passes through the sight glass to as ± 2 seconds.

Figure 4.1 shows the uncertainty bars in the calculated oil retention volume if the error in the time of oil detection at the sight glasses is ± 2 seconds. For OMF at or below 3 wt. % this human error does not affect significantly the reported ORV_n because the time of integration is long, that is, of several minutes. For OMF higher than 3 wt.%, the error bars in the ORV_n resulted ± 0.01 , which could be significant. In order to achieve an error of within ± 2 seconds in the time of detection of oil at the sight glasses, video recordings of the flow at the sight glasses were taken and synchronized during the oil retention tests. The digital images provided the time at which the oil arrived to the sight glass and covered its glass surfaces. Oil had a dye in it and it appeared as yellowish and greenish in color as opposed to refrigerant, which appeared as transparent fluid inside the sight glass. During a tests, video recordings of the sight glasses with actual time indicators (i.e., a digital chronometers) next to them were taken, as shown in

Figure 4.2. Then, the recordings were synchronized in time, labeled, and archived. After the test was completed, the video recordings were played back at 3 time slower rate than real time. The digital frames of the sight glasses and chronometers indicated the instant in which the oil appeared first in a sight glass until the instant in which the oil covered the full length of the sight glass surfaces. The images of the digital chronometer, once synchronized, provided the exact times (within ± 2 seconds) at which the oil arrived approximately at the end of the sight glass. The overall theoretical uncertainty plus the uncertainty due to human operator on the ORV_N was estimated to ± 0.01 . For normalized oil retention volumes in the range of 0.05 to 0.1, this experimental uncertainty on the oil retention was 10 to 20 percent.

Figure 4.1: Uncertainty of ORV with $t \pm 2$ seconds

Figure 4.2: Oil layer observed for various OMFs

Uncertainty of pressure drop in microchannel evaporator was similar as the one described for the condenser tests. Four different differential pressure transducers were used based on the magnitude of the pressure drop across the microchannel evaporator. Each pressure transducer had a different full scale. For high mass flux tests, the pressure drop measured between microchannel evaporator inlet and outlet ranged from 5 psid to about 10 psid. Thus, for these cases, a differential pressure transducer of 15 psid full scale range or of 8 psid full scale range were used. For low mass flux tests, the differential pressure transducer with 3 psid full scale range or 5 psid full scale range were used in order to improve the accuracy of the pressure drop measurements.

The uncertainty in the HTF for microchannel evaporator was similar to that of condenser for the medium temperature evaporator tests and it was of $\pm 4.5\%$.

CHAPTER V

5 Experimental Results and Discussion

5.1 Microchannel Condenser

The experimental results of oil retention, pressure drop and heat transfer factor of R410A-POE oil mixture in the microchannel condenser are presented next.

5.1.1 Oil retention

5.1.1.1 Note on the range of OMFs in actual air conditioning systems, vending machines, water and wine coolers of refrigeration systems

It should be emphasized that OMF in actual air conditioning systems, vending machines, water and wine coolers, and refrigeration systems typically ranges from 0.5 to 1 w.t. % and sometimes it can be as high as 3 w.t. % for some operating conditions. The maximum OMF investigated in the present work was intentionally higher than 3 wt.% because the aim was to clearly highlight trends among the data of ORV_N , HTF and PDF. However, the results in the present study when OMF was higher than 3 wt.% should not be interpreted as representative case for actual systems in the field.

5.1.1.2 Air Conditioning Application with R410A and POE lubricant

The results of oil retention in the microchannel condenser for air conditioning applications and with refrigerant R410A and POE lubricant mixture are shown in Figure

5.1 and Figure 5.2. The test conditions are represented by open and full symbols and letters A to F and they are summarized in Table 5-1. The first three columns of this Table indicate the saturation temperature and mass flux during the tests while the last two columns show the range of solubility and miscibility for R410A and POE oil during the tests. The oil retention volume was normalized (ORV_N) with respect to the condenser total internal volume and it was plotted versus oil mass fraction (OMF) for each saturation temperature and each mass flux studied in the present work. The degree of superheat at the inlet of microchannel condenser was set to 10°F (~5 °C) in Figure 5.1, which was referred to as low degree of superheat, and to 65 °F (~36 °C) in Figure 5.2, which was referred to as high degree of superheat throughout these sections of the report. The results indicated that the oil retained in the condenser was strongly dependent on the OMF in the heat exchanger. The oil retention volume increased if the OMF increased and it was measured up to 11% of the total condenser internal volume, which consisted of the internal volume of all microchannel tubes plus the headers.

Table 5-1 Legend of the letters and symbols used in the figures reporting the tests results of microchannel condenser with R410A and POE

*Mass flux G is the mass flux inside each of microchannel tubes. It was calculated from the mass flow rate divided by the total cross sectional area of all the microchannel tubes that belong to condenser section ($G_{\text{condenser}}$) and that belong to the subcooler section ($G_{\text{subcooler}}$)

**Solubility values for the test ranges were obtained using Gravimetric method (ASHRAE, 1996)

***Miscibility range was based on Kang and Pate (1999)

Figure 5.1: Oil retention volume at low degree of superheat for R410A+POE oil in microchannel condenser

Figure 5.1 and Figure 5.2 show that the oil retention volume for high mass flux conditions (open symbols and letters D, E, and F) are higher than those for low mass flux conditions (full symbols and letters A, B, and C). The effect of mass flux on the oil retention was small for low OMFs and becomes more evident for OMFs higher than 3 wt.%. The oil retention volume was from 1.6 to 3 times higher for the cases of high mass flux compared to those of low mass flux cases.

For similar mass flux, the effects of saturation temperature on the oil retention were small for low superheat inlet condition (see Figure 5.1). The most marked effect of the refrigerant mass flux on the oil retention volume was observed for the test at low superheat condition and $T_{\text{sat}} = 130 \text{ }^\circ\text{F}$ ($54 \text{ }^\circ\text{C}$), and it is reported in Figure 5.1 with the series C and F. An increase of the mass flux from $16 \text{ to } 24 \text{ lb}_m/\text{ft}^2\text{-s}$ ($80 \text{ to } 120 \text{ kg/m}^2\text{-s}$) doubled the oil retention volume in the microchannel condenser. This can be explained by considering that at high refrigerant mass flux more liquid phase was present inside the condenser than at low mass flux because the air side entering conditions were kept constant between the two series of tests. The liquid phase travelled along the condenser with lower mass velocity with respect to the refrigerant vapor phase velocity. If more liquid was present inside the condenser then more oil was present inside the condenser because the concentration of the oil in the mixture was constant (for example looking at constant OMF line of 3 wt.% for the series at high and low mass flux).

Figure 5.2: Oil retention volume at high degree of superheat for R410A+POE oil in microchannel condenser

When the saturation temperature increased, the miscibility of R410A and POE oil mixture decreased until the critical solution temperature could be reached and the mixture became completely immiscible. The critical solution temperature of R410A-POE oil mixture at high refrigerant mass fraction of about 0.8 (which is equivalent to OMF of 20 wt.%) was about 113 °F (45 °C) (Kang and Pate, 1999). At saturation temperature of 130 °F (54 °C), a decreased degree of miscibility of POE oil in R410A liquid refrigerant occurred with respect to the other (much lower) saturation temperatures tested in the present work. Because of this decreased miscibility, an increase in viscosity of the liquid phase occurred, especially near the internal walls of the condenser tubes. In addition, at

high mass flux of refrigerant-oil mixture, more oil mass was injected during the test period into the heat exchanger in order to set the OMF. Because of the reduced liquid phase velocity and of the augmented liquid viscosity, more oil can potentially be hold up inside the microchannel condenser.

If we assume that the liquid phase formed a distinct layer separated from the vapor phase inside the microchannel tubes when the mixture undergoes a the two phase flow change process and inside the inlet headers of the condenser, then a low degree of superheat of the entering refrigerant vapor resulted in a lower superficial velocity when compared to the similar tests with high degree of superheat. This contributed to increase the oil retention volume because carrying the oil became more difficult when the refrigerant vapor had low superficial velocity and when the oil was less miscible with the liquid refrigerant. That was the case when saturation temperature was 130 °F (54 °C) and the degree of superheat was low, as that for the series C and F in Figure 5.1.

Different trends were observed for high superheat inlet conditions, shown in Figure 5.2. The oil retention volume decreased as the saturation temperature increased and for both low and high mass fluxes. At high superheat conditions, most of the condenser internal volume was filled with refrigerant and oil in the two phase flow and the initial entering section of the condenser had superheated vapor. Because the degree of superheat was high, there was less liquid refrigerant in the internal volume of the condenser and the dominant effect for oil retention was not the miscibility of oil in the refrigerant liquid anymore.

By comparing the oil retention volume in Figure 5.1 with the corresponding data in Figure 5.2, it can be deduced that at T_{sat} of 105°F (41°C) the oil retention volume was higher when the inlet condition of the condenser was lower degree of superheat. In this condition, the refrigerant in the condenser internal volume was predominantly in two-phase flow and the refrigerant vapor had lower superficial velocity in average when entering with low degree of superheat. For example, at T_{sat} of 105 °F (41 °C) the superficial vapor velocity of the refrigerant entering the condenser was about 187 ft/s (57 m/s) for the low degree of superheat case and low mass flux (solid triangles data points with letter B in Figure 5.1). This velocity increased to 239 ft/s (73 m/s) for the corresponding case of high degree of superheat and for same mass flux in the solid triangles data points with letter B in Figure 5.2. This increase of the refrigerant vapor velocity reduced the oil retention volume inside the condenser. It should be noticed that the oil existed as either homogenous solution in liquid refrigerant or as a separate layer of oil rich-film at the microchannel tube wall. The presence of oil on both cases promoted oil held up in the microchannel condenser but in different ways. The two-phase region of the condenser was the main part where the oil was retained and oil was a component of the liquid phase mixture. The higher was the liquid phase volume inside the condenser, the higher was the oil retained in it. On the other hand, in the superheated section of the condenser, oil existed as liquid droplets and as film near the wall. The higher was the refrigerant vapor velocity, the higher was the oil carry over with it. The total oil volume retained in the condenser was depended on those two mechanisms, and the dominant mechanism varied for the saturation temperatures investigated in the present work. While a low degree of superheat tended to increase the oil retention, as reported in the data of

Figure 5.1 with respect to that of Figure 5.2, a generalization of this result to all saturation temperatures of the present work should not be made. For example, by comparing the oil retention data of series B, at OMF of 3 wt.% the ORV_N is about 0.07 with low degree of superheat in Figure 5.1 and it is reduced to 0.02 with high degree of superheat in Figure 5.2. However, the oil retention at $T_{sat} = 85\text{ }^\circ\text{F}$ ($29\text{ }^\circ\text{C}$) was basically the same for both low and high degree of superheat cases, as shown in the series A and D of the two figures.

5.1.1.3 Refrigeration Application with refrigerant R134a and POE lubricant

The results of oil retention in microchannel condenser for refrigeration applications with refrigerant R134a and POE oil mixture are shown in Figure 5.3. Test conditions are represented by open and full symbols and letters A to F summarized in Table 5-2.

Table 5-2 Legend of the letters and symbols used in the figures reporting the tests results of microchannel condenser with R134a and POE

*Mass flux G is the mass flux inside each of microchannel tubes. It was calculated from the mass flow rate divided by the total cross sectional area of all the microchannel tubes that belong to condenser section ($G_{\text{condenser}}$) and that belong to the subcooler section ($G_{\text{subcooler}}$)

**Solubility values for the test ranges were obtained using Gravimetric method (ASHRAE, 1996)

***Miscibility range was based on Kang and Pate (1999)

The oil retention volume was normalized with respect to the condenser total internal volume, (ORV_N), and it was plotted versus oil mass fraction (OMF) for each saturation temperature and each mass flux studied in the present work. The degree of superheat at the inlet of microchannel heat exchanger was 65 °F (36 °C). The experimental results of Figure 5.3 indicated that the oil retained in the condenser was strongly depended on the OMF. The oil retention volume increased if the OMF increased and for refrigerant R134a and POE mixture it was measured up to 10 % of the total condenser internal volume.

Figure 5.3: Oil retention volume at high degree of inlet superheat for R134a+POE oil in microchannel condenser

By comparing Figure 5.2 and Figure 5.3, the oil retention volume for both R410A+POE oil and R134a+POE oil are strongly dependent on OMF and have maximum oil retention at the lowest saturation temperature. With refrigerant R134a and POE oil, the effect of refrigerant mass flux on oil retention was small for OMF below 2 wt.% and the oil hold up in the condenser was less than 3 % of condenser internal volume (Figure 5.3). This was not the case with R410A and POE oil where the mass flux effect was already important at OMF about 1 wt.% (see again Figure 5.2 for OMF of 1 wt.% and compare with Figure 5.3 at OMF of 1 wt.%).

It can also be seen from Figure 5.3, that at the same condensation temperature, the increase mass flux decreased oil retention volume with R134a and POE oil (series with solid line and dashed line). However, the opposite was observed for R410A and POE oil as depicted in Figure 5.2.

If the OMF increased to above 3 wt.%, the high mass flux data (dashed lines in Figure 5.3) had lower oil retention than the corresponding low mass flux data (solid lines in Figure 5.3) for all three saturation temperatures tested in the present work. At low condensation saturation temperature of 95°F (35°C), oil retention increased quite significantly if the mass flux decreased, as represented by the series with letters A and D in Figure 5.3. For these series, at OMF of 5 wt.%, the oil retention increased by about 50% if the mass flux of the condenser section decreased from 18 lb_m/ft²-s (88 kg/m²-s) to 10 lb_m/ft²-s (49 kg/m²-s).

The lowest oil retention volume for R134a and POE oil was observed at highest saturation temperature and mass flux of 130°F (54°C) and 18 lb_m/ft²-s (88 kg/m²-s),

respectively (Series F). This can be explained with the high refrigerant-oil solubility at high temperature and coupled with high mixture velocity due to high mass flux.

5.1.2 Effect of oil retention on the heat transfer rate of the condenser

As described in the data reduction section, the heat transfer factor (HTF) of the refrigerant and POE oil mixture was defined as the ratio of the measured heat transfer rate of the microchannel condenser when oil was retained inside the heat exchanger over the heat transfer rate of the microchannel condenser for the case when there was not any oil inside the heat exchanger. Both heat transfer rates were measured at similar total mass flow rate, i.e., the refrigerant flow rate entering the condenser in the case with no oil was similar to the mixture (refrigerant plus oil) mass flow rate in the cases with oil. This means that the refrigerant flow rate was decreased slightly down 4 to 5% when OMF increased from 0 to 5 wt. %. The saturation pressures of condensation were also the same between the case with no oil and the tests with oil. And the degree of superheated vapor refrigerant entering the condenser was a third variable kept constant in between the two test. Finally, the air inlet temperature and velocity were also constant between the cases of tests with oil and the baseline references with no oil. In other words, by comparing the heat transfer rates at same flow rate, pressure, and superheat, the HTF is a performance parameter that isolated and quantified the effect that oil retained inside the condenser had on the microchannel condenser refrigerant-side total heat transfer rate.

5.1.2.1 HTF for air conditioning applications with R410A and POE lubricant

When OMF is 0 (i.e., no oil), the HTF resulted 1 by its own definition and it varied with OMF as shown in Figure 5.4 and Figure 5.5 for the microchannel condenser investigated in the present work. The test conditions are represented by open and full symbols and letters A to F and they were summarized in Table 5-1. At high saturation temperatures (cases with letters C and F), the HTF decreased if the OMF increased. Different trends were observed for medium saturation temperature and most intriguing results were observed at low saturation temperatures for both refrigerant mass fluxes and inlet superheat conditions (tests A and D). For medium saturation temperature of 105°F (41°C), indicated as B and E in the figures, the refrigerant-side heat transfer capacities seemed to be independent of the OMF for both mass fluxes and superheat inlet conditions. It is interesting also to note here that at low saturation temperature, the presence of oil was observed to increase the refrigerant-side heat transfer rate, although in non-monotonic fashion. The HTF in these conditions increased slightly as the OMF increased to about 3 wt.%; then the HTF started to decline at higher OMFs. POE oil did not change phase during the condensation process and it did not have as good heat transfer properties as that of refrigerant R410A. POE oil was a contaminant that added an additional thermal resistance to the heat exchange process between the air and the refrigerant in the microchannel condenser. Thus, the result of HTF decreasing when OMF increased could be somewhat intuitive because if POE oil was present in the two-phase flow mixture, then the convective heat transfer coefficient of the refrigerant-side was expected to diminish.

Figure 5.4: Heat transfer factor at low degree of superheat for R410A+POE oil in microchannel condenser

On the other hand, the tendency of the HTF to increase if OMF increased to 3 w.t. % or more was unexpected. For several tests, which were conducted in different days and repeated several times, and particularly for low saturation temperature of 85°F (29°C), both series A and D in Figure 5.4 and Figure 5.5 indicated that the presence of oil augmented the refrigerant-side heat transfer rate. An in-depth thermodynamic and heat transfer analysis of this interesting behavior is provided later in this dissertation.

Figure 5.5: Heat transfer factor at high degree of superheat for R410A+POE oil in microchannel condenser

The effects of refrigerant mass flux on the heat transfer rate had different results that were dependent on saturation temperature. At low saturation temperature, the HTF was slightly higher for high mass flux compared to that of low mass flux as shown in both Figure 5.4 and Figure 5.5 (cases A and D). On the other hand, at high saturation temperature (cases C and F), the HTF decreased significantly as the mass flux increased. At saturation temperature of 105 °F (41 °C), the HTF was not affected by the change of mass flux (series B and E). The effect of refrigerant mass flux on the condensation heat

transfer of refrigerant and oil mixtures was also reported to be small in the paper of Shao and Granryd (1995), in which they tested R134a-PAG oil mixture. The authors reported that for three different mass fluxes and for oil mass fraction up to 5 wt.%, there was no considerable change on the refrigerant-side heat transfer rate.

Shao and Granryd (1995) findings agreed with the results of the present work from the test series B and E, that is, only for one saturation temperature of 105°F (41°C). This is a common reference used in air conditioning applications. However, in the present work, the effect of oil on heat transfer rate was depended on the saturation pressure of condensation. The HTF decreased as the saturation temperature increased. The degradation of heat transfer capacity was due to the augmentation of the liquid mixture viscosity of refrigerant-oil mixture compared to that of pure refrigerant R410A. Based on the viscosity analysis of the R410A-POE oil mixture as reported by Zhang and He (2009), the liquid mixture kinematic viscosity for the experiments of the present work increased by over 28% for the range of saturation temperatures tested in their work. The higher viscosity, along with the higher surface tension of the liquid refrigerant-oil mixture reduced the molecular and turbulent transport in the condensate film, hence decreasing the condensation heat transfer. This effect was further augmented by the annular flow regime that is typically established inside microchannel tubes.

At low saturation temperature, the presence of oil increased the heat transfer capacity for low oil mass fractions. Again, similar results were also reported in the open domain literature by Shao and Granryd (1995) with R134a-PAG mixture. A possible reason for this observation is that the refrigerant-oil mixture had higher condensation temperature compared to that of pure refrigerant. This was also confirmed using vapor pressure

correlation suggested by Jeng *et al.* (2001) for R410A and POE oil mixture for the tests of the present work. At the same ranges of saturation pressure, the saturation temperature for the refrigerant and oil mixture at OMF of 5wt.% was up to 1.4°F higher than that of refrigerant R410A only. The higher saturation temperature caused the mixture to condense earlier at the beginning of microchannel condenser and increased the overall heat transfer capacity of the condenser.

The test results at high degree of superheated vapor at inlet of the condenser had slightly higher HTF than the corresponding tests at low degree of superheated vapor. In other words, the reduction of the refrigerant-side heat transfer rate due to oil retention was smaller when the refrigerant entered the condenser with high degree of superheated vapor. This result was associated with lower oil retention volume when high superheated vapor entered the condenser. In the superheated section of the condenser, oil was present as liquid droplets entrained in the refrigerant vapor bulk flow and as oil-rich liquid film at the tube wall interface. Less oil in the superheated section of the condenser yielded to convective heat transfer process inside the microchannel tubes that was similar to that of refrigerant only case. Since the refrigerant-side heat transfer rate of the superheated section of the condenser was secondary to the heat transfer rate of the phase change section of the condenser, the higher was the superheated vapor, the lesser was the oil retention volume, and the lesser was the penalization of the heat transfer rate when oil was present.

5.1.2.2 HTF for refrigeration applications with R134a and POE lubricant

Refrigerant R134a and POE oil mixture was tested for refrigeration applications and the effects of oil on the refrigerant-side heat transfer rate of the microchannel condenser are shown in Figure 5.6. Test conditions are represented by open and full symbols and letters A to F summarized in Table 5-2. When OMF is 0 (i.e., no oil), the HTF resulted 1 by its own definition and for R134a and POE mixture, the HTF varied with OMF as shown in Figure 5.6 for the microchannel condenser investigated in the present work. At high saturation temperatures (cases with letters C and F) and at medium saturation temperature for low mass flux (cases with letter B) and low saturation temperature for low mass flux (letter A), the HTF always decreased if the OMF increased.

The presence of oil in the condenser reduced the heat transfer rate and the penalty was fairly significant at low refrigerant mass flux. These findings were consistent with the previous results on the oil retention where low refrigerant mass flux resulted on higher oil retention. The oil retained in the form of liquid rich layer inside the microchannel condenser hindered the convective heat transfer exchange between the refrigerant and internal walls of the heat exchanger. The heat transfer capacity penalization was less than 10% at the highest saturation temperature tested in the present work.

For medium saturation temperature of 105°F (41°C), indicated as E in Figure 5.6, and for low saturation temperature of 95°F (35°C), indicated as D, the refrigerant-side heat transfer capacities seemed to be independent of the OMF. It is interesting also to note here that at low saturation temperature of 95°F (35°C), indicated as D, the presence of oil was observed to slightly increase the refrigerant-side heat transfer rate, although this

increase was considered an experimental uncertainty of the measurements. The HTF in these conditions increased slightly by up to 3% as the OMF increased to about 3wt.%; then the HTF started to decline at higher OMFs.

Figure 5.6: Heat transfer factor at high degree of superheat for R134a+POE oil in microchannel condenser

5.1.3 Pressure drop on the refrigerant side of the heat exchanger

5.1.3.1 Air Conditioning Application with R410A and POE lubricant

As described in the data reduction section, the pressure drop factor (PDF) of R410A-POE oil mixture was defined as the measured pressure drop across the microchannel condenser when oil was inside divided by the reference pressured drop across the microchannel condenser when there was not any oil and at constant total mass flow rate, saturation pressure, and degree of vapor superheat entering the condenser. The air inlet temperature and velocity were also constant between the cases of tests with oil and the baseline references with no oil. In simpler terms, the PDF was the parameter that isolated and quantified the effect of oil that was retained inside the condenser on the refrigerant side pressure drop across the entire condenser. When OMF was 0 wt.% (i.e., no oil), the PDF resulted 1 by definition and it varied with OMF as shown in Figure 5.7 and Figure 5.8. The figures indicate that the pressure drop factor increased if OMF increased. Up to 19 % increase of pressure drop was measured at $T_{sat} = 130^{\circ}\text{F}$ (54°C) with high inlet superheat of the condenser. The increasing pressure drop with oil presence was due to high refrigerant-oil mixture viscosity compared to that of refrigerant only. This increase of viscosity caused the increase on shear stress and of the frictional pressure drop associated with it. The increase of oil mass fraction also introduced higher amount of oil retention in the microchannel and it reduced the flow cross sectional area for the refrigerant vapor. This led to increasing pressure drop during the condensation process. Another reason for the pressure drop increase was the predominant annular flow established in microchannel during flow condensation(Schlager *et al.*, 1987). For annular flow, the increasing

refrigerant-oil mixture viscosity increases the shear stress significantly compared to that of other flow regimes, such as stratified flow and wavy flow types.

Figure 5.7: Pressure drop at low degree of superheat for R410A+POE oil in microchannel condenser

As indicated in both Figure 5.7 and Figure 5.8, the pressure drop increased as the refrigerant mass flux increased although with varying magnitude. Both figures show that the effects became more important as oil mass fraction increased to about 3 wt.%. A significant rise of pressure drop was observed with the increase of refrigerant mass flux at high saturation temperature (case C and F in both Figures), while the results showed smaller effects for other conditions. In the same figure, at saturation temperature of 130°F

(54°C), the pressure drop factor at low mass flux (case C) was approximately 10% higher when OMF was 3 wt.% compared to that of without oil case, and the PDF doubled for high mass flux (case F). It is interesting to note that at this higher saturation temperature, the effect of refrigerant mass flux became more important although the viscosity of R410A-POE oil mixture decreased (Zhang and He, 2009).

Figure 5.8: Pressure drop at high degree of superheat for R410A+POE oil in microchannel condenser

It seems that the pressure drop during this condition was mainly affected by the oil-rich film that was separated and retained in the microchannel due to immiscibility of the mixture at higher saturation temperature (Kang and Pate, 1999). This observation was

also confirmed by the findings that for the above conditions (case C and F in Figure 5.7), both pressure drop and oil retention results showed positive relation i.e. when the oil retention increased, the measured PDF also increased. The oil-driven viscosity augmentation of the refrigerant-oil mixture and the presence of oil retention near the microchannel wall contributed to increase the PDF.

The effect of saturation temperature on PDF at low superheat inlet conditions was small. While for high superheat inlet condition, as depicted in Figure 5.8, the increase of saturation pressure increased the pressure drop factor, the PDF for saturation temperatures of 105 and 130°F (41 and 54°C) were comparable and a significantly lower PDF was observed for lower saturation temperature of 85°F (29°C).

The effect of superheat inlet condition on pressure drop can be observed by comparing data on Figure 5.7 with the corresponding symbol/letter in Figure 5.8. First the superheat effects on PDF were not monotonic. At low saturation temperature, the increase of superheat at the inlet caused the PDF to decrease (cases A and D in Figure 5.7 and Figure 5.8), while at high saturation temperature, the increase of superheat led the PDF to decrease (cases C and F in Figure 5.7). The PDF for intermediate saturation temperature of 105°F (41°C) were not significantly altered by the change in the superheat inlet conditions.

5.1.3.2 Refrigeration Application with R134a and POE lubricant

The effect of oil presence on pressure drops in microchannel condenser for refrigeration applications are presented in Figure 5.9. For all saturation temperatures tested, the PDF was higher at lower refrigerant and oil mass flux. It is important to emphasize here that

the PDF represents the relative fraction of pressure drop between the tests with oil (numerator of the PDF definition in Eq. 4-9) and without oil (denominator of the PDF definition in Eq. 4-9) at the similar mass flux and inlet saturation pressure conditions. The PDF does not represent the absolute pressure drop at a given mass flux. Hence, although the pressure drop was higher at higher mass flux, the corresponding PDF depends only on the amount of oil and on the effect that the oil had on the pressure drop during the tests.

As depicted in Figure 5.9, the oil presence significantly penalized the refrigerant side pressure drop in the microchannel condenser when refrigerant R134a and POE were used. Although there was some scattering of the pressure drop data, Figure 5.9 shows that even small OMFs of 1 wt.% can increase the PDF from 1.01 up to 1.10, that is, that even small amount of oil in the refrigerant flow increased the pressure drop from about 1% up to 10%. The effects were more marked at lower refrigerant and oil mass flux. These results were consistent with the oil retention volume test results, presented previously in Figure 5.3, where the amount of oil retained was higher for lower mass flux. While at OMF of 3 wt.% the PDF ranged from 1.03 up to 1.20 (i.e. up to 20% increase of pressure drop due to the presence of excessive oil inside the microchannel condenser), the maximum PDF in the microchannel condenser tested in the present work was 1.37, and it was measured for OMF of about 5 wt.%.

Figure 5.9: Pressure drop factor at high degree of superheat for R134a+POE oil in microchannel condenser

5.1.4 Thermodynamic and Heat Transfer Analysis of Condenser Experimental

Results for the Heat Transfer Factor

As mentioned in section 5.1.2.1 for R410A and POE mixture and in section 5.1.2.2 for R134a and POE mixture, the results for heat transfer capacity when oil was present varied among the oil mass fractions and saturation temperatures investigated. Some of the HTFs when oil was present were higher than 1, which meant that small amount of oil retained in the condenser augmented the heat transfer capacity of the microchannel heat

exchanger. This was an intriguing and counterintuitive finding and this section discusses further analysis of the effects of oil retention on saturation temperature, flow regime, and free flow area of the microchannel condenser.

The influence of oil in the condensation heat transfer can be explained by one or more of the following mechanisms (Thome, 2004):

1. Bubble point temperatures; the presence of oil with much higher saturation temperature compared to that of the pure refrigerant, increase the bubble point temperature of the oil-refrigerant mixture
2. Oil alters the transport properties of the liquid phase; due to much higher molecular weight of the oil compared to that of pure refrigerant, the presence of oil notably change the density, liquid viscosity, specific heat and surface tension
3. Foaming; the oil-rich liquid film at the microchannel heat exchanger's wall promote the formation of foam. The foam may have positive effects on heat transfer due to the wetting of the top wall on otherwise stratified flow condition. Notable increase on heat transfer coefficient by about 10-60 % due to the presence of oil have been reported at intermediate vapor qualities (Zürcher *et al.*, 1998)
4. Oil promotes wetting of the microchannel heat exchanger's wall due to its larger surface tension compared to that of pure refrigerant
5. The presence of oil influences the flow pattern transition, such as annular flow and stratified-wavy flow

The presence of oil has been found to change the saturation temperature of the refrigerant-oil mixture (Takaishi and Oguchi, 1987; Wei *et al.*, 2008). In order to account for this effect, the saturation temperature of the refrigerant-oil mixture was estimated by using the thermodynamic approach proposed by Thome (Thome, 1995) and for the limits of OMF of 0 to 5 wt.%. The saturation (or the bubble point) temperature of refrigerant mixture of R410A and 5wt.% POE oil resulted in an increase of saturation temperature of about 1.8°F. This change of saturation temperature with the presence of oil shifted the baseline heat transfer capacity ($Q_{\text{without oil}}$) that should be taken in the denominator of Equation 4-10. As a result the potential variation of heat transfer factor (HTF) was found to be less than 1% with respect to the HTFs reported in Figure 5.4 and Figure 5.5. From this analysis, we concluded that the change of saturation temperature during condensation of the refrigerant and oil mixture when oil was present was not a main contributing factor to the increase of HTF observed in Figure 5.4 and Figure 5.5.

Another effect of the oil in the condenser has been related to the change of flow regimes during condensation (Shao and Granryd, 1995; Shen and Groll, 2005; Huang *et al.*, 2010). Notable changes with the oil introduction in MCHX condenser is the flow regimes and refrigerant distribution in the header, microchannel passages and the connection between them. The presence of oil shifts the flow regimes toward laminar flow (Huang *et al.*, 2010) inside the microchannels. In addition the presence of oil in MCHX condenser with vertical header has been reported to create change in refrigerant distribution (Jin and Hrnjak, 2014). The distribution changes are not linearly correlated with oil mass fraction, instead the distribution is worse as OMF increases upto 3 wt.% then become more uniform at higher OMFs. The experimental data for the refrigerant R410A and the

mixture of R410A with 5 wt.% POE oil were plotted on the Mandhane (1974) flow map. At the inlet of the microchannel condenser, the flows were found to be in the annular type flow regime region in the Mandhane flow map for both cases of refrigerant only and refrigerant and oil mixture circulating in the condenser. The presence of oil increased the liquid superficial velocity by increasing the density of oil-rich liquid phase. Analysis for the change of liquid density at OMF of 5 wt.% showed that the increase of liquid superficial velocity up to 0.36 ft/s (0.11 m/s) due the presence of oil did not change the flow regime according to the map. Thus the flow with the presence of oil remained in annular and mist-annular flow regime.

Following the above analysis on the change of phase velocity, although the presence of oil did not alter the vapor phase density (the vapor phase consisted of only refrigerant), there was considerable effect on the flow area reduction that might lead to increasing heat transfer during condensation in microchannel. Further analysis of cross-sectional flow area reduction alone with the presence of 5 wt.% oil at the inlet of microchannel condenser was performed using correlation from Huang *et al.* (2010). The reduction on flow area at 5 wt. % caused the Nusselt number to increase about 2.4% compared to that of no oil case.

From the above considerations, it seems that increase of heat transfer factor up to 13.5% when oil was present with respect to oil free conditions, as observed in Figure 5.4 and Figure 5.5, was not completely due the variation of saturation temperatures, the change of flow regime, or the increase in the superficial velocity of the refrigerant vapor inside the microchannel tubes. While high oil concentrations will ultimately decrease the heat transfer capacity of the condenser, some other phenomena must occur when oil was

present in small quantities in the refrigerant flow inside the microchannel tube during phase change condensation. For the present study, a potential cause can be ascribed as the foaming and increasing wettability of the liquid phase due to the presence of the oil and improved refrigerant distribution. These hypotheses requires visual observation of the refrigerant-oil flow in the microchannel tubes and its headers. Because the HTFs of the present work were obtained as global values for the entire heat exchanger, we were unable to identify such phenomena. Further research on local heat transfer phenomena in microchannel tubes is needed to be able to identify and quantify possible causes that contributed increasing of heat transfer rate when OMFs were small and below 3 wt.%.

5.2 Microchannel Evaporator

This chapter discusses the experimental results of oil retention measurements in microchannel evaporators in terms of normalized oil retention volume (ORV_N), pressure drop factor (PDF) and heat transfer factor (HTF). The definitions of these three variables are same used for the condenser and they are given in Equations 4-8, 4-9, and 4-10. When oil was present in the evaporator, the heat transfer rate and refrigerant-side pressure drop were compared to those of the oil free case at same total mass flow rate, same saturation pressure, and similar degree of vapor superheated at the outlet of the evaporator.

5.2.1 Oil retention volume in the evaporators

This section discusses the oil retention in microchannel evaporator A with R410A and POE oil and R134a and POE oil and for two mass flux and several saturation temperatures. The oil retention volume was measured by using the timing and video recording method of the oil flow entering and existing the test section; this method was discussed in section 3.3.3.4. The information of test conditions and the legend for the symbols used for the test series of R410A and POE oil and R134a and POE oil during the tests on evaporators are given in

Table 5-3 and Table 5-4.

An example of the calculation of mass flux inside each microchannel tube is provided below for test series represented by the letter G and the solid round black symbol in Table 5-3. The mass flow rate during the test of series G was 200 lb_m/hr (90.7 kg/hr). This was the total mass flow rate, i.e., the refrigerant mass flow rate if OMF = 0 wt. % or the total mixture (refrigerant plus oil) flow rate if OMF > 0 wt. %.

For evaporator A, the overall cross sectional area of each microchannel tube was 0.01953 in² (or 0.126 cm²), that is, 0.000135625 ft². Since there were 98 tubes for microchannel evaporator A, the overall cross sectional flow area resulted:







$$A_{cross,overall,Evap A} = 0.000135625 ft^2 * 98 = 0.013291 ft^2$$

Then, the total mass flux for the series G for the evaporator A resulted

$$m''_{G,Evap A} = \frac{mass\ flow\ rate}{flow\ area} = \frac{200\ (lb/hr)}{(0.013291\ ft^2 * 3600\ s/hr)} = 4.2\ \frac{lb_m}{ft^2 - s}\ or\ 20.4\ \frac{kg}{m^2 - s}$$

It should be emphasized in here that this is the total mass flux in each microchannel tube, i.e., the refrigerant mass flux if OMF = 0 w.t. % or the total mixture (refrigerant plus oil) mass flux if OMF > 0 w.t. %.

Table 5-3 Legend of the letters and symbols used in the figures reporting the tests results of microchannel evaporators with R410A and POE

Symbol	Letter	T_{sat}	
		$^{\circ}F$	$(^{\circ}C)$
	G	33	(0.5)
	H	38	(3.3)
	I	48	(9)
	J	33	(0.5)
	K	38	(3.3)
	L	48	(9)

*G is the mass flux inside each microchannel tubes. It was calculated from the total mass flow rate entering the evaporator divided by the total cross sectional area of microchannel tubes in the evaporator

5.2.1.1 Microchannel evaporator A with R410A and POE oil

The experimental results of oil retention volume (ORV_N) in evaporator A with refrigerant R410A and POE oil are summarized in Figure 5.10. This figure shows the oil retention volume in the microchannel evaporator A on the y-axis and the oil mass fraction (OMF) of POE oil in refrigerant R410A on the x-axis. The oil retention volume normalized, ORV_N , was the ratio of the oil retention volume over the total internal volume of the evaporator A, including the headers internal volume. The effect of mass flux is represented as void and solid symbols and corresponding letters. Low mass flux series are

represented by the solid symbols (G, H, and I) while high mass flux tests are represented as void symbols (J, K and L series) (for details see Table 5-3). Each saturation temperature is given with a void and a solid symbol with same color and shape of the symbol. For example, the black circle data points in Figure 5.10 represent saturation temperature of 33°F (~0.5°C) but the solid circle points (series G) are for low mass flux while the void circle points (series J) are for high mass flux. From a quick glance on those two series, it is evident that if the mass flux doubled then the oil retention in the evaporator was reduced by half. This result was observed when OMF was from 0 to 3 w.t. %.

The experimental results of ORV_N suggested that the amount of oil retained in the microchannel evaporator was strongly depended on the OMF and the oil retention in the microchannel increased as OMF increased. In the evaporator, oil existed in the liquid mixture because the entering fluid was a mixture of saturated refrigerant liquid and POE oil and the evaporation of liquid refrigerant along the microchannel tubes created refrigerant vapor in which the oil droplets entrainment was small. This assumption is supported by authors' previous work on refrigerant and oil flow visualization in air conditioning evaporators (Cremaschi et. al. 2005). During evaporation of the refrigerant along the length of microchannel tubes, the local concentration of oil in liquid mixture increased. Therefore the viscosity of liquid mixture increased along the length of microchannel tube, that is, along the direction of the refrigerant flow. For example, for OMF of 0.5 wt. %, the viscosity of liquid mixture in the microchannel tube increased by up to 40 times. In other words, the viscosity of the liquid mixture of saturated liquid refrigerant and POE at the inlet of the tube was 40 times lower than the viscosity of the

liquid mixture of POE oil and refrigerant dissolved in it at the outlet of the tube (most of the refrigerant was superheated vapor at the outlet of the microchannel tube but a small amount of refrigerant was still dissolved in the oil because of POE and refrigerant R410A are soluble and miscible at those temperatures and pressures). For OMF of 5 wt. % the liquid mixture viscosity increased by 7 times from inlet to outlet of the microchannel tube. The increase in the refrigerant R410A and POE oil mixture viscosity augmented the shear stress required to remove the oil, particularly the shear stress at the liquid-wall interface. Thus, oil increased its resistance to flow with and to be carried with the refrigerant vapor along the microchannel tube. It was sound to assume that oil tended to form a film layer around the wall, that is, to wet the internal walls of the microchannel tubes and of the outlet header. However, since the tests were conducted on a full size microchannel heat exchanger, this hypothesis was not verified in the present work and flow visualization experiments of refrigerant and oil mixtures in microchannel tubes are potential future work on this topic. In Figure 5.10, when OMF increased from 0 wt. % to 5 wt. % the oil retention volume in evaporator A also increased and it was measured up to 12.5 % of total internal volume of evaporator A. The trends in Figure 5.10 are clearly not linear. At OMF below 2 wt.%, the magnitude of the ORV_N for low mass flux cases (series G, H, and I) were different from that of high mass flux cases (J, K and L). For low mass flux series (G, H, and I), the amount of oil retention volume in evaporator A increased significantly as OMF increased from 0 to 1 wt. %. This finding was intriguing and the effect of potential systematic errors on the measured oil retention volume in the heat exchanger was further investigated. We recall the test methodology details described in section 3.3.3. The methodology was based mainly on timing and video recording

method of the oil flow when oil appeared at sight glasses. If we assume an operator error of ± 2 seconds on detecting such time instances, the results varied to within the experimental uncertainty of the oil retention measurements, which are shown in Figure 5.11 as an example. For OMF of 0.5 and 1 wt.% the actual time that the oil took to travel from inlet to outlet of the evaporator was of several minutes (that is, about 10 minutes or more). Thus, a human operator of 2 seconds on detecting the instant at which the oil appeared on the sight glasses had an impact on the ORV_N that was within the experimental uncertainty reported for one representative point in Figure 5.10. It should be noted that the experimental uncertainty bars reported for only one representative point in Figure 5.10 to Figure 5.12 applies to all data points of the figures. The bars were intentionally omitted for the other points to avoid compromising the readability and quality of the plots.

Figure 5.10: Oil retention volume (ORV_N) in microchannel evaporator A with R410A and POE oil

Figure 5.11: Oil retention volume (ORV_N) in microchannel evaporator A with respect to sight glass S1, sight glass S2, and effect of the variation of the observed time by 2 seconds (the results for series H)

Referring to Figure 5.11, the data in blue solid diamonds represent the actual measurements of oil retention in evaporator A for the series H. The green solid triangle data points represent the measured oil retention volume if the time of appearance at the sight glasses were to be shifted by ± 2 seconds with respect to the original time measured. This figure also shows the brown square solid data points, which represent the measured oil retention volume in the evaporator A if a second sight glass S2 was used to measure the oil travel time. The second sight glass was downstream S1 with respect to the direction of the refrigerant flow. The comparison of the ORV_N for the S1 series and S2 series indicates that the measured oil retention volume was independent of the location of

the sight glass used to measure the oil travel time. This was because the oil retention volume in the evaporator was obtained from a difference between two volumes, i.e, the volume retained from inlet injection port to the sight glass and volume retained from outlet inject port of the evaporator to the sight glass. Moving the sight glass downstream simply altered those two measured volumes by the same quantity but their difference (which was the oil retention volume in the evaporator) did not change. Nevertheless, we verified that the oil retention volume was independent on the sight glass location for several tests of the evaporator and we used the second sight glass as redundant method to confirm the measurements obtained from the first sight glass.

Even for small OMFs of 0.5 and 1 wt.%, the oil retained in the evaporator was quite significant and it was already 77 to 95 % of the oil retention volume measured when OMF was 3 wt.%. This result suggested that the geometry of the evaporator trapped a certain amount of oil regardless of the OMF in the main flow. Because only liquid mixture was present at the inlet of the evaporator, we concluded that the oil traps were most likely at the outlet header of the evaporator. In our experiments, recalling that the refrigerant flow inside the heat exchanger was vertical upward and that superheated refrigerant vapor was present at the outlet of the microchannel heat exchanger, we speculated that the oil was trapped in the valleys created between the microchannel tubes inserts into the outlet header. As the refrigerant and oil mixture flowed through the microchannel heat exchanger, the refrigerant evaporated leaving behind a liquid phase richer in POE oil. The oil-rich liquid mixture then filled the outlet header valleys until it flooded them. For these cases, the ORV_N increased sharply with OMFs and lower mass flux augmented significantly the filling time. This could explain the remarkable

difference in ORV_N in Figure 5.10 for low and high mass fluxes when OMF was below 1 wt.%. Once the minimum threshold volume defined by the volume of the valleys in the outlet header was filled with oil, then any additional oil was carried with the refrigerant vapor out from the evaporator header. For these cases, the ORV_N increase slowly with OMFs and the additional oil retention volume measured in the evaporator at OMF above 1 wt.% is mainly due to refrigerant and oil solubility. A similar phenomena was reported in the literature by Jin and Hrnjak (2014) but for condensers, where oil separated at the inlet header of the condenser and started to fill the bottom channels first. Furthermore, in the present evaporator A, the superheated vapor velocity at microchannel tubes decreased from around 2000 ft/s to 2.4 ft/s in the outlet header. Low vapor velocity inside outlet header reduced the vapor refrigerant and oil rich liquid layer interfacial shear force, which was responsible to carry the oil. This further promoted oil retention in the outlet header. At higher mass flux of refrigerant and oil mixture, the shear stress at the vapor-liquid interface was also high when compared to that of low mass flux. The interfacial shear stress was depended upon the difference between the refrigerant gas velocity and liquid oil film velocity (Lee, 2002). Thus, at higher mass flux, hence higher vapor velocity, more oil was carried over with the refrigerant vapor out form the evaporator and the oil retention volume decreased.



At the same saturation temperature, lower mass flux caused oil retention volume to increase between 5% and 3 times that for OMF ranging from 0.5 to 5 wt.%. It should be noted that for typical air conditioning applications, OMF is equal or less than 1 wt.%. From the experiments of the present work, the ORV_N at OMF of 1 wt.% was less than 4% of total internal volume for high mass flux series of J, K and L (represented as void

symbols in Figure 5.10) and the ORV_N was up to 10% of total internal volume of evaporator A for low mass flux series G, H, and I (represented as solid symbols in Figure 5.10).

5.2.1.2 Microchannel evaporator A with R134a and POE oil

This section discusses the experimental results of oil retention volume in microchannel evaporator A with refrigerant R134a and POE oil mixture. The experiments were carried out for saturation temperature of R134a at and above freezing temperatures, i.e. 33 °F (0 °C). Details of the test conditions are given in Table 5-4. The series (M, N, and O) for the oil retention experiments were carried out at mass flow rate of about 200 lbm/hr, and the saturation temperature was also varied in three stages ranging from 33 to 48 °F (0.5 °C to 9.5 °C).

Table 5-4: Legend of the letters and symbols used in the figures reporting the tests results of microchannel evaporator A with R134a and POE

Symbol	Letter	T_{sat}	$G_{Evaporator A}$
		$^{\circ}F (^{\circ}C)$	$lb_m/ft^2-s (kg/m^2-s)$
	M	33 (0.5)	3 (15)
	N	38 (3.3)	3 (15)

O 48 (9) 3 (15)



*G is the mass flux inside each microchannel tube. It was calculated from the total mass flow rate entering evaporator A divided by the total cross sectional area of all the microchannel tubes of the evaporator A ($G_{\text{Evaporator A}}$).

The results of oil retention volume (ORV_N) in evaporator A with refrigerant R134a and POE oil mixture for series (M, N and O) are given in Figure 5.12. The results indicated that the oil retention in evaporator A was strongly depended on the OMF and the oil retention volume increased if OMF increased. The oil retention volume was measured up to 7.5 % of internal volume of evaporator A.

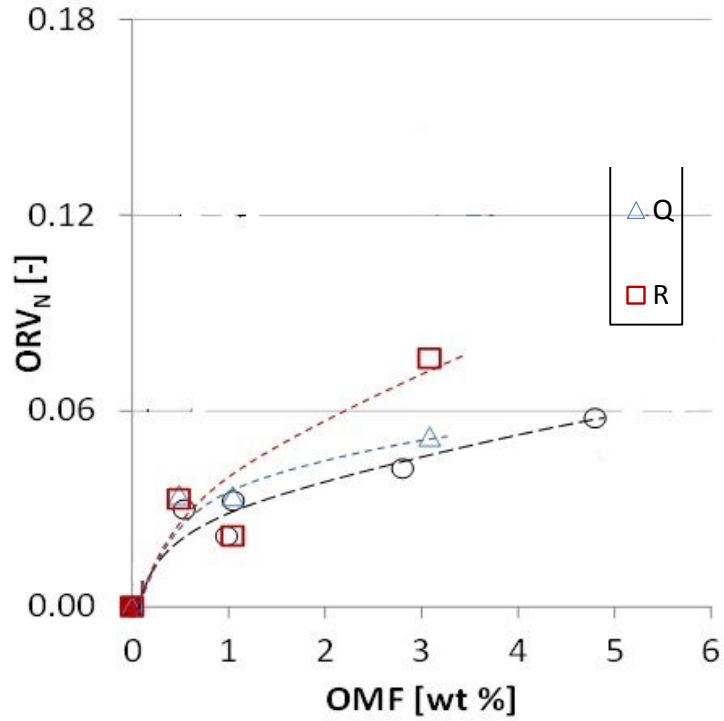


Figure 5.12: Oil retention volume for R134a+POE oil in microchannel evaporator A

As OMF increased from 0 to 1 wt. %, the ORV_N was up to 3 % of internal volume of evaporator A. The effect of saturation temperature was clearly visible when comparing the series (M, N and O) for oil mass fraction of 3 wt.%.

5.2.2 Heat transfer factors (HTFs) for microchannel evaporator

This section discusses the results of effect of oil on heat transfer rate of microchannel evaporator A with refrigerant R410A and POE oil mixture and with refrigerant R134a and POE oil mixture. The tests were conducted for two mass fluxes and at several saturation temperatures. The test conditions and the legend for the symbols used to report the experimental results from these tests were given in Table 5-3 and Table 5-4. The effect of oil on the heat transfer rate is provided in terms of heat transfer factor (HTF), which was the ratio of heat transfer rate measured from the air-side when oil was present over the heat transfer rate in oil-free conditions. Both heat transfer rates were evaluated at the same total mass flux, saturation pressure, and degree of superheated vapor at the outlet. Thus, the HTF isolated and quantified the effect of oil on the refrigerant-side heat transfer capacity. The results are summarized in plots in which OMF is on the x-axis and the HTF is on the y-axis. Low mass flux is represented by solid symbols (series G, H, and I) while the high mass flux is represented by the void symbols (series J, K and L series). Each saturation temperature was evaluated at both high and low mass flux. It should be emphasized in here that the refrigerant was well distributed across the microchannel tubes of the evaporators. Since we purposely decided to control the inlet conditions of the microchannel evaporators to slightly sub-cooled (or near saturated) liquid, the distribution of the refrigerant and oil mixture across the microchannel tubes was uniform during the tests of the present work. The flow distribution was only qualitatively observed by using thermal images of the evaporators during the tests. These images will be presented later in the manuscript but since the thermal image colors of the evaporator were uniform everywhere along the front face of the heat exchanger, we concluded that

all the microchannel tubes received approximately the same flow rate of refrigerant (or of refrigerant and oil mixture). The condition of saturated liquid at the inlet of the evaporator was not necessarily representative of real life evaporator applications but, in the present study, it avoided the challenge of non-uniform flow distribution of the refrigerant and oil mixture when oil was injected to the evaporator. As a result of the testing conditions imposed for the evaporators in the present work, the HTFs presented for the evaporators do not account for the effect that oil might have on the refrigerant flow distribution across the microchannel tubes and they do not account for the flow change, if any, inside the inlet headers of the microchannel heat exchangers. These effects, which are still due to the presence of oil in the mixture, might result in additional sources of heat transfer rate degradation in microchannel evaporators and their investigation could be part of future studies of this work.

5.2.2.1 HTF of microchannel evaporator A with R410A and POE oil

The experimental results of heat transfer factor (HTF) in evaporator A with refrigerant R410A and POE oil are summarized in Figure 5.13. This figure shows the HTF of the microchannel evaporator A on the y-axis and the oil mass fraction (OMF) of POE oil in refrigerant R410A on the x-axis. When OMF is 0 (i.e., no oil is present inside the evaporator), the HTF resulted 1 by its own definition and it decreased if OMF increased as shown in Figure 5.13. The effect of mass flux is represented as void and solid symbols and corresponding letters in the legend of the figures. Low mass flux series are represented by the solid symbols (G, H, and I) while high mass flux tests are represented as void symbols (J, K and L series) (for details about the legend, see Table 5-3). Each saturation temperature is given with a void and a solid symbol with same color and shape

of the symbol. For example, the black circle data points in Figure 6.14 represent saturation temperature of 48° F (9° C); the solid circle points (series G) are for low mass flux while the void circle points (series J) are for high mass flux. The results indicate that if the oil mass fraction (OMF) increased, the heat transfer factor of microchannel evaporator A decreased from 1 to 0.87. This represents a reduction of the refrigerant-side heat transfer rate due to oil by about 13%. However, at OMF of 1 wt.%, the reduction of the refrigerant side heat transfer rate was within the experimental uncertainty of $\pm 4.5\%$. From Figure 6.14 it is clear that the effect of oil on heat transfer rate was to decrease the refrigerant-side heat transfer rate but the impact of oil was not significant if OMF ranged from 0.5 wt. % and 1 wt. %. The impact of oil on the heat transfer rate was measurable for OMFs of 3 wt. % and of 5 wt. % and the heat transfer rate decreased by about 8 to 13%. The HTFs given in Figure 5.13 represent only the effect of oil because each test with oil was compared with the corresponding reference without oil at the same inlet saturation pressure, total mass flow rate, and degree of superheated vapor at the outlet of the evaporator. The air inlet temperature and velocity were also constant between the tests with oil and the baseline reference tests with no oil. Figure 5.14 provides the simulation results of the local refrigerant-side convective heat transfer coefficient of R410A and POE oil mixture along the direction of the refrigerant flow in a microchannel tube. Each tube was divided in 100 segments in order to compute 100 values (one for each segment) of the two phase flow boiling heat transfer coefficient inside the microchannel tube. The model used to obtain these results will be described in details in the next section but it is used here to highlight some insights on the convective heat transfer process inside the microchannel tube when oil was present. The simulation

results in Figure 5.14 indicate that the presence of oil in refrigerant R410A decreases the heat transfer coefficient when compared to refrigerant R410A heat transfer coefficient (blue series with legend 1-0OMF). This preliminary calculations show that oil tended to penalize the two phase flow heat transfer coefficient if refrigerant heat transfer coefficient correlations available in the literature were used for predicting the behavior of refrigerant and oil mixtures. This extrapolation of the heat transfer correlations might not be valid and should be carefully evaluated. However, developing local heat transfer coefficient correlations for refrigerant and oil mixtures was out of scope of the present work and might be potential future work.

The plots from Figure 5.15 to Figure 5.18 show the direct effect of oil on the heat transfer rate, $\dot{Q}_{evap,A}$, which was measured from the air-side of the evaporator during the actual heat transfer experiments. $\dot{Q}_{evap,A}$ was measured directly from the measurements of air flow rate (which was constant at all time during the tests) and of air inlet and outlet dry bulb temperatures. These figures shows how the heat transfer rate varied in real time during the tests when the oil was injected in the evaporator. The green solid line in each Figure represent the oil injection period. If the oil flow was zero than the green line is also zero; if the oil flow is greater than zero then the green line becomes high value. The measured data of instantaneous heat transfer rate in Figure 5.15 to Figure 5.18 were sampled every 2 seconds and the brown solid lines had some scattering. However, from these figures it was evident that when oil was introduced in the evaporator, the heat transfer rate decreased. The effect of oil on heat transfer rate was not directly visible from the instantaneous measurements of heat transfer rate if OMF was 0.5 wt. % and 1 wt. % (see Figure 5.15 and Figure 5.16). But when OMF was 3 wt. % and 5 wt. %, there was a

marked shift of the instantaneous heat transfer rate to below 15,000 Btu/hr (4.4 kW), shown in Figure 5.17 and Figure 5.18.

Figure 5.13: Heat transfer factor in microchannel evaporator A with R410A and POE oil

Figure 5.14: Simulation results of the local convective heat transfer coefficient in one microchannel tube of evaporator A with R410A and POE oil mixture (Dell'orto, 2014, printed with permission)

Figure 5.15: Heat transfer rate measured from the air-side ($\dot{Q}_{evap,A}$) in microchannel evaporator A with R410A and POE oil at OMF at 0.5%

Figure 5.16: $\dot{Q}_{evap,A}$ in microchannel evaporator A with R410A and POE oil at OMF 1%

Figure 5.17: $\dot{Q}_{evap,A}$ in microchannel evaporator A with R410A and POE oil at OMF 3%

Figure 5.18: $\dot{Q}_{evap,A}$ in microchannel evaporator A with R410A and POE oil at OMF 5%

The worst case of decrease in HTF of the microchannel evaporator A in Figure 5.13 was measured at OMF of 5 wt. % and at low mass flux (series H) where HTF was reduced by 13 % when compared to no oil conditions. For air-conditioning applications, when OMF is typically less than 1 wt. %, the decrease in heat transfer rate was less than 4%. The oil decreased the heat transfer rate and its impact was also depended on the mass flux. The HTFs were close to 1 for OMF less than 1 wt. % and for both high and low mass flux. For OMF higher than 1 wt. %, the impact of mass flux on HTF was measurable. For example, at OMF of 3 wt.%, a reduction of mass flux from high mass flux of 8.4 lb_m/ft²-s (20.4 kg/m²-s, series K) to low mass flux of 4.2 lb_m/ft²-s (20.4 kg/m²-s, series H) decreased the HTF from 0.96 (series K in Figure 5.13) to 0.90 (series H) for the same

saturation temperature of 38°F (3.3°C). Hu et al. (2011) conducted heat transfer experiments to study the heat transfer coefficient of R410A and POE oil mixture during flow boiling in a 7 mm diameter smooth tube. Their analysis showed that decreasing the mass flux of R410A/POE mixture at particular quality and oil concentration resulted in diminished local heat transfer coefficient. Their finding was in agreement with the experimental results of Figure 5.13, in which the HTFs for low mass flux series (letters G, H, and I) tended to be slightly lower than the HTFs for the high mass flux series (J, K and L). Furthermore, we recall that for the same OMF and saturation temperature, oil retention in the low mass flux series (G, H, and I) was higher when compared to that of high mass flux series (J, K and L). Due to high oil retention for low mass flux series (G, H, and I) there could be additional resistance added to heat transfer process in microchannel tubes. Finally, for evaporator A, the saturation temperature did not have a marked effect on HTF. This might be due to the normalization of the heat transfer rate with oil over the corresponding heat transfer rate with no oil at the same saturation temperature. The low mass flux series (G, H, and I) in Figure 5.13 were close to each other and the high mass flux series (J, K and L) were close to each other. For each group, the HTFs were within the experimental uncertainties of $\pm 4.5\%$ for HTF, shown by the error bars for one representative data point in Figure 5.13 (the same experimental uncertainty bars applied to all data points of the figure).

5.2.2.2 HTF for microchannel evaporator A with R134a and POE oil mixture

This section discusses the experimental results of heat transfer factor in microchannel evaporator A with refrigerant R134a and POE oil mixture. The experiments were carried out for saturation temperature of R134a at and above freezing temperatures, i.e. 33 °F (0 °C). Details of the test conditions are given in Table 5-4. The series (M, N and O) for the oil retention experiments were carried out at mass flow rate of about 200 lbm/hr, and the saturation temperature was also varied in three stages ranging from 33 to 48 °F (0.5 °C to 9.5 °C). The mass fluxes and test conditions are provided in Table 3-4.

The HTFs in Figure 5.19 represent only the effect of oil because each test with oil was compared with the reference without oil at the same inlet saturation pressure, total mass flow rate, and degree of vapor superheated at the outlet of the evaporator. The air inlet temperature and velocity were also constant between the cases of tests with oil and the baseline references with no oil. The results indicates that the presence of oil decreased the heat transfer capacity of microchannel evaporator A with refrigerant R134a. For few exceptions it was observed that presence of oil slightly increased the heat transfer rate of the evaporator compared to case of oil free conditions. For OMF ranging from 0 wt.% to 5 wt.%, the HTF of microchannel evaporator A decreased up to 12%. For refrigeration applications in which the OMF is typically less than 1 wt. % the HTF was about 0.96, which indicates a maximum decrease of heat transfer rate of 4% when compared to oil free conditions. These were the results for series M, N and O in Figure 5.19.

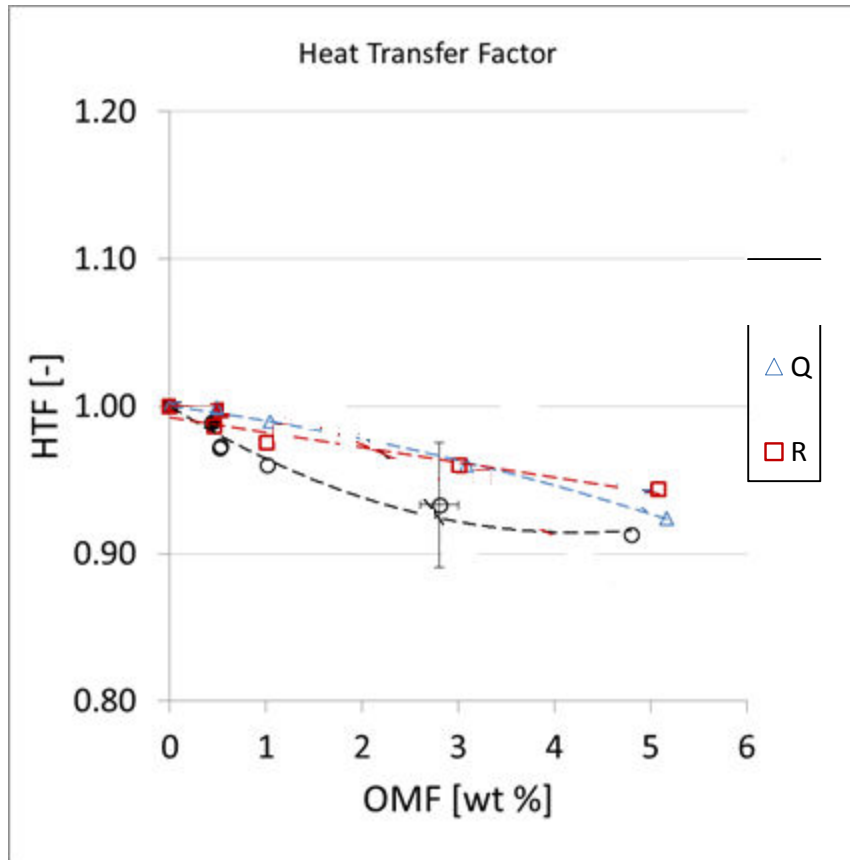


Figure 5.19: Heat transfer factor in microchannel evaporator A with R134a and POE oil

5.2.3 Pressure drop factor of microchannel evaporator

This section discusses the results of the effect of oil on the refrigerant side pressure drop for microchannel evaporator A with refrigerant R410A and POE oil mixture and with refrigerant R134a and POE oil mixture. The tests were conducted for two mass fluxes and at several saturation temperatures. The test conditions and the legend for the symbols used to report the experimental results from these tests are given in

Table 5-3 and Table 5-4. The effect of oil on the pressure drop is provided in terms of pressure drop factor (PDF), which was the ratio of pressure drop measured across the refrigerant side of the microchannel evaporator when oil was present over the pressure drop in oil-free conditions (see again definition of PDF in Eq. 4-9). Both pressure drops were measured at the same total mass flux, saturation pressure, and degree of superheated vapor at the outlet. Thus, the PDF isolated and quantified the effect of oil on the refrigerant-side pressure drop. The results were summarized in plots in which OMF was on the x-axis and the PDF was on the y-axis. Low mass flux was represented by solid symbols (series G, H, and I) while the high mass flux was represented by the void symbols (series J, K and L series). Each saturation temperature was evaluated at both high and low mass flux. It should be emphasized in here that the refrigerant was well distributed across the microchannel tubes of the evaporators. The PDFs presented in this work did not account for the effect that oil might have on the refrigerant flow distribution across the microchannel tubes and they did not account for the flow change, if any occurred, inside the inlet headers of the microchannel heat exchangers. These effects, which are still due to the presence of oil in the mixture, might results in additional sources of pressure drop augmentation in microchannel evaporators and their investigation could be part of future studies of this work.

5.2.3.1 PDF of Microchannel evaporator A with R410A and POE oil

The experimental results of pressure drop factor (PDF) in evaporator A with refrigerant R410A and POE oil are summarized in Figure 5.20. This figure shows the PDF of the microchannel evaporator A on the y-axis and the oil mass fraction (OMF) of POE oil in refrigerant R410A on the x-axis. When OMF is 0 (i.e., no oil is present inside the

evaporator), the PDF resulted 1 by its own definition and it increased if OMF increased as shown in Figure 5.20. The effect of mass flux is represented as void and solid symbols and corresponding letters in the legend of the figures. Low mass flux series were represented by the solid symbols (G, H, and I) while high mass flux tests were represented as void symbols (J, K and L series) (for details about the legend, see Table 5-3). Each saturation temperature was given with a void and a solid symbol with same color and shape of the symbol. For example, the black circle data points in Figure 5.20 represent saturation temperature of 48° F (9° C); the solid circle points (series G) are for low mass flux while the void circle points (series J) are for high mass flux. The results indicate that if the oil mass fraction (OMF) increased, the pressure drop factor of microchannel evaporator A increased from 1 to 1.47. This represents an augmentation of the refrigerant-side pressure drop due to oil by about 47%. From Figure 5.20 it is clear that the effect of oil on pressure drop was to increase the refrigerant-side pressure drop. The impact of oil was still significant even when OMF ranged from 0.5 wt. % and 1 wt. %. The PDFs given in Figure 5.20 represent only the effect of oil because each test with oil was compared with the corresponding reference without oil at the same inlet saturation pressure, total mass flow rate, and degree of superheated vapor at the outlet of the evaporator. The air inlet temperature and velocity were also constant between the tests with oil and the baseline reference tests with no oil. The increase in pressure drop can be attributed to the increase in viscosity of liquid mixture of refrigerant and lubricant in the microchannels. Hu *et al.* (2009) reported that the presence of lubricant enhances two phase pressure drop, where penalty factor ranges from 1.0-1.9 for 3.0 mm O.D. tube. As the amount of oil in refrigerant increased the penalty factor also increased.

Figure 5.20: Pressure drop factor in microchannel evaporator A with R410A and POE oil

The worst case of increase in PDF of the microchannel evaporator A in Figure 5.20 was measured at OMF of 5 wt. % and at high mass flux (series J) where PDF was augmented by 47 % when compared to no oil conditions. For air-conditioning applications, when OMF is typically less than 1 wt. %, the increase in pressure drop was less than 20%. The PDFs were slightly above 1 for OMF less than 0.5 wt. % and for both high and low mass flux. At OMF of 3 wt.%, increase of mass flux from low mass flux of $4.2 \text{ lb}_m/\text{ft}^2\text{-s}$ ($20.4 \text{ kg}/\text{m}^2\text{-s}$, series H) to high mass flux of $8.4 \text{ lb}_m/\text{ft}^2\text{-s}$ ($20.4 \text{ kg}/\text{m}^2\text{-s}$, series K) increased the PDF from 1.15 (series H in Figure 5.20) to 1.32 (series K) for the same saturation temperature of 38°F (3.3°C). Hu *et al.* (2008) measured and correlated two phase

frictional pressure of R410A/POE mixture flow boiling inside 7 mm diameter tube. Their experimental parameters include the evaporation temperature of 5 °C for two mass flux, the heat flux from 7.56 to 15.12 kW/m², the inlet vapor quality from 0.2 to 0.7, and nominal oil concentration from 0 % to 5 %. Their results indicated that the frictional pressure drop of R410A/ POE oil mixture increases as mass flux increases for similar vapor quality. And frictional pressure drop was high in regions of high vapor quality due to high viscosity oil rich liquid mixture. Their findings are in agreement with the experimental results of Figure 5.20, in which the PDFs for high mass flux series (letters J, K, and L) tended to be significantly higher than the PDFs for the high mass flux series (G, H and I) and OMF above 1 wt.%.

For similar OMF and mass flux, the impact of saturation temperature on pressure drop was less significant for OMF less than 1 wt. % and the results for these conditions were within uncertainty range of experimental instruments. For same mass flux and OMF higher than 3 wt. %, pressure drop was highest for saturation temperature of 33 °F (0 °C) for each OMF, represented as series G and J. As saturation temperature increased from 33 to 38 °F (0 to 3.3 °C), the pressure drop factor decreased. Although change in liquid mixture viscosity at particular quality and saturation temperature from 33 to 38 °F (0 to 3.3 °C) was negligible, there was significant decrease in liquid mixture density by 2.56 % for R410A+POE oil mixture at 5 wt. % POE oil. Furthermore, there was considerable decrease in surface tension of R410A+POE oil at the same concentration by approximately 22 % as temperature decreased from 33 to 38° F (0 to 3.3° C) (Wei *et al.*, 2007). The decrease in surface tension could lead to decrease in wall shear stress which can lead to lesser pressure drop factor during evaporation in the microchannels. These

two effects coupled together could explain the high pressure drop factor at saturation temperature 33 °F (0 °C) with respect to the pressure drop factor measured at 38°F (3.3°C) in the present work. As saturation temperature increased from 38 to 48 °F (3.3 to 9 °C) there was no measurable effect on pressure drop, for similar mass flux and OMF. The reason behind this was due to decrease in density approximately by 1 %, surface tension decreased by approximately 5 % as saturation temperature increased from 38 to 48 °F (3.3 to 9 °C) (Wei *et al.*, 2007).

5.2.3.2 PDF of Microchannel evaporator A with R134a and POE oil mixture

This section discusses the experimental results of effect of oil on pressure drop factor in microchannel evaporator A with refrigerant R134a and POE oil mixture. The experiments were carried out for saturation temperature of R134a at and above freezing temperatures, i.e. 33 °F (0 °C). Details of the test conditions are given in Table 5-4. The series (M, N and O) for the oil retention experiments were carried out at mass flow rate of about 200 lbm/hr, and the saturation temperature was also varied in three stages ranging from 33 to 48 °F (0.5 °C to 9.5 °C). The mass fluxes, test conditions, and the legend for the symbols in Figure 5.21 are provided in Table 5-4.

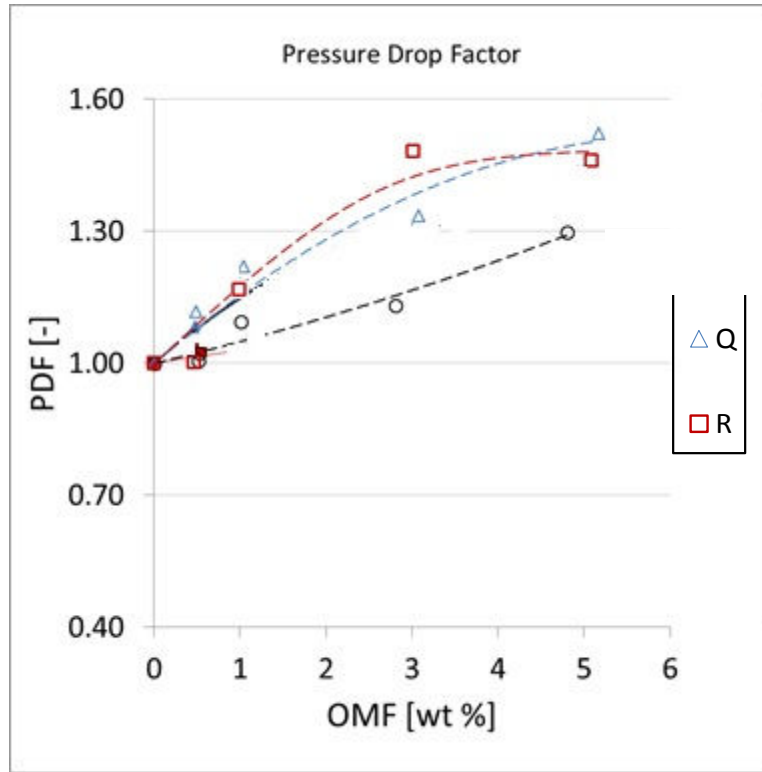


Figure 5.21: Pressure drop factor in microchannel evaporator A with R134a and POE oil

The PDFs in Figure 5.21 represent only the effect of oil because each test with oil was compared with the reference without oil at the same inlet saturation pressure, total mass flow rate, and degree of vapor superheated at the outlet of the evaporator. The air inlet temperature and velocity were also constant between the cases of tests with oil and the baseline references with no oil. The results indicates that the presence of POE oil increased the refrigerant-side pressure drop in microchannel evaporator A when refrigerant R134a was used. For OMF ranging from 0 wt.% to 5 wt.%, the PDF of microchannel evaporator A increased up to 57%. For refrigeration applications in which

the OMF is typically less than 1 wt. % the PDF was about 1.2, which indicates a maximum increase of pressure drop of 20% when compared to oil free conditions.

For series M, N and O, the pressure drop increased by 35% only when the saturation temperature increased from 33° to 38° F (0.5 to 3.3°C, series M and N) while there was no significant increase in pressure drop when the saturation temperature increased from 38° F to 48° F (3.3 to 9°C, series N and O).

CHAPTER VI

6 Oil Retention Model

The experimental work presented in the previous sections provided data on oil retention and its effects on microchannel condenser performance. A mechanistic model for oil retention model in microchannel condensers was developed in separate study and the results were used to help on analyzing the experimental results in this study. This section discusses briefly the model and its validation with the data of the present work and some data from the open domain literature. The model predicted the thermal performance of the microchannel condenser and the refrigerant-side operating conditions with and without oil (as well as the air-side conditions). The simulations of the entire heat exchangers were also used in the present work to provide some insights of the physics for oil retention, and to advance the understanding of the effects of oil on the heat transfer rates and pressure drops in microchannel condenser.

6.1 Microchannel Condenser Model

Microchannel type condensers have unique oil retention characteristics because of their small internal volume and of their header configuration. For microchannel heat exchangers, different models were developed to predict the heat transfer coefficient and to optimize the design of the heat exchanger for high performance. Often the models were based on a control volume approach and used an effectiveness-NTU method (Incropera and DeWitt, 2001) to solve the heat balance between the air side and the

refrigerant side. Huang (2012) developed a model to investigate various heat exchanger tube geometries. Schwentker (2005) developed a design tool for microchannel heat exchangers.

The model developed in this dissertation used a similar approach and it is based on the heat exchanger model originally developed by Iu (2007). The user defines the coil geometry parameters and selects the appropriate heat transfer and pressure drop correlations. Several researchers investigated correlations to predict the heat transfer and the pressure drop of both the refrigerant side and air side in condensers (Chang and Wang, 1997; Chang *et al.*, 2000). The behavior of the refrigerant and oil mixture during a condensation processes is also available in the literature (Schlager *et al.*, 1990; Thome, 1995; Bassi and Bansal, 2003). Huang (2012) investigated the influence of oil on condensation heat transfer coefficient of R410A for tubes of nominal diameters smaller than 5 mm. Their correlations were used in the present work as will be discussed later.

From the brief literature summary above, it appears that there are several models that are able to predict the heat transfer rate and pressure drop of refrigerant R410A two-phase flow condensation in microchannel condensers but they do not often consider the presence of oil in circulation with the refrigerant nor they have been experimentally verified when oil is retained in the condenser.

The model used a segmentation method to divide the heat exchanger into small sections along the refrigerant flow. By imposing a heat balance and by using the effectiveness-NTU method, the outlet conditions are predicted for each section and passed as input to the adjacent section until the entire refrigerant circuitry is completed. The model

calculates the local thermodynamic properties in each section for the refrigerant R410A and Polyester (POE) oil mixtures based on the local oil concentration, pressure, temperature, and mass flux. Then the model predicts the volume of oil retained in the microchannel tubes and its influence on the refrigerant-side heat transfer coefficient and pressure drop.

The present work used a numerical solver that was developed by Iu (2007) for numerically modeling heat exchangers. The model was implemented in FORTRAN and each single tube was divided in multiple segments whose capacity was computed using an effectiveness-NTU method.

6.2 Microchannel Condenser Model Validation

Experimental data of the oil retention and its effect on the heat transfer rate and pressure drop of microchannel type condensers were measured and were used to validate the predictions from the present model. The microchannel type condenser coil was tested at different operation conditions with refrigerant R410A and R134a and POE lubricant. The experimental data were obtained for two level of degree of superheat entering the condenser: one with low degree of superheat and one with high degree of superheat. The experimental setup, the test procedures, and test conditions for the experimental data of the microchannel condenser were described in details in the previous sections of this manuscript.

6.2.1 Air Conditioning Application with R410A and POE lubricant

The heat exchanger was tested at various operating conditions and with refrigerant R410A and with refrigerant-POE oil mixture; the saturation temperature ranged from 85

to 130°F (29 to 54°C) and the total refrigerant flow rate for the condenser varied between 400 to 600 lb_m/hr (0.05 and 0.075 kg/s). Finally, the oil mass fraction was also varied from 0.5 to 5 wt.%.

Before validating the model with the data of the present work, the air side heat transfer and the refrigerant side heat transfer and pressure drop with and without oil were independently verified with data from the literature. This was done to decouple the air side from the refrigerant side and isolate any potential sources of error in the model implementation. The numerical solver and algorithm was validated by Iu (2007). The air side heat transfer coefficients were verified with the correlations provided by Moallem *et al.* (2013), which were valid for a broad range louvered fin geometries commonly adopted in microchannel heat exchangers. The fin width, fin height, and fin depth of the present work were in the range of the correlation provided in Moallem *et al.* (2013).

The predictions of the refrigerant two phase flow condensation heat transfer coefficient for refrigerant R410A and oil mixture at different oil concentrations were verified against the literature data presented in Huang *et al.* (2010) and the results are summarized in Figure 6.1. The figure shows the simulation results of the present model for the heat transfer coefficient at different oil concentrations. The heat transfer coefficient was predicted with an error between $\pm 30\%$ and the model underpredicted the data of heat transfer coefficient. The deviation were larger at low oil concentration. In agreement with the data by Huang *et al.* (2010), the two phase flow condensation heat transfer coefficient was lower for higher oil concentrations. However, the prediction from the present model did not show a decrease of refrigerant side heat transfer coefficient as that reported by Huang *et al.* (2010).

Figure 6.1: Verification of the local refrigerant and oil mixture heat transfer coefficients during two phase flow condensation in microchannel tubes with data from the literature (Bigi, 2014)

The local surface temperature of the microchannel tube was predicted by the model and it was compared with the data collected in the present work by using an infrared thermal camera. For each segment, after the average heat capacity was computed, along with the outlet temperatures of air and refrigerant, the segment average surface temperature was calculated as in Equation 6-1 or with the equivalent expression reported in Equation 6-2.

$$\bar{T}_{\text{surface}} = \frac{T_{\text{air,inlet}} + T_{\text{air,outlet}}}{2} + \bar{Q}_{\text{seg}} * R_{\text{air}} \quad 6-1$$

$$\bar{T}_{\text{surface}} = \frac{T_{\text{ref,inlet}} + T_{\text{ref,outlet}}}{2} - \bar{Q}_{\text{seg}} * (R_{\text{ref}} + R_{\text{tube}}) \quad 6-2$$

The thermal measurements were taken by using an infrared camera (Fluke Infrared Solutions IR FlexCam), which had an accuracy of $\pm 1^{\circ}\text{C}$ ($\sim \pm 2^{\circ}\text{F}$). A surface thermocouple

(T-type thermocouple) was used for calibrating the emissivity on the infrared images. In order to be able to interpret correctly the information captured by the infrared images, additional tests were conducted on a sample of microchannel heat exchanger, similar in geometry to the one used for the oil retention tests. The sample was heated up inside an oven for about 60 minutes to ensure that the sample's temperature was uniform in all its parts. An infrared picture of the sample was then taken and its surface temperatures were also measured with an infrared thermometer (Fluke, Model: 62 MAX+; Accuracy: $\pm 1^{\circ}\text{C}$ ($\pm 2^{\circ}\text{F}$) or 1% of the reading).

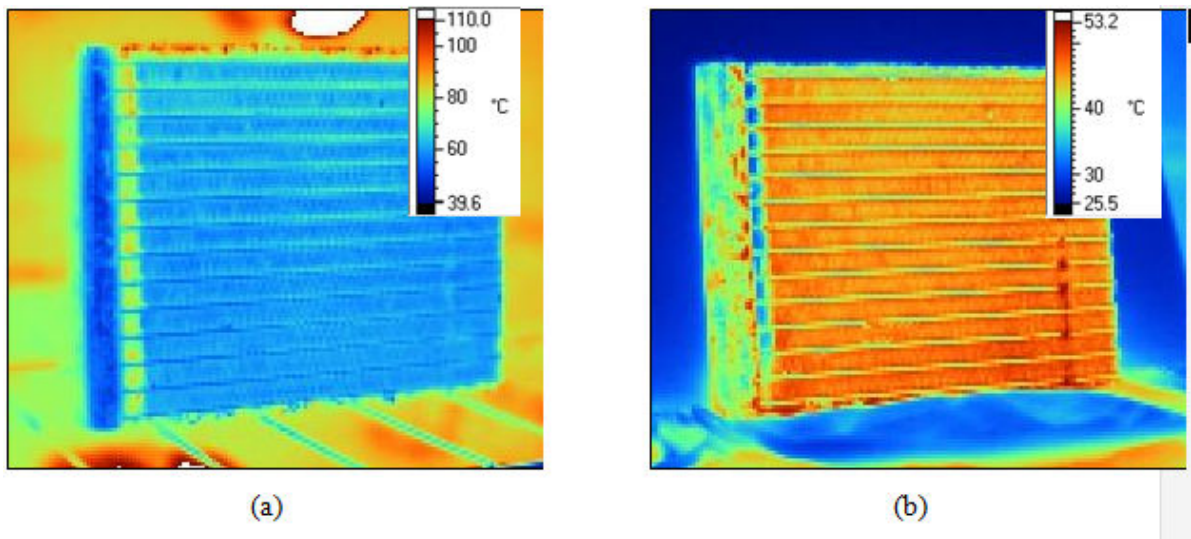


Figure 6.2: Infrared images of a small sample of microchannel heat exchanger inside (a) and outside (b) an oven; the images were taken to calibrate the emissivity factors of the thermal camera (Bigi, 2014)

The same procedure was repeated right after the sample was taken out of the oven. Figure 6.2 shows the temperature distribution captured by the infrared camera when the sample of microchannel heat exchanger was inside (a) and outside (b) the oven. It is noticeable how the images show a great change in temperature distribution between fins and tubes as soon as the sample was taken out of the oven. In particular, from Figure 7.6 (b) it looks

like the tubes were at a lower temperature than the fins; this observation was unexpected as the temperature of the sample should still be almost uniform or, at least, the fins' temperature was expected to decrease faster than the temperature of the tubes. Moreover, if the surface temperature measured with the infrared thermometer inside the oven was close to the one captured in the image (with a difference of about $\pm 1^{\circ}\text{C}$ ($\pm 2^{\circ}\text{F}$) between infrared camera and infrared thermometer), when the temperature was measured outside the oven, it was found to be closer to the temperature captured on the fins (with a difference up to $\pm 2.5^{\circ}\text{C}$ ($\pm 4.5^{\circ}\text{F}$) between infrared camera and infrared thermometer). It is possible that the captions of the infrared camera were disturbed by light reflection on the curved surface of the tubes. For these reasons, in order to validate the calculation of the surface temperature in the simulation, the temperature of the fins was used as a reference temperature for comparison, as opposed to the temperature of the tubes.

Figure 6.3: Infrared image of the microchannel condenser inlet with R410A and POE lubricant (a) and comparison of infrared image surface temperature with simulation results (b) for two different temperatures (Bigi, 2014)

Figure 6.3 (a) shows two thermal images of the microchannel condenser for two tests.

Figure 6.3 (b) shows the comparison of the tube surface temperature between the data and the simulation results. The cases reported in here are for a high degree of vapor superheat of about 63°F (35°C), for which the model had to predict a rapid decrease of surface temperature along the tube near the inlet header.

Some deviation was observed at the inlet region of the microchannel tube when the degree of superheat was high. At the inlet section of the condenser, which was the section

with the largest error, the surface temperature predicted by the model was about 5.5°F (3°C) or lower than the measured temperature. After both the air and the refrigerant side heat transfer coefficients and pressure drops were independently verified with data from the literature, the model was further validated with the data of the present work.

The model developed in the present work was also validated with the experimental data of this work when oil was retained in the microchannel condenser. Figure 6.4 shows the comparison between experimental data and predicted results for the oil retention volume (ORV) at low superheat conditions (top) and at high superheat conditions (bottom) of the microchannel condenser with refrigerant R410A and POE oil mixture. There is some scattering of the data in Figure 6.4 and the ORV was predicted from -50 to +70% with respect to the experimental data at low superheat conditions and within $\pm 70\%$ at high superheat conditions. Figure 6.4 provides the summary of the comparison between experimental data and predicted results for the oil retention volume (ORV) at high superheat conditions of the microchannel condenser with refrigerant R134a and POE oil mixture. Again there is some scattering of the data in Figure 6.5 and the ORV was predicted from -43 to +70% with respect to the experimental data.

The main reason for the discrepancy was due to the estimation of the oil retained in the headers and in the initial length of the microchannel tubes, in which refrigerant was superheated vapor. We observed that these sections of the condensers retained a significant portion of the total oil retained in the entire heat exchanger and sometimes they were dominant with respect to the oil miscible with the liquid phase of the refrigerant and oil mixture during two phase flow condensation. It is important to emphasize here that the sections of the condenser headers and microchannel tubes in

which refrigerant was in thermodynamic superheated vapor state, were assumed to retain oil in the form of a layer of oil rich mixture film that stretched and wetted the internal walls. While this assumption was sound the thickness of the liquid oil rich mixture film was estimated from the velocity of the vapor refrigerant and it was assumed constant among the various saturation temperatures. It was also assumed that the thickness varied linearly from 0 to a maximum value if the OMF increased from 0 to 5 wt.%. These assumptions might be the reason of the large error in the prediction of the ORV for some of the data points. However, overall the model provide the same order of magnitude of the oil retention that was measured during the tests. It should be finally noticed that for comprehensibility and for avoiding confusion, the uncertainty error bars are provided in only for few representative data points in the plots of Figure 6.4 but similar uncertainty error bars applied to all the experimental data points in the plot.

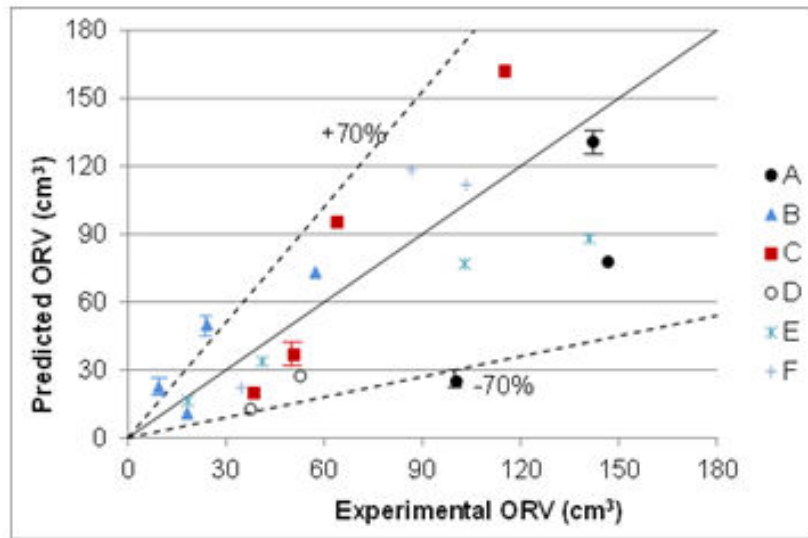
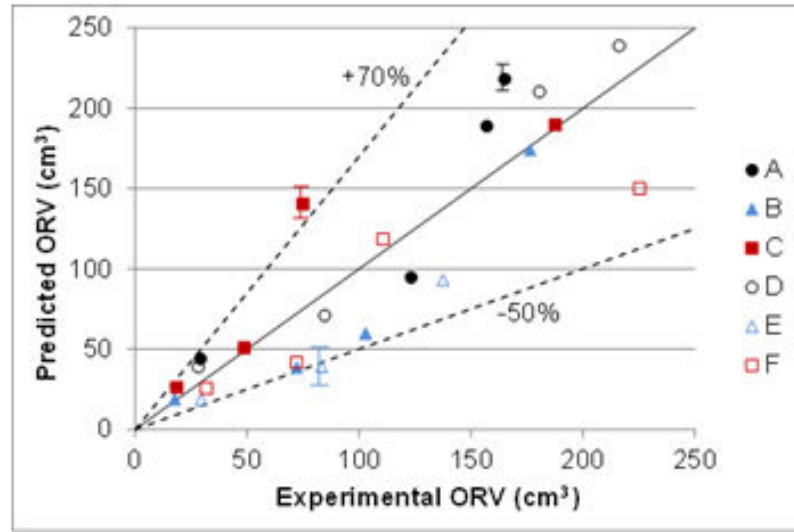


Figure 6.4 Comparison between experimental data and predicted results for the oil retention volume (ORV) at low superheat conditions (top) and at high superheat conditions (bottom) of the microchannel condenser with refrigerant R410A and POE oil mixture

Figure 6.5 Comparison between experimental data and predicted results for the oil retention volume (ORV) at high superheat conditions of the microchannel condenser with refrigerant R134a and POE oil mixture

Figure 6.6 and Figure 6.7 provide an example of the comparison between experimental data and predicted results for the HTF and PDF of the microchannel condenser with refrigerant R410A and POE oil mixture and R134a and POE oil mixture and at 105°F (41°C), low mass flux, and high and low superheat conditions. These results shows that the simulation results of PDF follow the same trend as the experimental data and provide similar PDFs, except for few isolated data points.

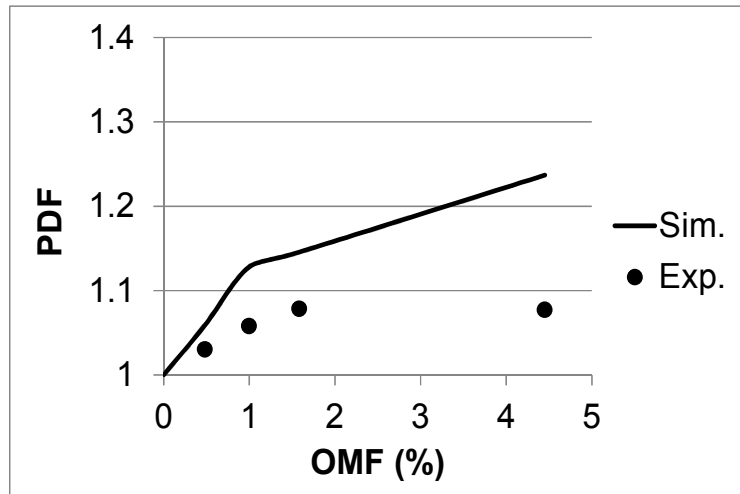
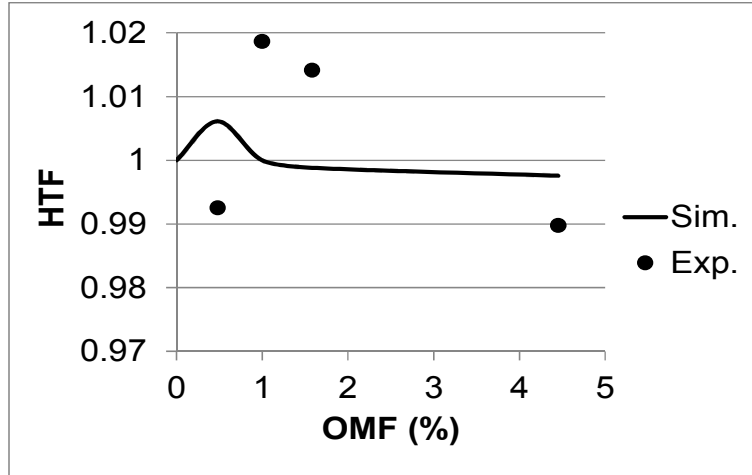


Figure 6.6: Comparison between experimental data and predicted results for the HTF (top) and PDF (bottom) of the microchannel condenser with refrigerant R410A and POE oil mixture at 105°F (41°C), low mass flux, and low superheat conditions

Figure 6.7: Comparison between experimental data and predicted results for the HTF (top) and PDF (bottom) of the microchannel condenser with refrigerant R410A and POE oil mixture at 105°F (41°C), low mass flux, and high superheat conditions

The predicted HTFs for R410A and POE mixture at both low and high superheat conditions were also in agreement with the experimental data as shown in Figure 6.6 and Figure 6.7 once the experimental uncertainty on the measured HTF data is considered. However, the simulation results for HTF seemed to under predict the degradation of heat transfer capacity due to the presence of oil when the OMF was higher than 3 wt.%. This was somewhat expected since the model assumed completely uniform refrigerant

distribution among the entire microchannel tubes regardless of the presence of oil. However, the oil might affect the internal distribution of the mixture in the condenser and subcooler and the distribution effects on the condenser heat transfer capacity are not accounted for in the model. The largest discrepancy was observed for refrigerant R134a and POE mixture, shown in Figure 6.8. The simulation results predicted a no change (or even a very small increase) of the heat transfer capacity and the HTF from the simulations ranged from 1 to 1.02 (i.e. an increase of 2%) if oil was retained in the heat exchanger. The experimental data showed a significant drop in capacity if the OMF was higher than 3 wt.%. One possible reason about the discrepancy of the HTF shown in Figure 6.8 might be the error in estimating the properties for the mixture of refrigerant R134a and VG 32 POE oil. This is not a common mixture and thus its property are not as well defined as the ones for the mixture of refrigerant R410A and VG 32 POE. Typically, VG 68 POE is more commonly used with the refrigerant R134a in refrigeration systems and thus further testing and modeling efforts might be required in future work by using this type of oil in combination with refrigerant R134a.

Figure 6.8: Comparison between experimental data and predicted results for the HTF (top) and PDF (bottom) of the microchannel condenser with refrigerant R134a and POE oil mixture at 105°F (41°C), low mass flux, and high superheat conditions

CHAPTER VII

7 Conclusions and Recommendations for Future Work

7.1 Conclusions from the Present Study

In vapor compression cycles the compressors need oil to prevent surface-to-surface contact, to remove heat, to provide sealing, to keep out contaminants, to prevent corrosion, and to dispose of debris created by wear. A small portion of the compressor oil circulates with the refrigerant through the cycle components, while most of the oil stays in the compressor. The oil amount carried with the refrigerant typically ranges from 0.5 to 1 percent of the refrigerant flow rate circulating in the air conditioning or refrigeration systems. This means that oil might be missing from the compressor because it can accumulate inside the heat exchangers during actual system operating conditions.

In refrigerant-to-air heat exchangers, the presence of oil increases the pressure losses and results in an additional thermal resistance to the heat exchange process; such effects are highly undesired yet unavoidable. In addition, improper oil management could lead to a lack of proper lubrication inside the compressor and ultimately to compressors mechanical failure.

Oil retention in heat exchangers is a complex function of fluid properties as well as geometry and configuration aspects. The circulating oil, which is missing from the compressor, can form a fairly homogeneous mixture with the liquid refrigerant or it can

exist as a separate oil film inside the tubes and headers of the heat exchangers and the amount of oil retained inside the heat exchangers is affected by the system operating conditions. The condensers and the evaporators of air conditioning and refrigeration systems have different oil retention characteristics, and large amounts of oil retained in refrigerant-to-air heat transfer equipment decrease the heat transfer rate and increase of pressure drop: both effects are highly undesired yet unavoidable.

The present study investigated the oil retention and its effects on heat transfer and pressure drop of refrigerants and oil mixtures in microchannel type condenser and evaporators. The present work used three different louvered-fin aluminum microchannel heat exchangers: one type for the condenser and two types for the evaporator. All three microchannel type heat exchangers were commercially available or installed in commercially available heat pump systems. The experiments were conducted in a custom-made test facility built ad-hoc for this research study in order to replicate at Oklahoma State University (OSU) laboratory the real life operating conditions of the heat exchangers of air conditioning and refrigeration systems. The OSU test facility also controlled the amount of oil in the heat exchangers and it measured the oil retention, the heat transfer rates, and the pressure drops. The test conditions were selected based on typical applications of refrigerant R410A in air conditioning applications and of refrigerant R134a in vending machines and water/wine coolers refrigeration systems. The oil used in the present work was synthetic polyol ester (POE) with viscosity grade of VG 32. The saturation temperatures for condenser applications varied from 85 to 130°F (29 to 54°C) while for evaporator applications, the range of saturation temperatures was ranged from 33 to 48°F (0 to 9°C).

The oil mass fraction (OMF) in actual air conditioning systems, vending machines, and water/wine cooler systems typically ranges from 0.5 to 1 wt. % (weight percent), and sometimes the OMF can be as high as 3 wt. % for some operating conditions. The maximum OMF levels investigated in the present work were intentionally higher than 1 wt.% and up to 5 wt.% because the aim was to clearly highlight trends among the experimental results. However, the results in the present study when OMFs were higher than 3 wt.% should not be necessarily interpreted as representative results for actual systems in the field.

The specific objectives that were achieved in the present study are as follows:

- 1) The study constructed an experimental apparatus capable of measuring the oil retention volume in microchannel heat exchangers used as both evaporators and condensers in R410A air conditioning systems and R134a coolers refrigeration systems
- 2) The study measured the quantity of oil held up in two microchannel heat exchangers, one for R410A air conditioning and one for R134a coolers applications, both operating in evaporator and condenser modes
- 3) The study provided data of oil retention in microchannel heat exchangers as function of oil mass fraction circulating in the heat exchangers, refrigerant flow rates, and refrigerant saturation temperatures
- 4) The study assessed the effect that oil held up inside the microchannel heat exchanger has on the heat transfer capacity degradation and refrigerant side pressure drop

- 5) The study performed analysis on the experimental data and utilized results from a model (developed from separate study) for oil retention and its effects to heat transfer and pressure drop in microchannel condenser

In the study, a methodology to measure oil retention in a refrigerant-to-air heat exchanger and to isolate and quantify the effect of oil on the heat transfer rate and pressure drop developed. A new test facility that consisted of three main systems, namely a refrigeration loop system, an oil injection system and an oil extraction system was designed, constructed, and calibrated. In the refrigeration loop system, a variable speed gear pump and a series of heat exchangers were used to control the refrigerant saturation temperature and the refrigerant flow rate to the microchannel heat exchangers. The details of the experimental apparatus are provided in the body text of the manuscript. After extensive calibration, and after repeating several tests, the experimental uncertainty in the measured oil retention volume was ± 10 percent. The uncertainty on the heat transfer rate was ± 5.2 percent and the uncertainty on the pressure drop was ± 0.25 percent. When reporting the volume of oil held up inside the heat exchanger, the measured volume of oil was normalized with respect to the total internal volume of the heat exchanger, which was the sum of the internal volume of the microchannel tubes plus the internal volume of the headers. This normalization of the oil retention volume made it possible to compare the oil retention characteristics among heat exchangers with very different dimensions. The normalized oil retention volume increased from 0 if the OMF was zero (i.e., no oil) up to 0.15 when oil was present, which meant that 15 percent of the internal volume of the microchannel heat exchanger was filled with oil. In the variation of 0 to 0.15, the normalized oil retention volume experimental uncertainty due to

instrumentation accuracy, random error, human operator, and repeatability was within ± 0.01 .

When comparing the heat transfer rate for the case in which oil was present versus the case of oil free conditions, the air flow rate and air inlet temperature were constant. This resulted in the definition of the heat transfer factor (HTF), which is the parameter that was used in the present study to isolate and quantify the effect of oil on the refrigerant side heat transfer rate. The HTF varied from 1 if the OMF was zero (i.e., no oil) down to 0.85 when oil was present and the experimental uncertainty on the HTF was within 2% (that is, ± 0.01). Similarly, the effect of oil on the refrigerant-side pressure drop were given in terms of pressure drop factor (PDF). The PDF increased from 1 if the OMF was zero (i.e., no oil) to up to 1.9 when oil was present and the experimental uncertainty on the PDF was also within ± 0.01 .

The experimental results obtained in the present study were analyzed and used in the validation of a separately developed model that calculated the oil retention, the overall heat capacity, and pressure drops.

The main conclusions from the experimental efforts and the use of the model are presented below for the microchannel condenser, microchannel evaporators, and model validation results

Microchannel condenser.

For microchannel type condenser, the results from the present work indicated that the oil retained in the condenser was strongly depended on the OMF of the mixture. The oil

retention volume increased if the OMF increased and it was measured up to 11% of the total condenser internal volume, which consisted of the internal volume of all microchannel tubes plus the headers. The internal volume of the condenser was about 2,436 cm³ (that is, 2.4 liters or 149 inch³). The oil retention volume for high mass flux conditions were higher than those for low mass flux conditions and the effect of mass flux on the oil retention was small for low OMFs but it became more evident for OMFs higher than 3 wt.%. This was explained by considering that at high mass flux more liquid phase was present inside the condenser than that at low mass flux condition and similar saturation temperature. The liquid phase travelled along the condenser with low mass velocity with respect to the refrigerant vapor phase velocity. Oil existed as either homogenous solution in liquid refrigerant or as a separate layer of oil rich-film at the microchannel tube wall. The presence of oil on both cases promoted oil held up in the microchannel condenser but in different ways. The two-phase region of the condenser was the main section of the heat exchanger where the oil was retained and in this section oil was simply mixed with the liquid refrigerant. When the oil concentration is 1 wt.%, the higher was the liquid phase volume inside the condenser, the higher was the oil amount mixed in it and thus the higher was the oil retention in the condenser. On the other hand, in the superheated section of the condenser, oil existed as liquid droplets and as film near the wall. The higher was the refrigerant vapor velocity, the better the oil was carried over with the refrigerant. The total oil volume retained in the condenser was depended on these two mechanisms, and the dominant mechanism was different based on the saturation temperature of condensation. While a low degree of superheat tended to

increase the oil retention, a generalization of the results from the present work to all saturation temperatures of condensation should not be made.

Oil affected the heat transfer rate of the microchannel condenser and it penalized the heat transfer capacity by as much as 10 percent if the oil mass fraction was 3 wt.%. Different trends were observed for medium saturation temperature and intriguing results were observed at low saturation temperatures for two refrigerant mass fluxes and inlet superheat conditions. For medium saturation temperature of 105°F (41°C) the refrigerant-side heat transfer capacities were fairly constant, even when a lot of oil was present inside the condenser. These results were observed for two mass fluxes and two level of superheated vapor at the inlet of the condenser. It is interesting also to note that at low saturation temperature of 85 to 95°F (29 to 35°C), the presence of oil was observed to increase the refrigerant-side heat transfer rate, although in non-monotonic fashion. For both refrigerant R410A and POE mixture and refrigerant R134a and POE oil mixture, the heat transfer rate at low saturation temperature increased slightly if the OMF increased up to about 3 wt.%; then the heat transfer rate started to decline at higher OMFs. POE oil was a contaminant that added an additional thermal resistance to the heat exchange process between the air and the refrigerant in the microchannel condenser. Thus, the reasons as to why the heat transfer rate of the condenser increased when oil was present at low the saturation temperature of condensation were not clear and required further research in future work.

Oil also increased the refrigerant-side pressure losses of the microchannel condenser up to 19 percent with respect to oil free conditions. This was due to high refrigerant-oil mixture viscosity compared to that of liquid refrigerant for the flow inside the

microchannel tubes. The increase of oil mass fraction also resulted in oil retention in the microchannel condenser and the oil might block some of the channels and/or reduce the refrigerant flow cross sectional area in the condenser. Both phenomena led to higher pressure drop during the condensation process due to the presence of oil.

Microchannel evaporators.

During in-tube flow evaporation the local concentration of oil in liquid refrigerant mixture increased as the thermodynamic vapor quality increased. Therefore more oil is typically retained in the superheated region of the evaporator, where the viscosity of liquid mixture is at its highest. The oil retention volume in the microchannel evaporators was measured up to 13 % of total internal volume of evaporator. For typical air conditioning application, OMF is less than 1 wt.%, and the oil retention volume varied from 3 to 10% of total internal volume, depending on the configuration of the outlet header and direction of the refrigerant flow at the outlet of the evaporator. When the microchannel tubes in the evaporator entered the outlet header vertically from the top and the refrigerant flow was vertical downward, then the valleys in between the tube inserts inside the outlet header were not potential traps for oil accumulation. On the other hand, in a vertical upward flow with microchannel tube entering the outlet header from the bottom. Valleys created in the outlet header were potential locations for trapping the oil inside the evaporator due to reduced refrigerant vapor velocity, separation of the oil from the bulk stream, and accumulation of the oil in the valleys by gravity.

The effect of saturation temperature was clearly visible. If the saturation temperature decreased then there was a significant increase in oil retention volume.

Oil affected the heat transfer rate of the microchannel evaporators and it penalized the heat transfer capacities by as much as 14% if the oil mass fraction was 5 wt.%. For air-conditioning applications and water and wine cooler applications, when OMFs were equal to or less than 1 wt. %, the decrease in heat transfer rates were within 4 %. The oil decreased the heat transfer rate and its impact was also depended on the mass flux. The heat transfer factors (HTFs) were close to 1 for OMF less than 1 wt. % and for both high and low mass flux. For OMF higher than 1 wt. %, the impact of mass flux on HTF was measurable. For example, at OMF of 3 wt.%, a reduction of mass flux by half, that is from high mass flux of 8.4 lb_m/ft²-s (20.4 kg/m²-s) to low mass flux of 4.2 lb_m/ft²-s (20.4 kg/m²-s), decreased the HTF from 0.96 to 0.90. This represented a decrease of 6% in the heat transfer rate for the same evaporation saturation temperature of 38°F (3.3°C) in the microchannels due to the decrease of mass flux from that of full load to part load conditions. These findings confirmed that the presence of oil in the evaporator was more marked at part load conditions. The refrigerant-side pressure drop across the microchannel evaporators increased by 10 to 25 percent when oil was present inside the heat exchangers and when the OMF was in the range of typical of air conditioning systems and refrigeration systems.

Validation of model of microchannel condenser with refrigerant and POE oil mixtures.

The extensive experimental work of this project RP 1564 provided data that were used to develop and experimentally validate a model for oil retention and for predicting the oil effects on microchannel heat exchangers heat transfer capacities and pressure drops. The model developed in this work used a segmentation approach of the heat exchanger to

divide the microchannel tubes into hundreds of short sections along the refrigerant flow direction. By imposing a heat balance and by using the effectiveness-NTU method on each segment, the outlet conditions from each segment were calculated and passed as input conditions for the adjacent segment until the entire refrigerant circuitry was completed. The user defined the coil geometry parameters and selected the appropriate heat transfer and pressure drop correlations based on refrigerant type, mass flux, and tube and fin geometries. These correlations are summarized in the modeling sections of the present report.

The model was able to capture correctly the trends and the magnitude of the penalization due to the oil on the heat transfer capacities and pressure drops of the microchannel heat exchangers at various oil mass fractions. The predicted oil retention volume was often lower than the measured oil retention volume. The main reason for the discrepancy was due to the estimation of the oil retained in the headers and in the length of the microchannel tubes, in which refrigerant was superheated vapor. We observed that these sections of the heat exchangers retained a significant portion of the total oil retained in the entire heat exchanger and sometimes they were dominant with respect to the oil miscible with the liquid phase of the refrigerant and oil mixture during two phase flow condensation and evaporation. The sections of the condenser headers and evaporator headers and the length of the microchannel tubes in which refrigerant was in thermodynamic superheated vapor state, were assumed to retain oil in the form of a layer of oil rich mixture film that stretched and wetted the internal walls. While this assumption was sound the thickness of the liquid oil rich mixture film was estimated from the velocity of the vapor refrigerant and it was assumed constant among the various

saturation temperatures. It was also assumed that the thickness varied linearly from 0 to a maximum value if the OMF increased from 0 to 5 wt.%. These assumptions might be the reason of the large error in the prediction of the ORV for some of the data points. However, overall the model provide the same order of magnitude of the oil retention volume that was measured during the tests of the present work. Preferential sites for oil accumulation in the microchannel heat exchangers headers were also identified in the present work and the amount of oil potentially retained in the headers was a significant portion of the total oil retention amount in the heat exchanger. Literature showed (and the experimental work of this project confirmed) that oil accumulated in the headers in the valleys created by the tube inserts inside the headers. This preferential sites for oil accumulation in the microchannel heat exchangers used in the experiments were not completely accounted for in the model. Thus, the model missed to predict a contribution to the oil retention volume due to the amount of oil held up inside the headers.

Finally the simulation results of the microchannel type heat exchangers predicted the heat transfer capacities and the pressure drop with and without oil. The model predictions of the heat transfer capacities were in general quite good and had an error of about ± 5 to $\pm 8\%$ with respect to the experimental data of the present work. The pressure drop were estimated by the newly developed model with an error that range from ± 20 to $\pm 50\%$ and the error increased significantly for some of the tests when oil was retained in the heat exchangers.

7.2 Recommendations for Future Work on this Research Topic

The overarching goal of this study was to investigate the effect of lubricant on heat transfer rate and pressure drop of refrigerant during flow boiling and condensation in microchannels and to use the results to validate a model for oil retention in microchannel heat exchangers. The approach in the present work was to consider the entire heat exchanger, that is, the microchannel tubes and the inlet and outlet headers all together. While this approach had the advantages of being feasible and accurate for the measurements of oil retention volume, heat transfer rate, and pressure drop, it also had certain limitations such as the determination of local heat transfer coefficient and local flow conditions. This present study addressed several key questions on this research topic (as discussed in the previous conclusion section) but also opened new questions for future work on this topic.

The main future work suggested are as follows.

1. Future work might be to extend the results of the present work to additional microchannel heat exchangers with different microchannel tube internal geometries and refrigerant flow configurations. Also, the experiments can be carry out by changing the flow direction and the heat exchanger orientation (i.e. vertical vs horizontal microchannel tubes and vertical vs horizontal headers).
2. Future work might be to extend the results of the present work to additional microchannel heat exchangers with different headers internal geometries and refrigerant flow configurations in the headers. The inlet and outlet (and intermediate headers for heat exchangers will multiple passes) are important elements that affect

- the oil retained in a microchannel heat exchanger and oil retention studies in the headers are recommended in future work on this research topic.
3. Future work might be to extend the results of the present work to additional refrigerant and oil mixtures and to expand the range of temperatures to very low temperatures for refrigeration applications (of -40°F (-40°C), for example). Measuring the oil retention is such low temperature conditions is not a trivial task and a future study on this topic is suggested.
 4. The oil retention was observed to be dependent on oil mass fraction, saturation temperature and inlet of superheat. These parameters were linked to the variation of mixture properties and possible disturbances of two-phase flow regimes encountered in microchannel heat exchangers. Further studies on two phase flow regimes with refrigerant and oil mixtures and the effect that oil has on altering the flow regime in microchannel tubes with respect to refrigerant only case might lead to a better understanding about how the oil impact the heat transfer coefficient and frictional pressure drops inside the microchannel tubes.
 5. It was observed that for OMF of 5 wt. % the liquid mixture viscosity increased by 7 times from inlet to outlet of the microchannel tube in an evaporator. The increase in the refrigerant R410A and POE oil mixture viscosity augmented the shear stress required to remove the oil, particularly the shear stress at the liquid-wall interface. Thus, oil increased its resistance to flow with and to be carried with the refrigerant vapor along the microchannel tubes. In the present work it was sound to assume that oil tended to form a film layer around the wall, that is, to wet the internal walls of the microchannel tubes and of the outlet header. However, since the tests were conducted

on full size microchannel heat exchangers, this hypothesis was not verified in the present work and the addition of flow visualization experiments of refrigerant and oil mixtures in microchannel tubes is potential future work on this topic.

6. In the present work we emphasized that the refrigerant was well distributed across the microchannel tubes of the evaporators. Since we purposely decided to control the inlet conditions of the microchannel evaporators to slightly sub-cooled (or saturated) liquid, the distribution of the refrigerant and oil mixture across the microchannel tubes was uniform during the tests of the present study. The flow distribution was only qualitatively observed by using thermal images of the evaporators during the tests. These images showed uniform color of the evaporator everywhere along the front face of the heat exchanger and we concluded that all the microchannel tubes received approximately the same flow rate of refrigerant (or of refrigerant and oil mixture). The condition of saturated liquid at the inlet of the evaporators is not necessarily representative of real life evaporator applications but, in this study, it avoided the challenge of non-uniform flow distribution of the refrigerant and oil mixture when oil was injected to the evaporators. As a result of our method of testing for the evaporators, the HTFs presented in the present work do not account for the effect that oil might have on the refrigerant flow distribution across the microchannel tubes and the HTFs do not account for the flow change, if any, inside the inlet headers of the microchannel heat exchangers. These effects, which are still due to the presence of oil retained inside the microchannel heat exchanger, might result in additional sources of heat transfer rate degradation in microchannel evaporators and their investigation is suggested in future studies of this work.

7. The experimental results of the present study were used to validate a model in predict the refrigerant charge, the heat transfer rate, and the pressure drop of a microchannel condenser. Preliminary calculations showed that oil tended to penalize the two phase flow heat transfer coefficient if heat transfer coefficient and pressure drop correlations, which were available from the literature and developed primarily from refrigerants only data, were used for predicting the phase change heat transfer behavior of refrigerant and oil mixtures. This extrapolation of the heat transfer correlations might not be valid and should be carefully evaluated. Developing local heat transfer coefficient correlations and pressure drop correlations for refrigerant and oil mixtures flow condensation in microchannel tubes might be potential future work.
8. In addition the oil retention model in the present works tended to underestimate the oil hold up in the heat exchangers. This was due to the lack of modeling of the microchannel headers internal geometries details. Literature showed (and the experimental work of this study confirmed) that oil accumulated in the headers, that is, in the valleys created by the tube inserts. Not only this accumulation might change the refrigerant flow distribution across the microchannel tubes but a model of the oil filling process of these valleys is missing. Future work might focus on modeling the oil retention in the headers of microchannel type heat exchangers in order to improve the accuracy of the oil retention model used in this study.

Nomenclature

A	area, m^2 (ft^2)
AB	alkylbenzene
CFC	chlorofluorocarbon
COP	coefficient of performance, dimensionless
c_p	specific heat capacity, $J/kg.K$ ($Btu/lbm.^{\circ}F$)
D	inner microchannel diameter, mm (inches)
EF	enhancement factor
f	friction factor
g	gravity acceleration, m^2/s (ft^2/hr)
G	mass flux, $kg/m^2\text{-s}$ ($lb_m/hr\text{-ft}^2$)
h	heat transfer coefficient, $W/m^2.K$ ($Btu/hr\text{-ft}^2.^{\circ}F$) or enthalpy J/kg (Btu/lb)
h_{fg}	enthalpy of vaporization, J/kg (Btu/lb)
HFC	hydrofluorocarbons
HTF	heat transfer factor, dimensionless
j	superficial phase velocity, m/s (fpm)

Ja	Jacob number
K_f	two-phase number
l	length of microchannel tubes, cm (inches)
m	mass, grams (or lbm)
\dot{m}	mass flow rate, grams/s or (lbm/min)
MO	mineral oil
MCHX	microchannel heat exchanger
NTU	number transfer unit
Nu	Nusselt number, dimensionless
OCR	oil circulation ratio, same as OMF
OMF	oil mass fraction, wt. %
ORV_N	oil retention volume normalized, dimensionless
P	pressure, Pa (psi) or perimeter, m (ft)
PAG	polyalkylene glycol
PDF	pressure drop factor
PF	penalty factor
POE	polyolester

Pr	Prandtl number, dimensionless
\dot{Q}	heat transfer rate, kW (Btu/hr)
R	thermal resistance, m ² .K/W (hr-ft ² .°F/Btu)
RH	relative humidity, %
Re	Reynolds number, dimensionless
s	solubility of refrigerant and oil mixture, % wt./wt.
S	sight glass
SUS	Saybolt universal second viscosity measurement method
t	time, second
T	temperature, °C (°F)
u	absolute uncertainty
v	velocity, m/s (fpm)
V	volume, cm ³ (or inch ³)
VG	viscosity grade
We	Weber number, dimensionless
X _{tt}	Martinelli parameter, dimensionless

Greek symbols

ΔP	refrigerant side pressure drop, kPa (psi)
α	heat transfer coefficient, W/m ² .K (Btu/hr-ft ² .°F)
ε	void fraction or efficiency, %
β	velocity ratio
δ	difference or uncertainty
ρ	density, grams/cm ³ (lb/inch ³)
σ	surface tension, N/m
μ	dynamic viscosity, Pa-s
ν	kinematic viscosity, cSt
$\tilde{\nu}$	viscosity ratio, dimensionless
γ	refrigerant-oil miscibility, dimensionless
ω	oil concentration by weight
ϕ	two phase multiplier
λ	thermal conductivity, W/m.K (Btu/hr-ft.°F)

Subscripts

f, L	liquid phase,
hx	heat exchanger

I	inlet
LO	liquid only
mchx	microchannel heat exchanger
mix	mixture
N	nozzle
NcB	nucleate boiling
o	oil or outlet
OR	oil retention
r	refrigerant
g, v	gas phase
sat	saturation
w	wall
tp	two phase
x	vapor quality

References

- A. Cicchitti, C. L., M. Silversti, G. Soldaini, R. Zavattarlli (1960). "Two-phase cooling experiments – pressure drop, heat transfer, and burnout measurements." *Energia Nucl.* 7(6): 407-425.
- Ackers, W. W., H. A. Deans and O. K. Crosser (1959). "Condensing heat transfer within horizontal tubes." *Chemical Engineering Progress Symposium* 55(29): 171-176.
- Ackers, W. W. and H. F. Rosson (1960). "Condensation inside a horizontal tube." *Chemical Engineering Progress Symposium* 56(30): 145-150.
- Agostini, B. and J. R. Thome (2005). Comparison of an extended database for flow boiling heat transfer coefficients in multi-microchannels elements with three-zone model. *ECI Heat Transfer and Fluid Flow in Microscale*, Italy.
- ASHRAE (1987). ANSI/ASHRAE 41.2-1987, Standard methods for laboratory airflow measurements, ASHRAE.
- ASHRAE (1988). ANSI/ASHRAE Standard 37-1988: Methods of testing for rating unitary air-conditioning and heat pump equipment Atlanta, GA, USA, ASHRAE: 25.
- ASHRAE (1996). ANSI/ASHRAE Standard 41.4-1996 (RA 2006) -- Standard Method for Measurement of Proportion of Lubricant in Liquid Refrigerant (ANSI approved). USA, ASHRAE.
- ASHRAE (2009). "American Society of Heating, Refrigerating and Air Conditioning Engineers Handbook: Fundamental SI Edition."
- ASHRAE (2010). "American Society of Heating, Refrigerating and Air Conditioning Engineers Handbook: Refrigeration SI Edition."
- ASHRAE (2013). "Standard 41.1-2013 -- Standard Method for Temperature Measurement."
- ASHRAE (2014). 41.3 Standard Methods for Pressure Measurement.
- Bai, X. and T. A. Newell (2002). Investigation of Two-Phase Viscous Liquid Flow. *9th Int. Refrigeration and Air Conditioning Conference at Purdue*. P. Univ. West Lafayette, IN (USA).
- Bandarra Filho, E. P., L. Cheng and J. R. Thome (2009). "Flow boiling characteristics and flow pattern visualization of refrigerant/lubricant oil mixtures." *International Journal of Refrigeration* 32(2): 185-202.
- Bassi, R. and P. K. Bansal (2003). "In-tube condensation of mixture of R134a and ester oil: Empirical correlations." *International Journal of Refrigeration* 26(4): 402-409.
- Bergles, A. E. and S. G. Kandlikar (2005). "On the Nature of Critical Heat Flux in Microchannels." *Journal of Heat Transfer* 127(1): 101-107.
- Biancardi, F. R., H. Michels, H., T. Sienel, H., and D. Pandey, R. (1996). Study of Lubrication Circulation in HVAC Systems - ARTI MCLR Project Number 665-53100, DOE/CE/23810-71 *The Air Conditioning and Refrigeration Technology Institute*. ARTI. East Hartford, Connecticut (US), United Technologies Research Center (UTRC). 1.
- Bigi, A. M., Cremaschi, L., Fisher, D. E. (2014). Modeling of Lubricant Effects in a Microchannel Type Condenser. *15th International Refrigeration and Air Conditioning Conference at Purdue*. West Lafayette, IN (USA).
- Cavallini, A., D. Del Col, L. Doretti, M. Matkovic, L. Rossetto and C. Zilio (2004). Condensation heat transfer inside multi-port minichannels. *Proceedings of the Second International*

- Conference on Microchannels and Minichannels (ICMM2004), June 17, 2004 - June 19, 2004, Rochester, NY, United states, American Society of Mechanical Engineers.*
- Cavallini, A., D. Del Col, L. Doretti, M. Matkovic, L. Rossetto and C. Zilio (2005). Condensation heat transfer and pressure gradient inside multiport minichannels, Taylor and Francis Ltd.
- Cavestri, R. C., J. Munk and M. Menning (1994). Solubility, viscosity, and density measurements of refrigerant-lubricant mixtures - part I: branched acid pentaerythritol polyolesters with R-134a. *Proceedings of the ASHRAE Annual Meeting, June 25, 1994 - June 29, 1994, Orlando, FL, USA, ASHRAE.*
- Cawte, H. (1992). "Effect of lubricating oil contamination on condensation in refrigerant R22." *International Journal of Energy Research* 16(4): 327-340.
- Chang, Y.-J., K.-C. Hsu, Y.-T. Lin and C.-C. Wang (2000). "A generalized friction correlation for louver fin geometry." *International Journal of Heat and Mass Transfer* 43(12): 2237-2243.
- Chang, Y.-J. and C.-C. Wang (1997). "A generalized heat transfer correlation for louver fin geometry." *International Journal of Heat and Mass Transfer* 40(30): 533-544.
- Chen, J. C. (1963). *A correlation for Boiling Heat Transfer to Saturated Fluids in Convective Flow*. Boston, ASME preprint 63-HT-34 presented at 6th National Heat Transfer Conference.
- Choi, J. W., M. S. Kim, J. S. Shin, S. K. Oh, B. Y. Chung and M. S. Kim (2009). "A numerical study on oil retention and migration characteristics in the heat pump system." *Journal of Mechanical Science and Technology* 23(7): 1858-1865.
- Choi, J. Y., M. A. Kedzierski and P. A. Domanski (1999). *Generalized pressure drop correlation for evaporation and condensation in smooth and micro-fin tubes*.
- Collier, J. G. and J. R. Thome (1994). *Convective boiling and condensation*. Oxford, Oxford Science Publications.
- Cremaschi, L. (2004). Experimental and Theoretical Investigation of Oil Retention in Vapor Compression Systems. Ph.D. Dissertation Ph.D. thesis, University of Maryland.
- Cremaschi, L., Y. Hwang and R. Radermacher (2005). "Experimental investigation of oil retention in air conditioning systems." *International Journal of Refrigeration* 28(Compendex): 1018-1028.
- Cremaschi, L. and E. Lee (2008). "Design and Heat Transfer Analysis of a New Psychrometric Environmental Chamber for Heat Pump and Refrigeration Systems Testing." *ASHRAE Transactions* 114(2): 619-631.
- Deokar, P. S. (2013). Development of an experimental methodology for measurement of oil retention and its effect on the microchannel heat exchanger. 1553402 M.S., Oklahoma State University.
- Dittus, F. W. and L. M. K. Boelter (1930). "Heat transfer in automobile radiators of the tubular type." *University of California Publications in Engineering* 2: 443-461.
- Dobson, M. K. and J. C. Chato (1998). "Condensation in smooth horizontal tubes." *Journal of Heat Transfer* 120(1): 193-213.
- Dukler, A. E. (1964). "Pressure drop and holdup in two phase flow." *AIChE Journal* 10(1): 38-51.
- Eckels, S. J., T. M. Doerr and M. B. Pate (1998). Heat transfer coefficients and pressure drops for R-134a and an ester lubricant mixture in a smooth tube and a micro-fin tube. *Proceedings of the 1998 ASHRAE Winter Meeting. Part 1 (of 2), January 18, 1998 - January 21, 1998, San Francisco, CA, USA, ASHRAE.*
- Eckels, S. J., S. C. Zoz and M. B. Pate (1993). Using solubility data for HFC-134a and ester lubricant mixtures to model an in-tube evaporator or condenser. *Proceedings of the 1993 Annual Meeting of the American Society of Heating, Refrigerating and Air-Conditioning Engineers, Inc., June 27, 1993 - June 30, 1993, Denver, CO, USA, Publ by ASHRAE.*

- Foster, P. and N. Zuber (1974). Point of Vapor Generation and Vapor Void Fraction. *5th Int. Heat Transfer Conf.*
- Friedel, L. (1979). *Improved frictional pressure drop correlations for horizontal and vertical two-phase pipe flow.*
- Garimella, S. (2004). "Condensation Flow Mechanisms in Microchannels: Basis for Pressure Drop and Heat Transfer Models." *Heat Transfer Engineering* 25(3): 104-116.
- Gnielinski, V. (1976). "New equation for heat and mass transfer in turbulent heat channel flow." *Int. J. Chem. Eng.* 16(2): 359-367.
- Gorenflo, D. (1993). "Pool Boiling." *VDI Heat Atlas, VDI Verlag, Düsseldorf.*
- Haraguchi, H., S. Koyama and T. Fujii (1994). "Condensation of refrigerants HCFC 22, HFC 134a and HCFC 123 in a horizontal smooth tube (2nd report, proposals of empirical expressions for local heat transfer coefficient)." *Nippon Kikai Gakkai Ronbunshu, B Hen/Transactions of the Japan Society of Mechanical Engineers, Part B* 60(574): 2117-2124.
- Hu, H.-T., G.-L. Ding, X.-C. Huang, B. Deng and Y.-F. Gao (2011). "Experimental investigation and correlation of two-phase heat transfer of R410A/OIL mixture flowboiling in a 5-MM microfin tube." *Journal of Enhanced Heat Transfer* 18(3): 209-220.
- Hu, H., G. Ding, X. Huang, B. Deng and Y. Gao (2009). "Measurement and correlation of flow-boiling heat transfer of a R-410A/Oil mixture inside a 4.18 mm straight smooth tube." *HVAC and R Research* 15(2): 287-314.
- Hu, H., G. Ding and K. Wang (2008). "Heat transfer characteristics of R410A oil mixture flow boiling inside a 7mm straight microfin tube." *International Journal of Refrigeration* 31(6): 1081-1093.
- Huang, L. (2012). A generalized effectiveness-ntu based variable geometry microchannel heat exchanger model. *Proceedings of the 14th International Refrigeration and Air Conditioning Conference at Purdue.* West Lafayette, IN: 2191.
- Huang, X., G. Ding, H. Hu, Y. Zhu, Y. Gao and B. Deng (2010). "Condensation heat transfer characteristics of R410A oil mixture in 5mm and 4mm outside diameter horizontal microfin tubes." *Experimental Thermal and Fluid Science* 34(7): 845-856.
- Huang, X., G. Ding, H. Hu, Y. Zhu, H. Peng, Y. Gao and B. Deng (2010a). "Influence of oil on flow condensation heat transfer of R410A inside 4.18 mm and 1.6 mm inner diameter horizontal smooth tubes." *Int. J. of Refrigeration* 33(1): 158-169.
- Huang, X., Y. Zhu, G. Ding, Y. Gao, H. Hu and B. Deng (2010b). "Two-phase frictional pressure drop characteristics of R410A-oil mixture flow condensation inside 4.18 mm and 1.6 mm I.D. horizontal smooth tubes." *HVAC&R Research* 16(4): 453-470.
- Hwang, Y., L. Cremaschi, R. Radermacher, T. Hirata, Y. Ozaki and T. Hotta (2004). Oil circulation behavior in low temperature CO₂ climate control systems. *Proc. of the SAE World Congress, Detroit, USA.*
- Incropera, F. P. and D. P. DeWitt (2001). *Fundamentals of Heat and Mass Transfer.* USA, Wiley.
- Iu, I. S. (2007). "Development of air-to-air heat pump simulation program with advanced heat exchanger circuitry algorithm."
- Jacobi, A. M. and J. R. Thome (2002). "Heat Transfer Model for Evaporation of Elongated Bubble Flows in Microchannels." *Journal of Heat Transfer* 124(6): 1131-1136.
- Jeng, Y.-R., C.-S. Chang and C.-C. Wang (2001). "Vapor pressure of R-410A/oil and R-407C/oil mixtures." *Applied Thermal Engineering* 21(8): 863-870.
- Jensen, M. K. and D. L. Jackman (1984). "Prediction of nucleate pool boiling heat transfer coefficients of refrigerant-oil mixtures." *Journal of Heat Transfer* 106(1): 184-190.
- Jiang, H. (2003). "Development of a simulation and optimization tool for heat exchanger design." *Ph.D. Dissertation University of Maryland at College Park.*
- Jin, S. and P. Hrnjak (2013). "Refrigerant and Lubricant Distribution in MAC System." *SAE Int. J. Passeng. Cars -Mech. Syst* 6(2).

- Jin, S. and P. Hrnjak (2014). An Experimentally Validated Model for Predicting Refrigerant and Lubricant Inventory in MAC Heat Exchangers. *SAE 2014 World Congress & Exhibition*. Michigan, USA.
- Jung, D. S. and R. Radermacher (1989). "Prediction of pressure drop during horizontal annular flow boiling of pure and mixed refrigerants." *International Journal of Heat and Mass Transfer* 32(12): 2435-2446.
- Kandlikar, S. G. (1990). "A general correlation for two-phase flow boiling heat transfer coefficient inside horizontal and vertical tubes." *Journal of Heat Transfer* 102: 219-228.
- Kandlikar, S. G. (2004). "Heat transfer mechanisms during flow boiling in microchannels." *Journal of Heat Transfer-Transactions of The ASME* 126(1): 8-16.
- Kandlikar, S. G. and M. E. Steinke (2003). Predicting heat transfer during flow boiling in minichannels and microchannels, Chicago, IL, United states, Amer. Soc. Heating, Ref. Air-Conditioning Eng. Inc.
- Kang, H.-M. and M. B. Pate (1999). Miscibility comparison for three refrigerant mixtures and four component refrigerants. *ASHRAE Annual Meeting, June 18, 1999 - June 23, 1999*, Seattle, WA, USA, ASHRAE.
- Kattan, N., Thome, J. R. and Favrat, D. (1998). "Flow Boiling in Horizontal Tubes: Part 1 - Development of a Diabatic Two-Phase Flow Pattern Map." *Journal of Heat Transfer* 120: 140-147.
- Kawahara, A., P. M. Y. Chung and M. Kawaji (2002). "Investigation of two-phase flow pattern, void fraction and pressure drop in a microchannel." *International Journal of Multiphase Flow* 28(9): 1411-1435.
- Kutateladze, S. S. (1961). "Boiling heat transfer." *International Journal of Heat & Mass Transfer* 4: 31.
- L Wojtan, T. U., J Thome (2005). "Investigation of flow boiling in horizontal tubes: Part I: A new diabatic two-phase flow pattern map." *International Journal of Heat and Mass Transfer* 48: 2955-2969.
- Lee, J. P. (2002). Experimental and Theoretical Investigation of Oil Retention in Carbon Dioxide Air-Conditioning System. Ph.D., University of Maryland.
- Li, H. and P. Hrnjak (2013). "Effect of lubricant on two-phase refrigerant distribution in microchannel evaporator." *Int. J. of Material and Manufacture* 6(3).
- Lockhart, R., W., and R. Martinelli, C., (1949). "Proposed correlation of data for isothermal two-phase, two-component flow in pipes." *Chemical Engineer Progress* 45: 39-48.
- Lottin, O., P. Guillemet and J.-M. Lebreton (2003). "Effects of synthetic oil in a compression refrigeration system using R410A. Part I: Modelling of the whole system and analysis of its response to an increase in the amount of circulating oil." *International Journal of Refrigeration* 26(7): 772-782.
- Lottin, O., P. Guillemet and J. M. Lebreton (2003). "Effects of synthetic oil in a compression refrigeration system using R410A. Part II: Quality of heat transfer and pressure losses within the heat exchangers." *International Journal of Refrigeration* 26(7): 783-794.
- Mandhane, J. M., Gregory, G. A., Aziz, K (1974). "A Flow Map for Gas-Liquid Flow in Horizontal Pipes." *Int. J. Multiphase Flow* 1: 537-553.
- McAdams, W. H. (1954). *Heat Transmission*. New York, McGraw-Hill.
- Mehendale, S. S. and R. Radermacher (2000). "Experimental and theoretical investigation of annular film flow reversal in a vertical pipe: Application to oil return in refrigeration systems." *HVAC&R* 6(1): 55-74.
- Memory, S. B., D. C. Sugiyama and P. J. Marto (1995). "Nucleate pool boiling of R-114 and R-114-oil mixtures from smooth and enhanced surfaces--I. Single tubes." *International Journal of Heat and Mass Transfer* 38(8): 1347-1361.
- Mishima, K. and T. Hibiki (1996). "Some characteristics of air-water two-phase flow in small diameter vertical tubes." *International Journal of Multiphase Flow* 22(4): 703-712.

- Monde, M. and E. Hahne (1987). "Boiling heat transfer on a fine horizontal wire in a refrigerant-oil mixture." *Heat Transfer-Japanese Research* 16(6): 48-60.
- Müller-Steinhagen, H. and K. Heck (1986). "A simple friction pressure drop correlation for two-phase flow in pipes." *Chemical Engineering and Processing: Process Intensification* 20(6): 297-308.
- Pierre, B. (1964). "Flow Resistance With Boiling Refhgerants-Part 1." *ASHRAE Journal* 6(9): 58-65.
- Popovic, P., R. L. Shimon, M. Pate and N. E. Schnur (2000). "Effects of lubricant miscibility and viscosity on the performance of an R-134a refrigerating system." *ASHRAE Transactions* 106: PA/.
- Radermacher, R., L. Cremaschi and R. A. Schwentker (2006). "Modeling of oil retention in the suction line and evaporator of air-conditioning systems." *HVAC&R Research* 12(1): 35-56.
- Ribatski, G., L. Wojtan and J. R. Thome (2006). "An analysis of experimental data and prediction methods for two-phase frictional pressure drop and flow boiling heat transfer in micro-scale channels." *Experimental Thermal and Fluid Science* 31(1): 1-19.
- Riedle, K. J., N. A. Macken and S. W. Gouse Jr (1972). "Oil Transport by Refrigerant Vapor: A literature Survey and Proposed Analytical Model." *ASHRAE Transactions* 78(Part 2): 124-134.
- Schlager, L. M., M.B. Pate, A.E. Bergles (1988). "Evaporation and condensation of refrigerant-oil mixtures in a smooth tube and a micro-fin tube." *ASHRAE transactions* 94(3112): 149.
- Schlager, L. M., M. B. Pate and A. E. Bergles (1987). Survey of refrigerant heat transfer and pressure drop emphasizing oil effects and in-tube augmentation. *ASHRAE Trans.*, New York, NY, USA, ASHRAE.
- Schlager, L. M., M. B. Pate and A. E. Bergles (1990). Oil quantity measurements in smooth and micro-fin tubes during evaporation and condensation of refrigerant-oil mixtures. *ASHRAE Annual Meeting*, St. Louis, USA.
- Schubring, D., E. T. Hurlburt, A. C. Ashwood and T. A. Shedd (2009). Optical measurement of base film thickness in annular two-phase flow, Jacksonville, FL, United states, American Society of Mechanical Engineers.
- Schwentker, R. (2005). Simulation and design tool for microchannel heat exchangers. *5th International Conference on Enhanced, Compact, and Ultra-Compact Heat Exchangers: Science, Engineering, and Technology*. Whistler, British Columbia, Canada.
- Schwentker, R. A. (2005). "Advances to a computer model used in the simulation and optimization of heat exchangers." *M.Sc. Dissertation University of Maryland at College Park*.
- Shah, M. M. (1979). "General correlation for heat transfer during film condensation inside pipes." *International Journal of Heat and Mass Transfer* 22(4): 547-556.
- Shao, D. W. and E. Granryd (1995). "Heat transfer and pressure drop of HFC134a-oil mixtures in a horizontal condensing tube." *International Journal of Refrigeration* 18(8): 524-533.
- Shedd, T. A. and T. A. Newell (1998). "Automated Optical Liquid Film Thickness Measurement Method." *Review of Scientific Instruments* 69(12): 4205-4213.
- Shedd, T. A. and T. A. Newell (2004). "Characteristics of the liquid film and pressure drop in horizontal, annular, two-phase flow through round, square and triangular tubes." *J. of Fluids Eng. Trans.* 126(5): 807-817.
- Shen, B. and E. A. Groll (2005). "Review Article: A Critical Review of The Influence of Lubricants on the Heat Transfer and Pressure Drop of Refrigerants-Part II: Lubricant Influence on Condensation and Pressure Drop." *HVAC&R Research* 11(4): 511-526.

- Shen, B. and E. A. Groll (2005). "Review Article: A Critical Review of the Influence of Lubricants on the Heat Transfer and Pressure Drop of Refrigerants, Part 1: Lubricant Influence on Pool and Flow Boiling." *HVAC&R Research* 11(3): 341-359.
- Steiner, D. and J. Taborek (1992). "Flow boiling heat transfer in vertical tubes correlated by an asymptotic model." *Heat Transfer Engineering* 13: 43-69.
- Sunami, M. (1999). Physical and chemical properties of refrigeration lubricants. *ASHRAE Annual Meeting, June 18, 1999 - June 23, 1999*, Seattle, WA, USA, ASHRAE.
- Sundaresan, S. G. and R. Radermacher (1996). "Oil return characteristics of refrigerant oils in split heat pump system." *ASHRAE Journal* 38(8): 57-61.
- Takaishi, Y. and K. Oguchi (1987). Measurements of Vapor Pressures of R22/Oil Solutions. *18th international Congress of Refrigeration*, Vienna.
- Tandon, T. N., H. K. Varma and C. P. Gupta (1995). "Heat transfer during forced convection condensation inside horizontal tube." *International Journal of Refrigeration* 18(3): 210-210.
- Tang, L., M. M. Ohadi and A. T. Johnson (2000). "Flow condensation in smooth and micro-fin tubes with HCFC-22, HFC-134a and HFC-410A refrigerants. Part I: experimental results." *Journal of Enhanced Heat Transfer* 7(5): 289-310.
- Taylor, B. N. and C. E. Kuyatt (1994). Guidelines for evaluating and expressing the uncertainty of NIST measurement results, U.S. Dept. of Commerce, Tech. Adm., NIST, Gaithersburg, MD, USA. 20: 28 cm.
- Teodorescu, M., L. Lugo and J. Fernandez (2003). "Modeling of Gas Solubility Data for HFCs-Lubricant Oil Binary Systems by Means of the SRK Equation of State." *International Journal of Thermophysics* 24(4): 1043-1060.
- Thome, J. (2004). Engineering Databook III, Wolverine Inc.
- Thome, J. R. (1995). "Comprehensive thermodynamic approach to modeling refrigerant-lubricating oil mixtures." *HVAC&R Research* 1(2): 110-110.
- Thome, J. R. (1998). "Boiling and evaporation of fluorocarbon and other refrigerants: A state-of-the-art review." *ARTI Report*.
- Thome, J. R. (2004). "Boiling in microchannels: A review of experiment and theory." *International Journal of Heat and Fluid Flow* 25(2): 128-139.
- Thome, J. R., V. Dupont and A. M. Jacobi (2004). "Heat transfer model for evaporation in microchannels. Part I: presentation of the model." *International Journal of Heat and Mass Transfer* 47(14-16): 3375-3385.
- Thome, J. R., J. El Hajal and A. Cavallini (2003). "Condensation in horizontal tubes, part 2: new heat transfer model based on flow regimes." *International Journal of Heat and Mass Transfer* 46(18): 3365-3387.
- Tichy, J. A., J. Duque-Rivera, N. A. Macken and W. M. B. Duval (1986). Experimental investigation of pressure drop in forced-convection condensation and evaporation of oil-refrigerant mixtures. *ASHRAE Transactions 1986. Technical Papers Presented at the 1986 Annual Meeting*, Portland, OR, USA, ASHRAE.
- Vaughn, R., S., (1971). "Refrigerant Compressors, Lubricating Oil, and Refrigerant - An Uneasy Trio." *ASHRAE Symposium Bulletin*(1): 14-18.
- Wang, H. S., J. W. Rose and H. Honda (2004). "A Theoretical Model of Film Condensation in Square Section Horizontal Microchannels." *Chemical Engineering Research and Design* 82(4): 430-434.
- Wei, W., G. Ding, H. Hu and K. Wang (2007). "Influence of lubricant oil on heat transfer performance of refrigerant flow boiling inside small diameter tubes. Part I: Experimental study." *Experimental Thermal and Fluid Science* 32(1): 67-76.
- Wei, W., G. Ding, H. Hu and K. Wang (2008). "Models of thermodynamic and transport properties of POE VG68 and R410A/POE VG68 mixture." *Frontiers of Energy and Power Engineering in China* 2(2): 227-234.

- Yang, C. Y. and R. L. Webb (1997). "A Predictive Model for Condensation in Small Hydraulic Diameter Tubes Having Axial Micro-Fins." *Journal of Heat Transfer* 119(4): 776-782.
- Yokozekei, A. M. (1994). Solubility and Viscosity of Refrigerant-Lubricant Mixtures. *Purdue International Refrigeration Conference*, West Lafayette.
- Zhang, Y. and M. He (2009). "Kinematic Viscosity of R410A and R407C Refrigerant–Oil Mixtures in the Saturated Liquid Phase with Lubricant Mass Fraction in the Range of (0 to 0.0001)." *J. Chem & Eng Data* 55(8): 2886-2889.
- Zhao, Y., M. Molki, M. Ohadi, M., F. Franca, H., R., R. Radermacher, G. Mathur, D., and K. Cho (2002). "Flow Boiling of CO₂ with Miscible Oil in Microchannels." *ASHRAE Transactions* 108(1): 135-144.
- Zürcher, O., J. R. Thome and D. Favrat (1998). "In-Tube Flow Boiling of R-407C and R-407C/Oil Mixtures Part II: Plain Tube Results and Predictions." *HVAC&R Research* 4(4): 373-399.

VITA

Ardiyansyah Saad Yatim

Candidate for the Degree of

Doctor of Philosophy

Thesis: OIL RETENTION AND ITS EFFECTS ON PRESSURE DROP AND HEAT TRANSFER IN MICROCHANNEL HEAT EXCHANGERS OF AIR CONDITIONING AND REFRIGERATION SYSTEM

Major Field: Mechanical and Aerospace Engineering

Biographical:

Education:

Completed the requirements for the Doctor of Philosophy in Mechanical and Aerospace Engineering at Oklahoma State University, Stillwater, Oklahoma in July, 2015.

Completed the requirements for the Master of Engineering in Refrigeration Engineering at Chonnam National University, Yeosu, Republic of Korea in 2006.

Completed the requirements for the Bachelor of Engineering in Mechanical Engineering at University of Indonesia, Depok, Indonesia in 2003.

Experience: -

Professional Memberships: American Society of Heating, Refrigerating and Air Conditioning Engineering (ASHRAE)